From Average to Marginal: A Novel Way to Measure the Mortality Risk of an Infectious Disease*

Adibah Abdulhadi†, Hanbat Jeong‡, Kurt Lavetti§, Rebecca McKibbin¶, Bruce A. Weinberg‖

November 4, 2025

Abstract

We propose a new measure of the mortality risk of infectious diseases, the marginal case-fatality rate (MCFR), which quantifies the effect of one additional case on aggregate subsequent mortality, including direct deaths and indirect deaths from downstream transmission. To estimate the MCFR, we develop a dynamic geospatial framework that incorporates transmission within and across places, spatial heterogeneity, lags between infections and death, and mortality spillovers to other causes of death. This framework can assist policymakers in disease mitigation decisions by consolidating multiple risk factors, including transmissibility and mortality, into a single interpretable measure that summarizes the full mortality consequences of an additional case. Applying this framework to 2020 US data, we estimate that one marginal COVID-19 case caused 0.63 subsequent all-cause deaths nationally. This MCFR estimate includes substantial spillover effects: a marginal case caused 0.15 COVID-19 deaths in the same county as the marginal infection, 0.33 COVID-19 deaths in other counties, and 0.15 non-COVID deaths. Ex post, mitigation policies like lockdowns were poorly targeted during the pandemic, contributing to a modest marginal benefit of $576 per person-week of lockdowns. The MCFR framework can help policymakers more efficiently target and coordinate interventions spatially and intertemporally.

Keywords: infectious disease, spatial dynamic models, mortality, epidemiology
JEL classification: I12, I18, C33

*We would like to thank participants of seminars/conferences held by the Ohio State University, the Social, Behavioral, and Economic COVID Coordinating Center (SBE CCC), the American Society of Health Economists, and the Econometric Society World Congress 2025 for their thoughtful feedback. This research was supported financially by the National Institute on Aging (NIA), the National Institute of General Medical Sciences (NIGMS), and the National Institutes of Health (NIH) Office of the Director (Grant U01AG076549).

†Department of Economics, The Ohio State University, E-mail: abdulhadi.9@osu.edu

‡Department of Economics, Macquarie Business School, Macquarie University, Sydney, Australia, E-mail: hanbat.jeong@mq.edu.au

§Department of Economics, The Ohio State University, E-mail: lavetti.1@osu.edu

¶School of Economics, The University of Sydney, E-mail: rebecca.mckibbin@sydney.edu.au

‖Department of Economics. The Ohio State University, 1945 N. High Street, Columbus, Ohio. E-mail: weinberg.27@osu.edu

1 Introduction

How many deaths are generated by an additional case of an infectious disease? The answer to this question is important for setting and communicating the value of policies to mitigate diseases. Epidemiology offers valuable measures, including the case fatality rate (CFR), which quantifies mortality, and the reproduction number ($\mathcal{R}_t$)[1], which quantifies transmission. However, there is no integrated measure that captures the total mortality impact of an additional case, nor is there a clear way of combining existing metrics to generate such a policy-relevant summary statistic.

This paper introduces the marginal case fatality rate (MCFR), a measure of the cumulative effect of one additional case at a point in time on subsequent mortality, accounting for both downstream transmission and mortality among infected people. As a single forward-looking, time- and location-specific measure of the total number of lives lost per additional case, the MCFR facilitates the spatial and temporal targeting of mitigation policies. To do so, our MCFR framework models both the time path from infection to death and the spread of disease within and across regions.

To demonstrate the policy relevance of the MCFR, we apply it to the COVID-19 pandemic in 2020. We estimate that one additional case led to 0.4757 additional COVID-19 deaths nationally—20 times greater than the CFR—and an additional 0.1498 non-COVID deaths. However, despite this large MCFR, we estimate that lockdowns aimed at reducing infections had a modest marginal benefit of $576 per person per week of lockdown, perhaps explaining mixed public views of the merits of lockdowns. Ex post, we also find that lockdowns were often poorly targeted – the MCFR is generally highest prior to spikes in cases, whereas lockdown policies during the pandemic often tracked mortality, which lags cases. This suggests that better-timed interventions based on the MCFR could have saved more lives without increasing the length or severity of lockdowns. While we focus on COVID-19 as an application, the MCFR framework we develop is generalizable and can be applied to other infectious diseases.

The framework underlying the MCFR is a novel combination of two well-established econometric components: a spatial dynamic panel data model for transmission and a finite distributed lag model for mortality. These components have not been previously applied together to study infectious diseases, but they are ideally suited to the context because they can capture important features of an infectious disease, like the spatial spread of disease and the delay between infections and death. Our spatial dynamic panel data model describes disease propagation over time and across locations using spatial weights to capture geographic and social connectedness between counties, allowing these relationships to influence patterns of disease spread (Yu, de Jong and Lee, 2008; Shi and Lee, 2017; Jeong and Lee, 2020; Han et al., 2021). To characterize disease transmission, we model the strength of relationships between counties using data on population flows from SafeGraph mobile phone locations (Kang et al., 2020). The finite distributed lag model (Almon, 1965; Griliches, 1967) describes the time path connecting mortality to infection by assigning distinct lag parameters to different points in time. Additionally, it extends the traditional CFR by allowing mortality risks to vary with county characteristics and demographics while explicitly linking mortality to past case levels.

[1]The effective reproduction number, $\mathcal{R}_t$, is a time-varying version of the well-known basic reproduction number, $\mathcal{R}_0$.

Our empirical framework yields a closed-form and additive summary statistic that can be decomposed in ways that are useful for a variety of policy questions. For example, we consider the effect of an additional case on mortality geographically and estimate that about one-third of COVID-19 deaths (31%) occur in the same county as the focal additional case, 36% occur in other counties in the same state, and 33% of deaths spill over to other states. By capturing these substantial geographic spillovers, our MCFR framework highlights that local mitigation policies produce externalities at the national level beyond their immediate jurisdictions, underscoring the value of strategic, coordinated interventions. We also alternatively decompose the MCFR into two channels: "direct" mortality of the person infected with the focal case of 0.0262 within 5-6 weeks (a figure comparable to the average CFR during out study period of 0.0210) and 0.4495 "indirect" deaths caused by subsequent COVID-19 propagation.[2] This decomposition highlights how the MCFR can inform policies to target different facets of the disease (e.g., reducing transmission versus investing in better treatments).

Another advantage of our empirical approach is that it can be easily and flexibly modified to evaluate externalities in mortality from causes other than the focal disease. This is important because the total mortality burden may be underestimated if the analysis focuses only on mortality from the focal disease. By contrast, mortality from other conditions is usually examined in separate epidemiologic models instead of in a single unified framework.[3] Using a broader model of all-cause mortality, we estimate that an additional case of COVID-19 generates 0.6255 additional deaths across the U.S. of which 24% (or 0.1498 deaths) are due to non-COVID-19 causes. These estimates incorporate both direct and indirect pathways, including strain on healthcare systems and mental health effects.

The regression form of our empirical framework can also be adapted to study disparities by demographic and socioeconomic characteristics. We estimate that the mortality risk to older adults from COVID-19 was 20 times larger than that of the young population; the risk among individuals with a high school diploma or less is 3.6 times larger than that of individuals with some college or more. Among older adults, the MCFRs among Non-Hispanic Blacks and among Hispanics were 2 and 1.4 times larger, respectively, than the MCFR among non-Hispanic Whites. (There are also smaller disparities within the young population.) These results corroborate evidence from prior studies that found disparities in outcomes like excess deaths[4] and, at the same time, offer another perspective to quantify the disparate mortality impact of COVID-19 and evaluate how the effects of mitigation policies might vary across groups.

The MCFR combines information on the fatality and transmission rates to produce policy-relevant metrics that cannot be easily inferred from traditional epidemiological measures like the CFR and $\mathcal{R}_t$. To demon-

[2]The CFR is the ratio of cumulative mortality to cumulative cases. It can be interpreted as the probability of deaths conditional on being infected and conceptually corresponds to the part of the MCFR on direct mortality.

[3]Other epidemiology measures that incorporate the spillover effects on deaths of causes other than the focal infectious disease include the mortality rate, the excess death rate, and the years of life lost (YLL). YLL is a measure of premature death and is usually calculated by subtracting the age at death from 65 (Alsan, Chandra and Simon (2021)). This measure incorporates age into the calculation of the burden of a disease, with younger ages associated with a larger burden. The mortality rate and excess death rate can also be adjusted for age. Apart from incorporating deaths of other causes, an advantage of these measures over the CFR is that they can overcome variation in how cause of death is coded across places (Beaney et al., 2020; Morgan et al., 2020). However, these measures are not directly linked to cases and are averages, not marginal measures, which, while useful in characterizing the severity of a disease, cannot directly inform decisions on whether to impose a policy to mitigate disease spread.

[4]For instance, see Weinberger et al. (2020); Alsan, Chandra and Simon (2021); Polyakova et al. (2021); Schwandt et al. (2022); Finkelstein et al. (2024).

strate the distinct information it captures, we attempt to reconstruct the MCFR using combinations of the CFR and $\mathcal{R}_t$, and find that based on the R^2 value, 54% of the variation in the MCFR is unexplained (conditional on state and time fixed effects), indicating that the MCFR adds considerable information over existing measures.

We further investigate the interaction between fatality and transmissibility in their relationship to the MCFR through comparative statics exercises that vary key disease parameters. These exercises illustrate how the MCFR behaves in settings with different epidemiological characteristics (for instance, if COVID-19 were to evolve) and demonstrate its applicability to other infectious diseases. We find that the MCFR implies a mathematical complementarity between fatality and transmissibility. That is, the MCFR increases faster with respect to the fatality (transmission) rate at larger values of the transmission (fatality) rate. Furthermore, the gap between the values of the MCFR and a CFR analog widens as transmissibility increases because of increased downstream transmission. This exercise showcases that the MCFR framework is likely to add value relative to the traditional epidemiological measures in characterizing infectious diseases with high transmissibility like COVID-19. In short, these results highlight how embedding mortality and transmission in an integrated framework allows us to generate insights on how they interact to determine mortality.

Our framework contributes to a large epidemiology literature characterizing infectious diseases.[5] We explicitly relate our MCFR framework to the literature both empirically and theoretically. At a theoretical level, we detail how an integral element of the MCFR capturing marginal case propagation corresponds to $\mathcal{R}_t$.[6] At an empirical level, we build a compartmental model with similar features as our setup (e.g., cross-county transmission) to evaluate our own $\mathcal{R}_t$ using our marginal measure of case propagation.[7] We then show that it mirrors the dynamic patterns of the MCFR components that incorporate mortality from downstream cases of rising and peaking before an outbreak. Our estimate of $\mathcal{R}_t$ is within the range reported in the literature, although it is at the lower end,[8] which can be explained by differences in the study periods (large $\mathcal{R}_t$ estimates in the literature tend to come from the very early pandemic period while we cover much of 2020) and modelling approaches (our $\mathcal{R}_t$ captures *marginal* case transmission while the traditional $\mathcal{R}_t$ is more conventionally evaluated as the total or average impact of a case).[9]

The rest of the paper proceeds as follows: Section 2 outlines our framework and empirical approach, Section 3 describes the data we use to implement our model, Section 4 presents the main results, Section 5 presents selected robustness exercises, and Section 6 concludes.

[5] We derive the properties of our new measure and ground it in other well-established concepts because our empirical approach is built upon the finite distributed lag model and spatial dynamic panel data models that are widely used with well-understood features.

[6] This is the rate of new cases tomorrow generated from cases today.

[7] This is necessary because $\mathcal{R}_t$ is inherently model-specific, and we are not aware of any studies with the same empirical setup as ours.

[8] Relevant works are Al-Raeei (2021); Chinazzi et al. (2020); Li et al. (2020); Liu et al. (2020); Park et al. (2020); Salje et al. (2020); Fernández-Villaverde and Jones (2022).

[9] We note that around the early pandemic, our $\mathcal{R}_t$ is close to the higher end of the range in the literature, which is consistent with our model incorporating local as well as inter-regional transmission. For instance, see Katul et al. (2020); Sanche et al. (2020); Ke et al. (2021); Korolev (2021); Chudik, Pesaran and Rebucci (2022); Johnsson, Pesaran and Yang (2023).

2 Framework

Our objective is to quantify the effect of an additional case on all ensuing mortality, thereby producing a comprehensive measure that combines and innovates upon existing epidemiological metrics. We break down this problem into two relationships. First, to estimate the fatality rate conditional on infection, we relate mortality in location i at time t to lags of cases in that location. Second, because infectious diseases propagate, resulting in additional cases and ultimately more mortality, we model disease transmission within and across locations. In our analysis, we measure locations using counties and time periods using weeks. However, the framework can be extended to other infectious diseases, units of geography (e.g., state, country), and time periods (e.g., daily, monthly) to suit the context.

2.1 Model specification

We implement the MCFR framework with two well-established econometric models that map naturally onto the biology of an epidemic. Mortality conditional on infection is captured by a finite distributed lag model (Almon, 1965; Griliches, 1967), which assigns separate lag coefficients to successive post-infection weeks. This structure allows the data to inform the time path between symptom onset and death (which can be benchmarked against the clinical literature) while allowing fatality risk to vary with county demographics and other covariates. Transmission is modeled with a spatial dynamic panel-data specification. Spatial weights characterize geographic and social connectedness between counties; the spatial dynamic panel data equations then track how infections propagate across those links over time (Yu, de Jong and Lee, 2008; Shi and Lee, 2017; Jeong and Lee, 2020; Han et al., 2021). Our approach of combining finite distributed lag and spatial dynamic panel data models has not been previously applied to simultaneously model the mortality process and spread of diseases.

Because both components are linear,[10] their coefficients have straightforward marginal interpretations. Linearity also allows us to tractably aggregate the mortality impacts of an additional case, including effects from subsequently propagated cases, when constructing the MCFR. Together, the spatial dynamic panel data and finite distributed-lag components capture (i) the dynamic evolution of infections and deaths and (ii) the externalities created by cross-county spread—two features that compartmental models rarely handle explicitly, if at all.

Our framework differs from compartmental models because it does not explicitly model the resistant population (i.e., the recovered and/or vaccinated population), but this approach is reasonable early in a pandemic (Bertozzi et al., 2020), when the resistant population is small and vaccination is not yet widespread (Wu and McGoogan, 2020). Our analysis focuses on 2020, when both of these conditions hold (Atkeson, Kopecky and Zha, 2024).

[10] While nonlinear models also accommodate marginal effects, they typically require additional steps or assumptions to derive and interpret the marginal effects. Given our focus on explaining the incremental impact of each new case, a linear specification highlights this idea more transparently. More detailed discussions of this issue can be found in Appendices A.1 and D.1.3.

2.1.1 Mortality

Our first equation describes the determinants of mortality, $m_{i,t} = \ln(\text{mortality}_{i,t})$, where $\text{mortality}_{i,t}$ is the number of deaths plus one in county $i = 1, \cdots, n$, in week $t = 1, \cdots, T$.[11] We begin by focusing on mortality from the focal infectious disease but later apply the model to mortality from other causes. Formally,

$$m_{i,t} = \sum_{l=1}^{L} \theta_l h_{i,t-1} + \kappa z_i \sum_{l=1}^{L} h_{i,t-1} + \mathbf{x}_{i,t}^{M} \boldsymbol{\beta}^{M} + \zeta_i^{M} + \tau_t^{M} + e_{i,t}^{M}. \tag{1}$$

Mortality naturally depends on the levels of cases in the county in the previous weeks, $h_{i,t-l} = \ln(\text{case}_{i,t-l})$, where $\text{case}_{i,t-l}$ is the count of new confirmed cases plus one in county i in week $t - l$.[12] We allow for a fully flexible time relationship between mortality and lagged cases, as reflected by the parameters θ_l, and for cases to affect mortality over the time horizon of L weeks. The choice of L should be informed by the mortality process of the focal infectious disease (i.e., the recovery period),[13] which has important implications on the estimation, as described in detail in Section 2.1.3.

County heterogeneity. To provide flexibility and tractability in accounting for differences across counties, we allow county-level heterogeneity to affect mortality through three channels. First, we include time-invariant county characteristics, z_i, that may interact with cases to affect mortality. In our empirical application z_i is the prevalence of diabetes in county i.[14] Second, we include a range of time-varying county characteristics, $\mathbf{x}_{i,t}^{M} = \left(x_{i,t,1}^{M}, \cdots, x_{i,t,K_M}^{M}\right)$, that affect mortality. In our application, we include in $\mathbf{x}_{i,t}^{M}$ weather conditions (temperature and humidity) and the share of occupied inpatient beds to capture medical shortages. Third, we include county fixed effects, ζ_i^{M}, which account for all time-invariant differences across counties, and additionally, calendar week fixed effects, τ_t^{M}. The statistical error is $e_{i,t}^{M}$.

Of central interest is the direct effect of cases, $h_{i,t-l}$, on mortality, $m_{i,t}$ which captures mortality conditional on being infected and excludes downstream mortality caused by disease propagation, as discussed below.

[11] To ensure that $m_{i,t}$, is well defined even when there are no deaths, we add 1 to the count of mortality. We use the same transformation for confirmed cases. To justify this transformation, we focus on the 369 largest counties, in which there are few zeros, and conduct a sensitivity analysis for the transformation to evaluate the robustness of our specification (see Appendix D.1.3). Overall, the estimated coefficients remain stable as the transformation constant changes. Essentially, most of our identification comes from variation along the intensive margin with few zeros in the aggregated data, reducing variations along the extensive margin. Similarly, state-level lockdown/reopening policies effectively relate to counties already experiencing a significant number of positive cases rather than those transitioning from zero to positive cases or *vice versa*. For the relevant discussions, refer to Chen and Roth (2024).

[12] We use the log-log specification generating a linear-in-logs relationship between cases and mortality. Equation (1) can be written in Cobb-Douglas form as:

$$\text{mortality}_{i,t} = \prod_{l=1}^{L} \text{case}_{i,t-l}^{\overline{\theta}_{i,l}} \cdot \prod_{k=1}^{K_M} \left(X_{i,t,k}^{M}\right)^{\beta_k^{M}} \cdot \exp(\zeta_i^{M}) \cdot \exp(\tau_t^{M}) \cdot \exp(e_{i,t}^{M}),$$

where $X_{i,t,k}^{M} = \exp(x_{i,t,k}^{M})$. Comparable specifications can be found in Auster, Leveson and Sarachek (1969) and Ruhm (2015).

[13] The number of lags, L represents the termination of the biological process of infection. A person infected in week t would at the end of week $t + L$ either die or recover, so the recovery period refers to the time in which a person is still at risk of mortality.

[14] We use pre-pandemic characteristics to avoid simultaneity. County characteristics that might be used include demographics (e.g., the age distribution of the population), the prevalence of other pre-existing health conditions (e.g., asthma), and environmental factors (e.g., air pollution). To avoid multicollinearity, we include a single characteristic in z_i, the pre-pandemic prevalence of diabetes based on model fit (the likelihood) and its statistical significance in explaining COVID-19 mortality (see Section 3).

The direct mortality effect is given by:

$$\overline{\theta}_{i,l} = \theta_l + \kappa z_i.$$

$\overline{\theta}_{i,l}$ gives the impact of a 1 percent change in county i's cases on log mortality in county i at time $t+l$. κ captures county-level heterogeneity in the effect of cases on mortality related to time-invariant, pre-existing county characteristics z_i. Equation (1) can be modified to accommodate other functional forms and to include other regressors depending on the characteristics of the disease being studied.

Other outcomes. Equation (1) is sufficiently general to allow researchers to study the effects of cases on outcomes other than mortality from the focal infectious disease by replacing the left-hand-side variable, $m_{i,t}$ with another outcome of interest. For example, we also consider the effect of cases on non-COVID mortality (e.g., through delayed or foregone medical treatments from non-COVID diseases), as well as mortality (from COVID or other conditions) among different demographic and socioeconomic groups. As discussed below, the coefficient estimates can then be used to generate an equivalent MCFR for these outcomes. A researcher with access to the appropriate data could also consider other outcomes such as (quality-adjusted) life years lost or disability-adjusted life years lost.

2.1.2 Disease transmission

To model the geo-social transmission of cases, we use a spatial dynamic panel data model (Yu, de Jong and Lee, 2008; Shi and Lee, 2017; Jeong and Lee, 2020).[15] We assume that the number of new cases in county i at time t, $h_{i,t}$, depends on the number of cases in the previous period in that county, $h_{i,t-1}$, and the weighted average of cases in other counties, $\sum_{j=1,j\neq i}^{n} w_{ij}h_{j,t-1}$, where w_{ij} captures the weight that county i places on county j:

$$h_{i,t} = a_1 h_{i,t-1} + a_2 \sum_{j=1,j\neq i}^{n} w_{ij}h_{j,t-1} + \mathbf{x}_{i,t}^{H}\boldsymbol{\beta}^{H} + \zeta_i^{H} + \tau_t^{H} + e_{i,t}^{H}. \tag{2}$$

Our primary interest in equation (2) is to estimate coefficients a_1 and a_2, which give the marginal effects of previous cases in the same and other counties, respectively, on cases in focal county i. Since the weights on other counties $(w_{i1}, \cdots, w_{in})$ can be regarded as a characteristic of county i, they also describe regional heterogeneity. As detailed below, in our main specification, w_{ij} is constructed using population flows between counties as measured by location data from mobile phones. Section 5.2 reports estimates from alternative specifications of w_{ij}.

In addition to lags of cases, the transmission equation, like the mortality equation, includes county characteristics $\mathbf{x}_{i,t}^{H} = \left(x_{i,t,1}^{H}, \cdots, x_{i,t,K_H}^{H}\right)$ with corresponding parameters $\boldsymbol{\beta}^{H} = \left(\beta_1^{H}, \cdots, \beta_{k_H}^{H}\right)'$. In our application, we include in $\mathbf{x}_{i,t}^{H}$ all the variables in $\mathbf{x}_{i,t}^{M}$ and additionally, a measure of the intensity of lockdown policies. Lastly, we include county and week fixed effects, ζ_i^{H} and τ_t^{H}, and errors, $e_{i,t}^{H}$.

[15] Qiu, Chen and Shi (2020), Han et al. (2021), and Jeong, Lin and Weinberg (2023) model the geographic transmission of COVID-19 with spatial panel data models.

2.1.3 Estimation

The main parameters of interest are $\theta_1, \cdots, \theta_L, \kappa, a_1, a_2$, and the coefficient on lockdowns in $\boldsymbol{\beta}^H$, which we estimate using maximum likelihood. This method has two advantages. First, it provides a rigorous foundation to select the appropriate model (e.g., lag length L and proper spatial weighting matrices) based on well-established statistical criteria. Second, this approach allows us to employ control functions in our framework to address endogeneity in the transmission equation. We use standard errors generated from our quasi-maximum likelihood estimation method. Appendix A.5 details our methods for obtaining standard errors for the MCFR.

Equation (1). The main objects of interest in equation (1) are the coefficients on lagged cases (i.e., $\{h_{i,t-1}, \cdots, h_{i,t-L}, z_i \sum_{l=1}^{L} h_{i,t-1}\}$).[16] The model is identified from cross-sectional and temporal variations in lagged cases, conditional on $\mathbf{x}_{i,t}^M$, ζ_i^M, and τ_t^M. Choosing an appropriate L is essential for avoiding omitted variable bias (L must be sufficiently large) and multicollinearity between lagged cases (L should be parsimonious).

In our empirical application, we select $L = 5$ based on two considerations. First, existing medical research indicates that most deaths from COVID-19 occur within 5 to 6 weeks of infection (Barmen et al., 2020; SeyedAlinaghi et al., 2021; Tsegaye et al., 2022). Second, our choice can be empirically justified by Hannan and Quinn's (1979) information criterion, which compares likelihoods for various lags (explored in Appendix D.1.1)[17] and examining how the estimates vary and checking their statistical significance with different prespecified L (explored in Section 5).

Equation (2). The same strategy for identifying the coefficients on lagged cases (i.e., $\{h_{i,t-1}, \sum_{j=1,j\neq i}^{n} w_{ij} h_{j,t-1}\}$) applies in equation (2). However, identifying the effect of state-level lockdown policies, $\text{LRO}_{i,t-2}$, is more complicated because policies are decisions made by state policymakers and are unlikely to be randomly assigned. For instance, the error term $e_{i,t}^H$ in equation (2) may be correlated with $\text{LRO}_{i,t-2}$ if states expecting high transmission levels impose stricter lockdowns.

We use a control function approach in equation (2) to address this endogeneity issue. The main idea of the control function is to decompose the original error $e_{i,t}^H$ into two parts: (i) a part potentially correlated with $\text{LRO}_{i,t-2}$ and (ii) an uncorrelated part (purged errors). To implement this approach, we use two types of exogenous variation. The first comes from earlier levels of cases, COVID-19 mortality, and economic conditions not included in equation (2). This is based on the empirically-supported idea that: (i) state lockdown policies are responsive to realized COVID-19 mortality and case counts (see Section 4.5) and (ii) policymakers may also consider contemporaneous economic circumstances in deciding whether to impose a lockdown. The second type of exogenous variation is pre-pandemic demographic and political characteristics of counties that are correlated

[16] To allow for county-level heterogeneity as captured by κ, we include z_i, which has rich county-level variation. We allow the effects of z_i to interact with the sum, $\sum_{l=1}^{L} h_{i,t-1}$. Doing so (rather than estimating a separate value of κ for each lag, $\{h_{i,t-1}, \cdots, h_{i,t-L}\}$) reduces multicollinearity.

[17] We rely on Hannan and Quinn's (1979) information criterion because it selects the correct number of lags with probability one (i.e., is consistent). By comparing the likelihoods of models with varying lags, this criterion helps ensure that we neither underestimate L (excluding relevant weeks of the infection-to-mortality process) nor overestimate it (unnecessarily adding noise and complexity).

with lockdown policies, providing additional cross-sectional variation.[18]

To validate the assumptions behind this approach, we empirically verify the absence of serial correlation in the model's purged errors in Equation (2), which suggests that purged errors can be viewed as independently generated shocks across weeks. This implies that the error term at time t is unrelated to the lagged variables (e.g., cases, medical shortages) and that the parameters in equation (2) are identified. Further details are provided in Appendix A.2.

2.2 MCFR formula

2.2.1 Mortality within originating county

We begin by focusing on mortality from the focal infectious disease in the county in which the marginal case originates. We define the marginal case fatality rate in the origin county, $\text{MCFR}_{(i,t)\to(i,\Sigma L^*)}$, as the impact of a new case in county i in week t on subsequent mortality in the same county in weeks $t+1$ through $t+L^*$. The subscript in $\text{MCFR}_{(i,t)\to(i,\Sigma L^*)}$ describes the location and time of the focal case (i.e., origin county i in week t as denoted by the pair (i,t)) and the location and time of the resulting mortality (i.e., destination county i in weeks $t+1$ through $t+L^*$ as denoted by the pair $(i,\Sigma L^*)$). Appendix A.3 details our notation conventions.[19]

The $\text{MCFR}_{(i,t)\to(i,\Sigma L^*)}$ is the sum of two components – mortality of the person with the focal case, which we refer to as the direct channel and denote as $\text{MCFR}_{(i,t)\to(i,\Sigma L^*)^{\text{Direct}}}$, and mortality among people who are infected with subsequent cases propagated from the focal case, which we refer to as the propagation channel and denote as $\text{MCFR}_{(i,t)\to(i,\Sigma L^*)^{\text{Prop}}}$.

Because the MCFR quantifies the marginal effect of cases on mortality, the only parameters that enter it are the coefficients on cases (e.g., $\theta_1,\cdots,\theta_L$, κ, a_1, and a_2). The $\text{MCFR}^{\text{Direct}}_{(i,t)\to(i,\Sigma L^*)}$ uses the estimated parameters (e.g., $\theta_1,\cdots,\theta_L$, and κ) and county-specific characteristics (i.e., z_i) from equation (1). The $\text{MCFR}^{\text{Prop}}_{(i,t)\to(i,\Sigma L^*)}$, which incorporates case transmission, depends on the same parameters and z_i as well as those (i.e., a_1, a_2, and w_{ij}) from equation (2). Note that the MCFR is expressed in levels, while the relation-

[18] Note that $\text{LRO}_{i,t-2}$ varies by state, while this second-type varies by county, which enriches the cross-sectional variation in the control function.

[19] Briefly, since our model specification is based on spatial econometric models, each outcome (e.g., cases and mortality) has its own geographic location and time. Then, our MCFR measures represent how a case from origin pair (i,t) transitions to mortality for destination pair $(j,t+l)$ for $j=1,\cdots,n$, and $l=1,2,\cdots,L^*$. Thus, we want to highlight (i) the origin pair and (ii) the destination pair. The targeting unit j can be the same county ($j=i$), or not ($j\neq i$).

ships between cases and mortality in equations (1) and (2) are in logs. Formally,

$$\begin{aligned}\text{MCFR}_{(i,t)\mapsto(i,\Sigma L^*)} &= \sum_{l=1}^{L^*} \text{MCFR}_{(i,t)\mapsto(i,t+l)} \\ &= \sum_{l=1}^{L^*} \frac{d(\text{mortality}_{i,t+l})}{d(\text{case}_{i,t})} = \sum_{l=1}^{L^*} \frac{dm_{i,t+l}}{dh_{i,t}} \cdot \frac{\text{mortality}_{i,t+l}}{\text{case}_{i,t}} \\ &= \sum_{l=1}^{L^*} \left(\underbrace{\frac{\partial m_{i,t+l}}{\partial h_{i,t}}}_{\text{Direct channel}} + \underbrace{\sum_{p=1}^{l-1} \frac{\partial m_{i,t+l}}{\partial h_{i,t+p}} \frac{\partial h_{i,t+p}}{\partial h_{i,t+p-1}} \cdots \frac{\partial h_{i,t+1}}{\partial h_{i,t}}}_{\text{Propagation channel}} \right) \cdot \frac{\text{mortality}_{i,t+l}}{\text{case}_{i,t}}.\end{aligned} \tag{3}$$

Here, $\text{MCFR}_{(i,t)\to(i,\Sigma L^*)}$ is the increase in mortality in week $t+l$ from an additional case in week t.

For each lag l, equation (3) decomposes the $\text{MCFR}_{(i,t)\to(i,\Sigma L^*)}$ into the direct channel and the propagation channel by decomposing the elasticity $\frac{dm_{i,t+l}}{dh_{i,t}}$. The direct channel describes mortality conditional on being infected, so it is our counterpart to the CFR, although (as detailed in the next section) our approach differs from the conventional one in that we estimate the direct MCFR using a regression framework. The propagation channel describes mortality from newly transmitted cases; it is one of the primary innovations of our approach as it combines case fatality with case transmission. Specifically,

1) **Direct channel**, $\text{MCFR}^{\text{Direct}}_{(i,t)\mapsto(i,t+l)}$:
This channel captures the direct effect of $\text{case}_{i,t}$ on $\text{mortality}_{i,t+l}$ and it is evaluated as:

$$\text{MCFR}^{\text{Direct}}_{(i,t)\mapsto(i,t+l)} = \frac{\partial m_{i,t+l}}{\partial h_{i,t}} \cdot \frac{\text{mortality}_{i,t+l}}{\text{case}_{i,t}} = \overline{\theta}_{i,l} \cdot \frac{\text{mortality}_{i,t+l}}{\text{case}_{i,t}} \text{ for } l = 1, \cdots, L.$$

Note that $\text{MCFR}^{\text{Direct}}_{(i,t)\mapsto(i,t+l)}$ is zero for $l > L$ because all the people originally infected in week t are assumed to have either recovered or died by week $t+L$.

2) **Propagation channel**, $\text{MCFR}^{\text{Prop}}_{(i,t)\mapsto(i,t+l)}$:
This channel captures mortality in county i resulting from newly transmitted cases, which can propagate (i) within the originating county i and (ii) across county borders before returning to county i. A notable feature of $\text{MCFR}^{\text{Prop}}_{(i,t)\mapsto(i,t+l)}$ is the persistence of the propagation channel even beyond L, because cases at time t continue to propagate indefinitely. These additional new cases subsequently cause mortality. Formally,

$$\begin{aligned}\text{MCFR}^{\text{Prop}}_{(i,t)\mapsto(i,t+l)} &= \left(\sum_{p=1}^{l-1} \frac{\partial m_{i,t+l}}{\partial h_{i,t+p}} \frac{\partial h_{i,t+p}}{\partial h_{i,t+p-1}} \cdots \frac{\partial h_{i,t+1}}{\partial h_{i,t}} \right) \cdot \frac{\text{mortality}_{i,t+l}}{\text{case}_{i,t}} \\ &= \left(\sum_{p=1}^{l-1} \overline{\theta}_{i,l-p} \cdot [\mathbf{A}^p]_{ii} \right) \cdot \frac{\text{mortality}_{i,t+l}}{\text{case}_{i,t}} \text{ for } l = 2, \cdots, L^*.\end{aligned}$$

The matrix $\mathbf{A} = a_1\mathbf{I} + a_2\mathbf{W}$ in equation (2) governs the transmission of cases where $\mathbf{W} = [w_{ij}]$ denotes the spatial weighting matrix.[20] Note that $\text{MCFR}^{\text{Prop}}_{(i,t)\mapsto(i,t+l)}$ is zero at $l = 1$ because, by construction, a case requires at least one week to propagate and another to result in mortality. To illustrate the propagation channel, consider mortality in week $t+3$ generated by a case in week t. First, there are two sequences of within-county transmission: (i) $\text{case}_{i,t} \rightarrow \text{case}_{i,t+1} \rightarrow \text{case}_{i,t+2} \rightarrow \text{mortality}_{i,t+3}$ and (ii) $\text{case}_{i,t} \rightarrow \text{case}_{i,t+1} \rightarrow \text{mortality}_{i,t+3}$. These sequences can be represented by $a^2\overline{\theta}_{i,1} \cdot \frac{\text{mortality}_{i,t+3}}{\text{case}_{i,t}}$ and $a_1\overline{\theta}_{i,2} \cdot \frac{\text{mortality}_{i,t+3}}{\text{case}_{i,t}}$, respectively. Second, there is a "bring-home effect" represented by the sequence, $\text{case}_{i,t} \rightarrow \text{case}_{j,t+1} \rightarrow \text{case}_{i,t+2} \rightarrow \text{mortality}_{i,t+3}$ for some $j \neq i$, which can be formulated as $a_2^2 \sum_{j\neq i} w_{ij}w_{ji} \cdot \overline{\theta}_{i,1} \cdot \frac{\text{mortality}_{i,t+3}}{\text{case}_{i,t}}$. Hence, $\text{MCFR}^{\text{Prop}}_{(i,t)\mapsto(i,t+3)} = \left(a_1^2\overline{\theta}_{i,1} + a_1\overline{\theta}_{i,2} + a_2^2\sum_{j\neq i} w_{ij}w_{ji} \cdot \overline{\theta}_{i,1}\right) \cdot \frac{\text{mortality}_{i,t+3}}{\text{case}_{i,t}}$.

To summarize, $\text{MCFR}_{(i,t)\mapsto(i,\Sigma L^*)} \equiv \text{MCFR}^{\text{Direct}}_{(i,t)\mapsto(i,\Sigma L^*)} + \text{MCFR}^{\text{Prop}}_{(i,t)\mapsto(i,\Sigma L^*)}$ with $\text{MCFR}^{\text{Direct}}_{(i,t)\mapsto(i,\Sigma L^*)} \equiv \sum_{l=1}^{L} \text{MCFR}^{\text{Direct}}_{(i,t)\mapsto(i,t+l)}$ and $\text{MCFR}^{\text{Prop}}_{(i,t)\mapsto(i,\Sigma L^*)} \equiv \sum_{l=1}^{L} \text{MCFR}^{\text{Prop}}_{(i,t)\mapsto(i,t+l)}$. A detailed derivation of the MCFR is in Appendix A.4.

Note that the elasticity $\frac{dm_{i,t+l}}{dh_{i,t}}$ does not incorporate incidental components (e.g., covariates, county-level fixed effects, etc.), which, while useful in improving fit when estimating the coefficients of cases in equations (1) and (2), imply that there are parts of the cases transmission and mortality that are explained by the incidental components such as the fixed effects that are not included in the MCFR.

Given that our model employs a log-log specification, the elasticities are time-invariant. Therefore, all time variation in $\text{MCFR}_{(i,t)\mapsto(i,\Sigma L^*)}$ is due to the ratios $\frac{\text{mortality}_{i,t+l}}{\text{case}_{i,t}}$ for $l = 1, \cdots, L^*$. Moreover, a reasonable choice of L^* would encompass total downstream mortality including that from cases propagating from $\text{case}_{i,t}$. If cases propagate (i.e., $a_1 > 0$ and/or $a_2 > 0$), then the expectation is that $L^* > L$.[21]

The decomposition of the MCFR is valuable because it offers two distinct takeaways. First, it underscores a unique feature of the MCFR, which is that it combines the mortality rate of an infection and the transmission rate, producing a single, policy-ready measure of the total effect on mortality from one additional case. In contrast, while the CFR and the basic reproduction number, $\mathcal{R}_0$, are valuable, it is not clear how they interact or how they should be combined for policy purposes.

Second, the distinction between direct and propagation channels enables policymakers to target different facets of a disease. For instance, a disease with a high $\text{MCFR}^{\text{Direct}}_{(i,t)\mapsto(i,\Sigma L^*)}$ but a relatively low $\text{MCFR}^{\text{Prop}}_{(i,t)\mapsto(i,\Sigma L^*)}$ might best be addressed by investments in treating infected individuals. On the other hand, if the $\text{MCFR}^{\text{Prop}}_{(i,t)\mapsto(i,\Sigma L^*)}$ is high or spikes, that might prompt policymakers to consider interventions to limit disease spread.

[20] In evaluating $\text{MCFR}^{\text{Prop}}_{(i,t)\mapsto(i,t+l)}$, we use the diagonal elements of the matrix $\mathbf{A}^p$ for $p = 1, \cdots, l-1$ which capture the transmission sequences that result in cases in week $t+p$ in the origin county.

[21] Estimates for distant weeks are a product of future mortality levels, either realized or predicted. As L^* increases, we must rely more heavily on predictions generated by iterating on the prediction model, which introduces noise. We set $L^* = 16$ to reduce noise and provide robustness checks where $L^* = 52$ in the appendix. Additionally, given that we estimate a stable transmission process, the full effect of a case on mortality can be approximated with a finite value of L^*. Note that L^* should not be confused with L in equation (1), which represents the endpoint of the biological process of mortality conditional on infection.

2.2.2 Mortality across counties

Next, we turn to case transmission across borders and evaluate the effect of a focal case beyond the county in which it originates. The model's MCFR estimates are naturally represented in a $(n \times n \times T \times L^*)$ tensor, which describes the impact of a marginal case in each of the n origin counties at calendar time t on mortality in each of the n destination counties l weeks after the focal case occurred.[22] We consider three levels of geographic aggregation for the destination counties and introduce notation to denote each:

1) **Origin county**, $\text{MCFR}_{(i,t)\mapsto(i,\Sigma L^*)}$: The county in which the focal case originates.

2) **Same state**, $\text{MCFR}_{(i,t)\mapsto(\mathcal{S}_{s(i)},\Sigma L^*)}$: Counties in our sample in the same state as the origin county. That is, counties $j \in \mathcal{S}_{s(i)}$ where $\mathcal{S}_{s(i)}$ is the set of counties in state $s(i)$, where $s(i)$ is the state that includes county i.[23] This is constructed as $\text{MCFR}_{(i,t)\to(\mathcal{S}_{s(i)},\Sigma L^*)} \equiv \sum_{l=1}^{L^*}\sum_{j\in\mathcal{S}_{s(i)}} \frac{d(\text{mortality}_{j,t+l})}{d(\text{case}_{i,t})}$. Note that $\text{MCFR}_{(i,t)\to(\mathcal{S}_{s(i)},\Sigma L^*)}$ includes $\text{MCFR}_{(i,t)\to(i,\Sigma L^*)}$.

3) **National level**, $\text{MCFR}_{(i,t)\mapsto(\mathcal{N},\Sigma L^*)}$: All counties in the sample. This is constructed as $\text{MCFR}_{(i,t)\to(\mathcal{N},\Sigma L^*)} \equiv \sum_{l=1}^{L^*}\sum_{j=1}^{n} \frac{d(\text{mortality}_{j,t+l})}{d(\text{case}_{i,t})}$, where $\mathcal{N}$ denotes the set of all the counties in the sample. Note that $\text{MCFR}_{(i,t)\to(\mathcal{N},\Sigma L^*)}$ includes $\text{MCFR}_{(i,t)\to(\mathcal{S}_{s(i)},\Sigma L^*)}$.

Note that, as before, the subscripts in $\text{MCFR}_{(*)\to(*)}$ describe the origin of a marginal case and the destination of the resulting mortality. Similiarly, the notation ΣL^* refers to the summation from weeks $t+1$ through $t+L^*$.

Since $\text{MCFR}_{(i,t)\to(\mathcal{S}_{s(i)},\Sigma L^*)}$ and $\text{MCFR}_{(i,t)\to(\mathcal{N},\Sigma L^*)}$ are calculated based on the elasticities $\frac{dm_{j,t+l}}{dh_{i,t}}$ and the ratios $\frac{\text{mortality}_{j,t+l}}{\text{case}_{i,t}}$ for different $j = 1, \cdots, n$ and $l = 1, \cdots, L^*$, their derivations are analogous to that of $\text{MCFR}_{(i,t)\to(i,\Sigma L^*)}$ and are detailed in Appendix A.4.[24]

In short, $\text{MCFR}_{(i,t)\to(\mathcal{S}_{s(i)},\Sigma L^*)}$ and $\text{MCFR}_{(i,t)\to(\mathcal{N},\Sigma L^*)}$ reflect spillovers from a focal case in county i to other parts of the country. They also highlight the different geographical units relevant for disease control policy. For instance, a state, represented by s, might prioritize mortality occuring within its border, (i.e., $\text{MCFR}_{(i,t)\to(\mathcal{S}_s,\Sigma L^*)}$) and focus less on the national $\text{MCFR}_{(i,t)\to(\mathcal{N},\Sigma L^*)}$. In contrast, the key indicator for the federal government would likely be the national $\text{MCFR}_{(i,t)\to(\mathcal{N},\Sigma L^*)}$. Moreover, this framework is sufficiently general to decompose the MCFR based on other geographical aggregations, such as metropolitan statistical areas or Census divisions.

[22] T refers to the total number of calendar weeks. The impact of an additional case in county i at calendar time t on mortality in county j at calendar time $t+l$ would have indices (j,i,t,l) in the tensor of derivatives.

[23] A related notation is $\mathcal{S}_s$ which refers to all counties in state s, which could but need not be a function of any county i.

[24] As an example, $\text{MCFR}_{(i,t)\to(\mathcal{S}_{s(i)},t+l)}$ is constructed as $\sum_{j\in\mathcal{S}_{s(i)}} \frac{d(\text{mortality}_{j,t+l})}{d(\text{case}_{i,t})} = \sum_{j\in\mathcal{S}_{s(i)}} \frac{dm_{j,t+l}}{dh_{i,t}} \cdot \frac{\text{mortality}_{j,t+l}}{\text{case}_{i,t}} = \sum_{j\in\mathcal{S}_{s(i)}} \left(\overline{\theta}_{j,l} + \sum_{p=1}^{l-1} \overline{\theta}_{j,l-p} \cdot [\mathbf{A}^p]_{ji}\right) \cdot \frac{\text{mortality}_{j,t+l}}{\text{case}_{i,t}}$. Here, we take the elements of column i in $\mathbf{A}^p$ corresponding to counties in $\mathcal{S}_{s(i)}$ (rows j), which capture the sequence of transmission that results in cases in week $t+p$ in the state of county i. Note also that the resulting $\text{MCFR}_{(i,t)\to(\mathcal{S}_{s(i)},t+l)}$ is an element of the $n \times T \times L^*$ tensor which describes the impact of a case in each of the n origin counties in week t on mortality in week $t+l$ in counties within the same state as the origin county (forcusing on the state of origin means that the destination dimension of the tensor is eliminated, leading to a 3-dimensional tensor).

2.2.3 Other causes of mortality and all-cause mortality

We can similarly evaluate the increase in mortality from causes other than the focal infectious disease from a marginal case. We refer to this as the OCMCFR or "other-cause" marginal case fatality rate. We re-estimate equation (1) and replace the dependent variable, $m_{i,t}$, in our application with non-COVID mortality in county i in week t. We then calculate the OCMCFR using the new parameters $\theta_l^{\text{othercause}}$ for non-COVID mortality from equation (1), and the same parameters on case transmission from equation (2).

Consistent with our previous notation, we define $\text{OCMCFR}_{(i,t)\to(i,\Sigma L^*)}$ as the effect of a case in county i in week t on non-COVID mortality in the same county in weeks $t+1$ through $t+L^*$; $\text{OCMCFR}_{(i,t)\to(\mathcal{S}_{s(i)},\Sigma L^*)}$ and $\text{OCMCFR}_{(i,t)\to(\mathcal{N},\Sigma L^*)}$ are defined analogously. We can then add up the MCFR and the OCMCFR to arrive at an all-cause marginal case mortality rate, the ACMCFR following the same logic. Formally,

$$\text{ACMCFR}_{(i,t)\mapsto(\mathcal{N},\Sigma L^*)} = \text{MCFR}_{(i,t)\mapsto(\mathcal{N},\Sigma L^*)} + \text{OCMCFR}_{(i,t)\mapsto(\mathcal{N},\Sigma L^*)}.$$

2.2.4 Mortality by subgroups

We can also consider differences in the mortality impact of a case across different demographic and socioeconomic groups. In our application, we re-estimate equation (1) and replace the dependent variable, $m_{i,t}$, with all-cause mortality for specific groups (by age, rate and ethnicity, sex, and education). We then calculate the effect of a case on all-cause mortality in group g in county i, $\text{ACMCFR}_{g,(i,t)\to(i,\Sigma L^*)}$ using the parameters $\theta_{g,l}$ for each group from the re-estimated equation (1) and the same parameters on case transmission from equation (2). Because counties differ in their demographic and socioeconomic composition, we normalize the $\text{ACMCFR}_{g,(i,t)\to(i,\Sigma L^*)}$ by the population size of that group, $\text{pop}_{g,i}$ to make the estimates comparable across groups:

$$\text{ACMCFRpop}_{g,(i,t)\mapsto(i,\Sigma L^*)} = \text{ACMCFR}_{g,(i,t)\mapsto(i,\Sigma L^*)} \times \frac{1}{\text{pop}_{g,i}} \times 100,000.$$

$\text{ACMCFRpop}_{g,(i,t)\to(i,\Sigma L^*)}$ is interpreted as the effect of one additional COVID-19 case in county i in week t on all-cause mortality in group g in the same county per 100,000 population of the group.

2.3 Conceptual relation to existing epidemiology framework

We propose the MCFR as a way to comprehensively characterize the forward-looking mortality effects of an infectious disease in a single statistic. While this concept is new, it has clear connections to well-established epidemiology frameworks and measures. This section lays out the relationship between our MCFR measure and common epidemiological measures.

Fatality rates. A commonly used epidemiological measure is the case fatality rate, CFR.[25] It is frequently calculated using counts of mortality and cases within the same area, so here we focus on measures within a focal county. The CFR in county i in week t, $\text{CFR}_{i,t}$, is defined as the ratio of cumulative mortality to cumulative

[25] See Taubenberger and Morens (2006) and Heymann (2015) for examples of the application of the CFR to other infectious diseases.

cases up to week t. Formally,

$$\text{CFR}_{i,t} = \frac{\sum_{\tau=1}^{t} \text{mortality}_{i,\tau}}{\sum_{\tau=1}^{t} \text{case}_{i,\tau}}.$$

The MCFR has a few advantages over the CFR. First, the MCFR is arguably a more policy-relevant measure as it captures the mortality that can be avoided from reducing an additional case. In contrast, the CFR is an average measure, which is useful for expressing the severity of an infectious disease, but does not directly relate to the impact of a policy on mortality.

Second, the MCFR framework incorporates both the mortality and transmission aspects of an infectious disease, and can be readily adapted to study differences across groups (e.g., $\text{ACMCFR}_{g,(i,t)\to(i,\Sigma L^*)}$) and various externalities from an additional case (e.g., OCMCFR) that are relevant to policy decisions. In contrast, the CFR is usually evaluated for one geographical area and does not incorporate spillovers to mortality from other causes. Conceptually, it is closest to the $\text{MCFR}^{\text{Direct}}_{(i,t)\to(i,\Sigma L^*)}$ which measures mortality from the focal infectious disease within the geographical area of interest, conditional on being infected.

Third, the MCFR is better at capturing temporal variation in the mortality rate of an infectious disease and is forward-looking. The MCFR is evaluated using values of cases and mortality in week t through $t + L^*$. In contrast, the CFR incorporates all past values up to week t, so it is less responsive to current values and tends to stabilize over time. This forward-looking property of the MCFR makes it less vulnerable to large numbers of latent infections from the early pandemic. That is, in the case of COVID-19, there were many unmeasured infections early in the pandemic, causing the CFR to permanently overestimate the death probability conditional on infection.[26] The CFR at time t is more indicative of the entire history of the disease, so when comparing the two measures it is appropriate to compare the *average* $\text{MCFR}^{\text{Direct}}_{(i,t)\to(i,\Sigma L^*)}$ over a period to the CFR at the *end* of the period. Asymptotically, the CFR represents the endemic equilibrium rather than the comtemporary fatality rate and can be interpreted as the probability of mortality conditional on infection, simliar to the interpretation of the $\text{MCFR}^{\text{Direct}}_{(i,t)\to(i,\Sigma L^*)}$. Hence, $\text{MCFR}^{\text{Direct}}_{(i,t)\to(i,\Sigma L^*)} \simeq \text{CFR}_{i,t} =$ when $\text{MCFR}^{\text{Direct}}_{(i,t)\to(i,\Sigma L^*)}$ is stable over time.

We modify the CFR formula to make it more forward-looking and hence more comparable to the $\text{MCFR}^{\text{Direct}}_{(i,t)\to(i,\Sigma L^*)}$, and refer to the modified measure as the short-run CFR or SCFR. We sum up the cases and mortality over the next L weeks and calculate the ratio of the two.[27] To align with the MCFR, the sum of mortality leads to the sum of cases by one week. Formally,

$$\text{SCFR}_{i,t} = \frac{\sum_{l=1}^{L} \text{mortality}_{i,t+l}}{\sum_{l=1}^{L} \text{case}_{i,t+l-1}}.$$

In Section 4.8, we jointly examine the CFR, SCFR, and $\text{MCFR}^{\text{Direct}}_{(i,t)\to(i,\Sigma L^*)}$, and show that they are empirically comparable across time and counties.

[26] Intuitively, the denominator of the CFR (cumulative cases) is understated, while the numerator (cumulative COVID-19 mortality) is well measured (Atkeson, Kopecky and Zha, 2024).

[27] Note that because the direct channel ends at $L + 1$, we sum over L weeks instead of L^* weeks when calculating SCFR.

Disease transmission. A corresponding epidemiological measure for transmissibility that aligns with our framework is the effective reproduction number $\mathcal{R}_t$, which represents the average number of secondary cases generated by one infected individual under the population conditions at time t. As a time varying measure, $\mathcal{R}_t$ extends the conventional reproduction number ($\mathcal{R}_0$), which evaluates the average number of secondary cases from an initial infection. These transmissibility measures are typically derived from parameters of mathematical compartment models such as the Susceptible-Infectious-Recovered (SIR) model. Because there are numerous ways of forming compartment models, $\mathcal{R}_t$ (or $\mathcal{R}_0$) is inherently model-specific.

We can also derive an analogous measure of transmissibility in the MCFR framework through the marginal effect $\frac{\partial \text{case}_{j,t+1}}{\partial \text{case}_{i,t}} = [\mathbf{A}]_{ij} \cdot \frac{\text{case}_{j,t+1}}{\text{case}_{i,t}}$, which is a key element of the MCFR (in particular, its components that incorporate case propagation, such as $\text{MCFR}^{\text{Prop}}_{(i,t)\to(i,t+1)}$). The diagonal elements ($\frac{\partial \text{case}_{i,t+1}}{\partial \text{case}_{i,t}}$) represent the number of new cases in county i in week $t+1$ generated from an additional case in that same county in week t, while the off-diagonal elements (i.e., $\frac{\partial \text{case}_{j,t+1}}{\partial \text{case}_{i,t}}$ for $j \neq i$) capture geospatial transmission of a focal case to other counties in week $t+1$.

While our transmissibility measure and $\mathcal{R}_t$ have the same objective – characterizing the transmission of an infectious disease – a few key distinctions arise from the difference between our modeling strategy and that of a compartmental model. First, we model transmission by estimating the relationship between the flow of (new) cases at time t and time $t+1$, and show that $h_{j,t-1}$ ($j = 1, \cdots, n$) is a sufficient statistic to describe disease spread. We also do not explicitly model the infection period. In contrast, compartmental models attempt to imitate the biological process of disease transmission, commonly by explicitly specifying new infections as a product of contacts between the stock of susceptibles and the currently infected individuals. An advantage of our approach is that new cases are easier to measure than the stock of infections.

Moreover, our framework is designed for evaluating marginal effects, while $\mathcal{R}_t$ is more of an average. $\frac{\partial \text{case}_{j,t+1}}{\partial \text{case}_{i,t}}$ from our model gives the number of new cases in county j generated from previous cases in county i if all other factors are held constant. The incidental components that we include in our model help address unobservable factors, like behavioral changes, and improve the model fit. However, by including incidental components, some portion of the disease transmission process is necessarily explained by these incidental components.

Consequently, our measure of transmissibility cannot be directly mapped to the $\mathcal{R}_t$ because they are different objects. In Section 4.8, we evaluate $\mathcal{R}_t$ that closely aligns with our setup (e.g., inter-county disease spread) using our estimated parameters (as outlined in Appendix C.5), and then evaluate how it relates to specific components of the MCFR.

In summary, this paper provides a tractable framework to quantify the marginal impact of an additional case on mortality, which economic logic suggests is particularly policy-relevant metric compared to averages. We propose a range of measures relevant to COVID-19, although the framework is sufficiently flexible and can be adapted to the specifics of other infectious diseases. The measures we introduce are laid out in Figure 1, which also relates them to well-established epidemiology measures. In Section 4.7, we quantitatively relate the MCFR to combinations of the CFR and $\mathcal{R}_t$ from previous studies to elucidate how our measure captures and

unifies the insights from separate, well-established epidemiological measures.

Figure 1: Summary of concepts and notations

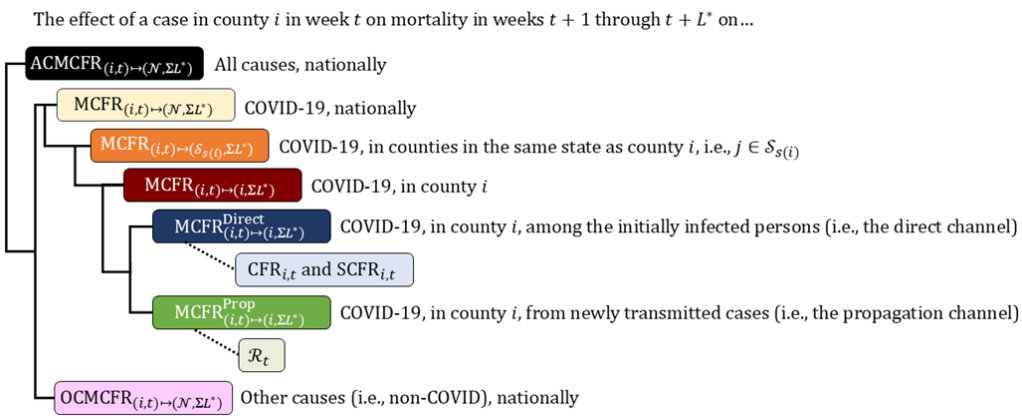

Notes: This figure summarizes the concepts and notation used in the paper. The MCFR refers to the impact of one additional case on COVID-19 deaths, while the ACMCFR and OCMCFR refer to the analogous impact on deaths from all causes and other (i.e., non-COVID) causes, respectively. The subscript (i,t) before the arrow describes the location and timing of the focal case (i.e., in county i in calendar week t). The subscript after the arrow describes the location and timing of resulting mortality. $\mathcal{S}_{s(i)}$ refers to the sum of impacts on mortality in all counties within the same state as county i. $\mathcal{N}$ refers to the sum of impacts on all counties nationally. ΣL^* refers to the sum of impacts in weeks $t+1$ through $t+L^*$. This annotation can be used to refer to concepts not included in this figure. For instance, the $\text{OCMCFR}_{(i,t)\mapsto(\mathcal{S}_{s(i)}\to\Sigma L^*)}$ is the effect of a case in county i in week t on other cause (i.e., non-COVID) mortality in the state of county i in weeks $t+1$ through $t+L^*$. The $\text{CFR}_{i,t}$ refers to the case fatality rate of county i in week t, the $\text{SCFR}_{i,t}$ to the short-term CFR, and $\mathcal{R}_t$ to the effective reproduction number.

3 Data

We use weekly panel data from $n = 369$ of the largest counties in the contiguous U.S., comprising 70% of the U.S. population. The data span from January 2020 through April 2021. This section lays out our primary variables, data, and data methods. Appendix B provides more details on how the variables are constructed.

COVID-19 cases. We retrieved data on confirmed COVID-19 cases from the website USAFacts, which compiles daily counts of cumulative cases for individual counties from state and local public health agencies (USAFacts, 2022). From these, we calculate the counts of new cases and aggregate the data to the weekly level, so that our observations are at the county-week level.

Mortality. We use individual-level mortality records from the National Center for Health Statistics. This dataset contains demographic and socioeconomic characteristics of the deceased, county of residence, month of death, and cause of death. We first collapse the data to the county-month-cause level and, depending on the specific application, we collapse the data more finely by adding a demographic or socioeconomic dimension. We consider a death to be caused by COVID-19 if COVID-19 is listed as one of the causes of death. All deaths that do not include COVID-19 among any of the causes are considered other cause (i.e., non-COVID) deaths. To obtain weekly-level data, we interpolate the monthly data using publicly available data from USAFacts and

the Centers for Disease Control and Prevention (CDC, 2022*a*,*b*,*c*). The interpolation methods are detailed in Appendix B.2 and an accompanying paper Abdulhadi and Weinberg (2025).

Covariates. We incorporate 2019 county-level data on diabetes prevalence, z_i, from the County Health Rankings and Roadmaps produced by the University of Wisconsin Population Health Institute (Population Health Institute, 2023). We normalize z_i to have a mean of 0 and a standard deviation of 1 among the counties in the sample.

We use weekly, county-level weather data on humidity and temperature from the National Centers for Environmental Information (NCEI, 2023) in $\mathbf{x}_{i,t}^M$ and $\mathbf{x}_{i,t}^H$. Previous research has consistently indicated that cold and dry conditions contribute to the spread and heightened mortality risk of COVID-19.[28] To capture the potential nonlinear influence of county temperatures, we incorporate both temperature and its square. To mitigate multicollinearity, humidity squared is excluded from $\mathbf{x}_{i,t}^M$ and $\mathbf{x}_{i,t}^H$. To account for the role of medical shortages on the spread of COVID-19 and mortality, we use the fraction of inpatient beds occupied in a county using data from the U.S. Department of Health & Human Services (HHS, 2023).

We use data on state-level COVID-19 lockdown and reopening policies (LRO) from the Henry J. Kaiser Family Foundation and the New York Times (KFF, 2022; The New York Times, 2021). LRO ranges from 0 to 5, with higher values indicating more restrictive policies (see Appendix B.3 for details).[29] For the control function, we consider two categories of (weakly) exogenous variables. The first category variables refer to values at $t-2$ or earlier, which are excluded from the main equation (2). Statistically, these variables capture serial correlation in $e_{i,t}^H$. In addition to historical cases and COVID-19 deaths, we employ the economic activity index, which is measured using the (seasonally adjusted) change in consumption expenditures from January 2020, drawn from Opportunity Insights' consumption spending index (Chetty et al., 2020). For the second category, we include two pre-pandemic, county-level demographic and political characteristics: the percentage of the county population with at least some college education and the percentage of Republican votes in the 2016 presidential election from MIT Election Data and Science Lab (MEDSL, 2017). These variables are expected to influence the imposition of states' LRO policies, but they predate the pandemic, making them suitable for addressing endogeneity in equation (2).

Spatial weights. We generate spatial weights using estimates of weekly population flows from Kang et al. (2020). These estimates were produced using mobile phone location data obtained from SafeGraph.[30] To create weights, we first sum the population flows, popflow_{ij} from county j to county i for all of 2019. Next, we sum popflow_{ij} for each pair of counties to create the total bilateral population flows between counties i and j, i.e.,

[28] Notable studies supporting this include Mecenas et al. (2020); Shi et al. (2020); Wu et al. (2020); Notari (2021).

[29] This discrete specification represents the strength of a state's lockdown policy with a finite policy space that facilitates the interpretation of policies and identifying optimal policies.

[30] The location data were created using Global Positioning System (GPS) pings from numerous mobile phone applications. The data are anonymized and do not contain demographic information. Coston et al. (2021) link SafeGraph data to voter roll data which contain race and age information on voters and voting locations and finds that the SafeGraph data underrepresent older adults and non-white voters.

$\breve{w}_{ij} = (\text{popflow}_{ij} + \text{popflow}_{ji})$ if $j \neq i$; and 0 if $j = i$.[31] We then row-normalize these values to generate the spatial weight $w_{ij} = \frac{\breve{w}_{ij}}{\sum_{k=1}^{n} \breve{w}_{ik}}$, which makes $\sum_{j=1, j\neq i}^{n} w_{ij} h_{j,t-1}$ the weighted average of log cases in other counties based on the strength of their connections to county i. We use this spatial weight in the baseline estimation. We consider other spatial weights in Section 5 and Appendix B.4.

Other variables. We use data on the resident population of each county from the US Census Bureau (Census Bureau, 2019). The dataset contains annual estimates of population counts by age, sex, race, and Hispanic origin. We use the population estimates for 2019, the year immediately prior to the pandemic, when calculating the $\text{ACMCFR}_{g,(i,t)\to(i,\Sigma L^*)}$ for each demographic and socioeconomic group.

Summary statistics. Table 1 shows summary statistics of the data for April 26, 2020 through December 26, 2020, the period covered in the figures presented in Section 4 on results. Note that some of the mortality values are not whole numbers because they were interpolated from monthly data on mortality counts using publicly available weekly data.

4 Results

We begin by presenting estimates of our two main equations – the mortality and disease transmission equations. We then present a series of other results derived from these estimates, including the direct effect of a COVID-19 case on mortality versus the indirect effect through propagation in the focal county, COVID-19 and non-COVID-19 mortality, geographic spread, simulations on the impact of state-level lockdown policies, demographic differences, a comparison to epidemiological models and measures, and an analysis of variations in model parameters.

4.1 Coefficient estimates

Mortality. Figure 2 and Table 2 present the estimates from our mortality equation (1). Here, our dependent variable is the log of COVID-19 mortality in a county in a given week, $m_{i,t}$. Figure 2 plots the coefficients, θ_l, which give the elasticities of mortality with respect to cases in the preceding weeks. The coefficients gradually decline over time, stabilizing around the fourth lag, θ_4. A 1% increase in cases is associated with a 0.35% rise in COVID-19 mortality one week later, declining to 0.07% after five weeks. These estimates refer to mortality conditional on infection and exclude subsequent mortality arising from newly transmitted cases. From these estimated θ_l, we evaluate in Section 4.2 the probability of death and the time paths of mortality conditional on infection based on the average $\text{MCFR}^{\text{Direct}}_{(i,t)\mapsto(i,\Sigma L^*)}$ and compare them to other related measures from the literature (e.g., CFR).

[31] We consider two directions of spread of COVID-19 cases in this specification. First, the population flow from county j to county i (popflow_{ij}) can impact log cases ($h_{i,t}$) in county i, as infected individuals from county j can spread infections upon arriving in county i. Second, the population flow from county i to county j (popflow_{ji}) can contribute to an increase in county i's cases, as individuals from county i may be exposed to cases in county j and subsequently "bring infections back" to their home county.

Table 1: Summary statistics

	Mean	Median	Std. Dev.
Count of total deaths per county-week			
Total deaths	111.16	72.67	134.56
By cause			
COVID-19	15.12	6.19	35.12
Other causes	96.04	64.71	109.24
By gender			
Female	52.88	35.03	62.17
Male	58.16	37.72	72.48
By age			
Young (age younger than 65)	29.80	18.78	38.62
Older (age 65 or older)	81.24	53.96	97.04
By race and ethnicity			
White	74.26	53.92	68.72
Black	17.54	7.19	32.28
Hispanic and others	19.21	5.00	55.96
By education			
High school or less	67.31	43.44	83.97
Some college or more	43.72	28.38	52.37
Other variables			
Cases	935.85	395.00	2320.99
Population	620,609	382,067	795,674
Temperature (°C)	19.93	21.37	7.86
Absolute humidity (g/m^3)	0.0094	0.0087	0.0045
Medical shortage (share of inpatient beds occupied)	0.68	0.70	0.17
Lockdown and reopening policies (LRO)	3.08	4.00	1.18
Percent change in consumption expenditures from January 2020	-8.2687	-6.5993	12.1791
Percentage population with some college or more	63.99	64.10	8.27
Share of Republican votes in 2016 presidential election (%)	46.22	48.58	9.39
Spatial weights, w_{ij}			
based on population flows, popflow$_{ij}$	0.00271	0.00025	0.02321

Notes: The statistics in this table cover the period from April 26 through December 26, 2020. The unit of observation is a county-week. Some of the mortality values are not whole numbers because they were interpolated from monthly data of mortality counts using publicly available weekly data. A higher value of the LRO indicates stricter measures.

Figure 2: Estimates of the coefficients θ_l on the log-past cases, $h_{i,t-l}$, from equation (1) for COVID-19 mortality

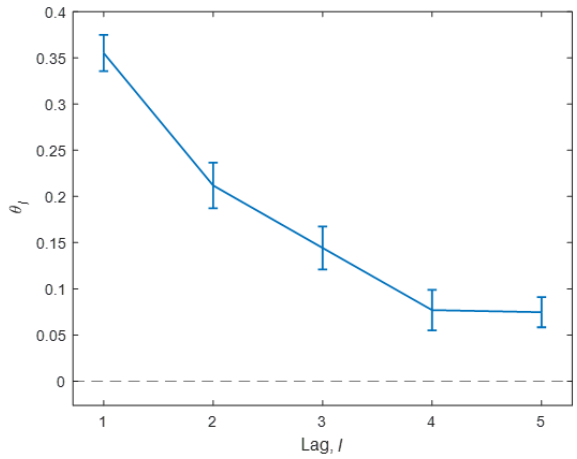

Notes: This figure shows estimates of θ_l from regressions of log mortality on the log of cases, $h_{i,t-l}$ in the preceding 5 weeks from equation (1). The estimates give the elasticity of mortality with respect to past cases. Other coefficient estimates are reported in Table 2. The vertical bars show 95 percent confidence intervals.

Table 2 reports other coefficient estimates from equation (1). The coefficient κ, on the interaction between diabetes prevalence, z_i, and the cumulative sum of cases, $\sum_{l=1}^{L} h_{i,t-l}$, is both positive and significant. This estimate suggests that diabetes increases mortality from COVID-19, which is in keepng with work that highlights diabetes as a significant risk factor (Stokes et al., 2020; Huang, Lim and Pranata, 2020; Kumar et al., 2020; Corona et al., 2021; Kastora et al., 2022; CDC, 2023). Holding lagged cases ($\sum_{l=1}^{L} h_{i,t-l}$) constant, a one standard deviation increase in the prevalence of diabetes is associated with 0.01% higher mortality.

Table 2: Coefficient estimates of covariates from equation (1) for COVID-19 mortality

κ: Diabetes$_i \cdot h^{\text{sum}}_{i,t-1} \mapsto m_{i,t}$	0.0096	(0.0006)
β^M_1: Temperature$_{i,t} \mapsto m_{i,t}$	-0.0263	(0.0025)
β^M_2: Temperature$^2_{i,t} \mapsto m_{i,t}$	0.0004	(0.0001)
β^M_3: Humidity$_{i,t} \mapsto m_{i,t}$	0.6386	(2.5863)
β^M_4: Medical shortage$_{i,t-1} \mapsto m_{i,t}$	0.0968	(0.0270)
Number of observations	17,712	
Log-likelihood	-8,212	

Notes: This table reports coefficient estimates from equation (1) for COVID-19 mortality. Diabetes gives the prevalence of diabetes in a county among adults in 2019. Temperature is measured in degrees Celsius (°C). Humidity refers to absolute humidity, measured in g/m^3. Medical shortage refers to the fraction of inpatient beds in a county that are occupied. Standard errors are reported in parentheses.

Medical shortages in the form of limited hospital capacity are also associated with increased mortality. Specifically, a 1 standard deviation increase in the share of occupied inpatient beds in a county is associated with a 1.65% increase in mortality. Intuitively, we expect increased mortality among people who are infected as medical resources become constrained.

High temperatures are associated with lower mortality, although this pattern weakens at high temper-

atures (i.e., mortality decreases as a function of temperature up to 33°C, a level corresponding to the 98th percentile of the sample). This pattern aligns with higher influenza-related mortality in the winter. While the literature suggests that humidity is associated with lower mortality,[32] our estimated coefficient on humidity is not statistically different from zero, which may be due to its collinearity with temperature.

Case transmission. Table 3 presents the estimates of equation (2), the disease transmission equation. We estimate that a 1% increase in cases in the previous week in a focal county results in a 0.748% rise in cases in the current week in that county. Cases in one county are also affected by those in other counties: A 1% increase in (the weighted average of) cases in surrounding counties induces a 0.201% increase in the focal county's cases. Thus, the magnitude of the cross-county marginal-effect coefficient, a_2, is roughly a quarter of the own-county marginal-effect coefficient, a_1. They sum to 0.949%, indicating that COVID-19 transmission conditional on the covariates is highly persistent, but bounded (i.e., close to, but less than 1).[33] It is important to note that while these estimates imply that COVID-19 is persistent (rather than explosive) on average, cases can increase rapidly at times due to the incidental components – covariates, county-level fixed effects, etc. (e.g., at the start of an outbreak) – and, at other times, spread slowly (e.g., at the end of an outbreak).

Table 3: Coefficient estimates from equation (2)

a_1: $h_{i,t-1} \mapsto h_{i,t}$	0.7480	(0.0055)
a_2: $w_{ij}h_{j,t-1} \mapsto h_{i,t}$	0.2007	(0.0082)
β_1^H: Temperature$_{i,t} \mapsto h_{i,t}$	-0.0039	(0.0018)
β_2^H: Temperature$^2_{i,t} \mapsto h_{i,t}$	0.0001	(0.0000)
β_3^H: Humidity$_{i,t} \mapsto h_{i,t}$	-6.5357	(2.1548)
β_4^H: LRO$_{i,t-2} \mapsto h_{i,t}$	-0.0360	(0.0046)
β_5^H: Medical shortage$_{i,t-1} \mapsto h_{i,t}$	0.0668	(0.0210)
Number of observations	17,712	
Log-likelihood	-29,871	

Notes: This table reports coefficient estimates from equation (2) on case transmission. Temperature is measured in degrees Celsius (°C). Humidity refers to the absolute humidity, measured in g/m^3. Lockdown (LRO) is expressed on a scale from 0 (no restriction) to 5 (most restrictive). Medical shortage refers to the fraction of inpatient beds in a county that are occupied. Standard errors are reported in parentheses.

One of the incidental components in our transmission equation is medical shortages, which also affect cases. A one standard deviation increase in the share of occupied inpatient beds is associated with a 1.14% rise in cases. A scarcity of available inpatient beds might leave people to travel further for medical care, potentially spreading COVID-19. Alternatively, individuals might opt to self-treat at home, rather than being isolated in a crowded hospital. Medical shortages may also be correlated with a lack of access to other medical resources

[32] Shaman et al. (2010) found that "the onset of increased wintertime influenza-related mortality in the United States is associated with anomalously low absolute humidity levels during the prior weeks." Similarly, Wu et al. (2020) verified the same pattern in relation to the COVID-19 pandemic.

[33] We verify that the equation system consisting of equations (1) and (2) does not contain a unit root conditional on our covariates. For instance, our tests in Appendices D.1 and D.3 show that $a_1+a_2 < 1$. If $a_1+a_2 \geq 1$, generated mortality from a case becomes unbounded (one confirmed case eventually leads to the death of the entire population). Although our model does not rule out this scenario, our estimation based on 2020 data suggests a highly persistent but stable dynamic process, which is consistent with the estimates from conventional epidemiological models.

and greater crowding, which might also increase transmission.

In terms of policy, our results indicate that stringent lockdown measures are associated with lower COVID-19 case transmission. Increasing lockdown stringency by one on a scale of 0 to 5 unit reduces cases in the focal county by 3.60%.

Regarding weather, we find that higher temperatures and humidity are associated with lower COVID-19 case propagation. The relationship with temperature is quadratic, with stronger effects at low temperatures. This observation aligns with existing studies of COVID-19 transmission (Mecenas et al., 2020; Shi et al., 2020; Wu et al., 2020; Notari, 2021). It also mirrors findings in the broader influenza literature that in temperate regions, influenza activity is highest when temperature and humidity are lower, typically during the winter (Shaman et al., 2010; Tamerius et al., 2013). Several theories have been posited to explain this pattern, such as improved viral survival, enhanced viral transmission via airborne droplets, increased viral shedding by hosts, and diminished antiviral defenses in colder, drier conditions (Shaman and Kohn, 2009; Deyle et al., 2016; Kudo et al., 2019).

4.2 Direct and Indirect COVID-19 Mortality in the Focal County

Having estimated COVID-19 mortality conditional on infection and the spread of COVID-19, we can now evaluate the MCFR using the coefficient estimates in Section 4.1. For each lag l, Figure 3 reports the mean values of $\text{MCFR}_{(i,t)\mapsto(i,t+l)}$ across origin counties and calendar weeks, that is $\overline{\text{MCFR}}_{(\cdot,\cdot)\to(\cdot,\cdot+l)} \equiv \frac{1}{nT}\sum_{i=1}^{n}\sum_{t=1}^{T}\text{MCFR}_{(i,t)\mapsto(i,t+l)}$. For tractability, MCFR estimates in the remainder of the paper refer to averages across some dimensions that are described explicitly and then referred to as simply the MCFR (e.g., without the upper bar) as a shorthand. For instance, the $\text{MCFR}_{(i,t)\mapsto(i,t+l)}$ in this subsection refers to $\overline{\text{MCFR}}_{(\cdot,\cdot)\to(\cdot,\cdot+l)}$ unless noted otherwise.[34]

Figure 3 shows that one additional COVID-19 case in week t on average leads to 0.0105 additional deaths in week $t+1$ in the same county. The estimate increases to 0.0151 in week $t+5$ before decreasing to 0.0026 in week $t+16$. Over 16 weeks, one additional case leads to 0.1489 additional deaths in the focal county. We then decompose the $\text{MCFR}_{(i,t)\mapsto(i,t+l)}$ into the increase in mortality among the initially infected person (the direct channel, $\text{MCFR}^{\text{Direct}}_{(i,t)\mapsto(i,t+l)}$, represented by the dark blue bars) and mortality attributed to cases that propagate from the focal case (the propagation channel, $\text{MCFR}^{\text{Prop}}_{(i,t)\mapsto(i,t+l)}$, represented by the green bars).

One week after an additional case occurs ($l=1$), all mortality is attributed to the direct channel. This is a product of the model's construction: a case requires at least one week to propagate and an additional week to result in mortality. The magnitude of the direct channel is governed by θ_l in equation (1), leading to a gradual decrease over time. The $\text{MCFR}^{\text{Direct}}_{(i,t)\mapsto(i,t+l)}$ is zero in weeks $t+6$ onwards because $L=5$ in equation (1). The probability of death conditional on contracting COVID-19, implied by $\text{MCFR}^{\text{Direct}}_{(i,t)\mapsto(i,\Sigma L)}$ in the first 5 weeks, is 0.0262. This is comparable to the CFR at the end of our sample period, which is 0.0210.[35] The $\text{MCFR}^{\text{Direct}}_{(i,t)\mapsto(i,t+l)}$

[34] Appendix D.2 presents results based on median values of the MCFR, which are largely consistent with those based on the means, although their magnitnudes differ.

[35] Conceptually, the mean value of $\text{MCFR}^{\text{Direct}}_{(i,t)\mapsto(i,\Sigma L)}$ over the sampling period corresponds to the CFR at the end of the period. The $\text{MCFR}^{\text{Direct}}_{(i,t)\mapsto(i,\Sigma L)}$ captures the contemporaneous probability of death at time t, so taking its average over a period is appropriate. In contrast, the CFR incorporates all past values. Thus, the average $\text{MCFR}^{\text{Direct}}_{(i,t)\mapsto(i,\Sigma L)}$ over a period is comparable to the CFR at the end of the period. This is discussed in Section 2.3 and explored further in Section 4.8.

Figure 3: Marginal case fatality from an additional COVID-19 case in the origin county by channel

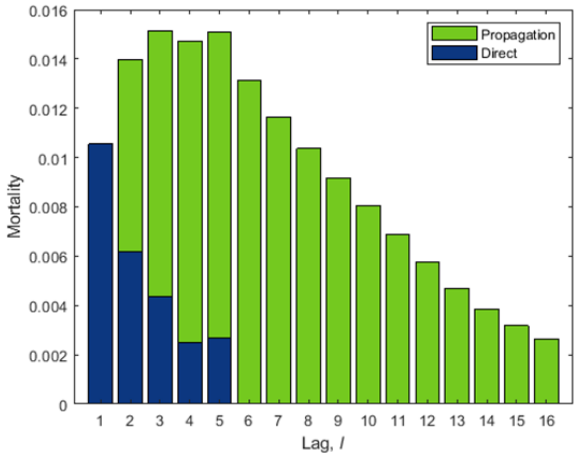

Notes: This figure shows the effect of an additional COVID-19 case in a focal county in week t on COVID-19 deaths in weeks $t+1$ through $t+L^*$ in that focal county. The total height of each bar shows the effect on mortality in the origin county for each lag l relative to week t, $\text{MCFR}_{(i,t)\mapsto(i,t+l)}$. We decompose this value into direct mortality among the initially infected persons, $\text{MCFR}^{\text{Direct}}_{(i,t)\mapsto(i,t+l)}$ in dark blue bars and mortality from newly propagated cases, $\text{MCFR}^{\text{Prop}}_{(i,t)\mapsto(i,t+l)}$ in green bars. For each lag l, we calculate the mean across counties and calendar weeks, for instance $\overline{\text{MCFR}}^{\text{Direct}}_{(\cdot,\cdot)\to(\cdot,\cdot+l)} = \frac{1}{nT}\sum_{i=1}^{n}\sum_{t=1}^{T}\text{MCFR}^{\text{Direct}}_{(i,t)\mapsto(i,t+l)}$.

also describes the time path between infection and mortality, which is not captured by the CFR. We estimate that 63.79% of these additional deaths occur by week $t+2$, and 80.33% by week $t+3$, consistent with the average time from onset to death of 17.8 days, as reported by Verity et al. (2020).

Mortality from newly transmitted cases (i.e., $\text{MCFR}^{\text{Prop}}_{(i,t)\mapsto(i,t+l)}$) exhibits an inverted U-shape over time. It initially increases from 0 in week $t=1$ to 0.0078 in week $t+2$, peaks at 0.0131 in week $t+6$, and then declines gradually. The initial increase can be attributed to the lag between infection and mortality. The effect of a new case in week $t+1$ that propagated from the focal case spans weeks $t+2$ through $t+6$, and so forth. The sum of these lagged effects from the initially propagated cases produces the initial increase.

However, the $\text{MCFR}^{\text{Prop}}_{(i,t)\mapsto(i,t+l)}$ eventually dissipates over time because we estimate a persistent but not permanent marginal effect of a current new case on future new cases (equation 2), implying that the cumulative effect of a case on mortality is bounded. The formula for the $\text{MCFR}^{\text{Prop}}_{(i,t)\mapsto(i,\Sigma L^*)}$ can be described as a finite weighted summation of a geometric series from a dynamic system, eventually resulting in declining values of $\text{MCFR}^{\text{Prop}}_{(i,t)\mapsto(i,t+l)}$ as l increases. Put differently, while the model allows for indefinite case transmissions, case propagation from one week to the next becomes smaller over time as the sum of the marginal effect coefficients a_1 and a_2 is less than 1, so the impact on mortality also declines.

Over 16 weeks, direct mortality on average accounts for 18% of the $\text{MCFR}_{(i,t)\mapsto(i,\Sigma L^*)}$, while case propagation accounts for the remaining 82%. These results highlight the magnitude of COVID-19 externalities – the effect of an additional case on mortality due to propagation is 4.6730 times that of the initially infected person.

The MCFR varies considerably temporally and spatially, which is masked by Figure 3 that presents the

average across these dimensions. As detailed in Section 4.8, the MCFR tends to increase substantially in the weeks preceding an outbreak and then decreases afterwards due to fluctuations in the ratio of mortality to cases, $\frac{\text{mortality}_{i,t+l}}{\text{case}_{i,t}}$, in the MCFR formula. The MCFR also varies across counties based on, among other factors, w_{ij} and z_i. Our empirical approach provides a disciplined and data-driven way to model these variations.

We further examine regional heterogeneity in the MCFR by analyzing its components averaged across calendar weeks, that is $\overline{\text{MCFR}}^{\text{Direct}}_{(i,\cdot)\to(i,\Sigma L)} \equiv \frac{1}{T}\sum_{t=1}^{T} \text{MCFR}^{\text{Direct}}_{(i,t)\to(i,\Sigma L)}$ and $\overline{\text{MCFR}}^{\text{Prop}}_{(i,\cdot)\to(i,\Sigma L)}$ (defined analogously). The standard deviation of $\overline{\text{MCFR}}^{\text{Prop}}_{(i,\cdot)\to(i,\Sigma L)}$ is 0.0904, which is 7.2120 times larger than that of $\overline{\text{MCFR}}^{\text{Direct}}_{(i,\cdot)\to(i,\Sigma L)}$ (0.0125). Notably, this ratio (7.2120) exceeds the ratio of their averages (4.6730), suggesting more pronounced variability in the propagation component. We find that counties with higher proportions of older, less educated, and uninsured populations exhibit larger county-level values of $\overline{\text{MCFR}}^{\text{Prop}}_{(i,\cdot)\to(i,\Sigma L)}$. Meanwhile, variation in $\overline{\text{MCFR}}^{\text{Direct}}_{(i,\cdot)\to(i,\Sigma L)}$ (standard deviation 0.0125, compared to 0.0093 for the county-level CFR) is higher for counties with older and less educated populations, as well as those with elevated rates of premature death (refer to Appendix C.1 for details).

4.3 Non-COVID Mortality

An advantage of our framework is that it allows us to estimate the effect of an additional COVID-19 case on non-COVID-19 mortality in the short run (16 weeks). COVID-19 cases have an ambiguous effect on non-COVID mortality in the short run due to competing mechanisms, making the net effect an empirical question. On one hand, a person close to death from a terminal condition (e.g., a late-stage cancer) may die of COVID-19 instead of their underlying condition. That is, thought of in terms of competing risks, COVID-19 cases can reduce mortality from non-COVID causes. On the other hand, social isolation during the pandemic may have also contributed to the increase in mortality related to mental illness, including substance use. Moreover, an increase in cases may lead people to delay or avoid treatment for non-COVID conditions, eventually leading to mortality that would otherwise have been avoided or delayed. Note that our approach is not well-suited to estimating the effect of COVID-19 cases on long-term mortality, such as that arising from complications due to missed diagnostic screenings that increase mortality many months or years in the future. The fact that even non-COVID mortality was higher in 2020 than in previous years suggests that COVID-19 cases increased non-COVID mortality.[36]

Table 4 reports the estimates from equation (1) for non-COVID mortality. Here, $L = 1$, based on Hannan and Quinn's (1979) information criterion (refer to Figure D.25 in Appendix D.1.1) and a comparison of the estimates with different values of L (Figure 16 in Section 5).[37] A 1% increase in cases is associated with a 0.03% increase in non-COVID mortality. The estimated elasticity, $\theta_1^{\text{othercause}}$, for non-COVID mortality is much smaller than that for COVID. However, since almost 90% of deaths in the counties in our sample during our

[36] Among counties in our sample, the raw count of non-COVID mortality is 6.8% higher in 2020 than all-cause mortality in 2019, which is equivalent to 122,168 excess deaths. The raw count of all-cause mortality in 2020 is 20.1% higher than in 2019, equivalent to 361,501 excess deaths. Mortality is higher in 2020 than in 2019 for almost all causes, except for chronic lower respiratory disease and suicide, which experience declines. Thus, it seems plausible that COVID-19 might have increased non-COVID mortality.

[37] Since specifying a "recovery period" for all non-COVID causes is daunting, we rely on statistical evidence (model selection criteria and robustness check) to select L for non-COVID mortality.

study period are attributed to non-COVID causes, the effect of an additional case on the level of non-COVID mortality is substantial (0.0594 deaths on average). This finding is consistent with Zhang (2021), which finds a drop in hospital visits among veterans during the very early part of the pandemic and worse presentations of those who arrived at emergency departments. The author attributes the excess in non-COVID mortality during the same period to hospital avoidance. Similarly, Ziedan, Simon and Wing (2022) found that cancelled medical appointments during the pandemic led to an increase in mortality.

Table 4: Coefficient estimates from equation (1) for non-COVID mortality

θ_1: $h_{i,t-1} \mapsto m_{i,t}$	0.0339	(0.0009)
κ: Diabetes$_i \cdot \bar{h}^{\text{sum}}_{i,t-1} \mapsto m_{i,t}$	0.0041	(0.0006)
β^M_1: Temperature$_{i,t} \mapsto m_{i,t}$	-0.0038	(0.0004)
β^M_2: Temperature$^2_{i,t} \mapsto m_{i,t}$	0.0001	(0.0000)
β^M_3: Humidity$_{i,t} \mapsto m_{i,t}$	-1.0011	(0.4532)
β^M_4: Medical shortage$_{i,t-1} \mapsto m_{i,t}$	0.0398	(0.0047)
Log-likelihood	16,846	
Number of observations	17,712	

Notes: This table reports estimates from equation (1) of other cause (i.e., non-COVID) mortality on lags of cases. We choose $L = 1$. Diabetes gives the prevalence of diabetes in a county among adults in 2019. Temperature is measured in degrees Celsius (°C). Humidity refers to absolute humidity, measured in g/m^3. Medical shortages refer to the fraction of inpatient beds in a county that are occupied. Standard errors are reported in parentheses.

The estimates of the other coefficients generally have the same sign as those for COVID mortality, but the magnitudes are smaller.[38] For instance, a one standard deviation increase in the share of occupied inpatient beds in a county is associated with a 0.68% rise in non-COVID mortality, which is smaller than the 1.65% increase observed for COVID-19 mortality.

We use these estimates to evaluate the OCMCFR$_{(i,t)\to(i,t+l)}$ for non-COVID-19 deaths in the focal county. As before, we then take the mean across counties and weeks (i.e., $\overline{\text{OCMCFR}}_{(\cdot,\cdot)\to(\cdot,\cdot+l)} \equiv \frac{1}{nT}\sum_{i=1}^{n}\sum_{t=1}^{T}\text{OCMCFR}_{(i,t)\to(i,t+l)}$), plotting it together with $\overline{\text{MCFR}}_{(\cdot,\cdot)\to(\cdot,\cdot+l)}$ for COVID-19 deaths from Figure 3. OCMCFR$_{(i,t)\to(i,t+l)}$ in this subsection refers to $\overline{\text{OCMCFR}}_{(\cdot,\cdot)\to(\cdot,\cdot+l)}$ unless otherwise noted.

Figure 4 shows that, on average, one additional COVID-19 case in week t generates 0.0139 additional non-COVID-19 deaths in week $t+1$; this number decreases monotonically to 0.0005 by week $t+16$. Over the 16-week period, an extra case leads to 0.0594 more non-COVID-19 deaths in the focal county.

In week $t+1$, more than half (57%) of the increase in mortality is attributed to non-COVID deaths. However, non-COVID mortality decreases monotonically and more rapidly over time. Over 16 weeks, 28% of the increase in mortality from an additional case is attributed to non-COVID causes with the remaining 72% from COVID-19. These results highlight the substantial spillovers that a COVID-19 case has on mortality from other causes. This estimate is likely a lower bound of the effect of COVID-19 cases on non-COVID mortality as it focuses only on the short-run effects. Other effects may take longer to manifest. For instance, missed cancer screenings may well lead to increased cancer mortality past our observation window.

We also examine regional heterogeneity in the OCMCFR by taking its average across calendar weeks, that

[38] An exception to this pattern is the coefficient on the level of humidity.

Figure 4: Marginal case fatality rate from an additional COVID-19 case by cause in the origin county

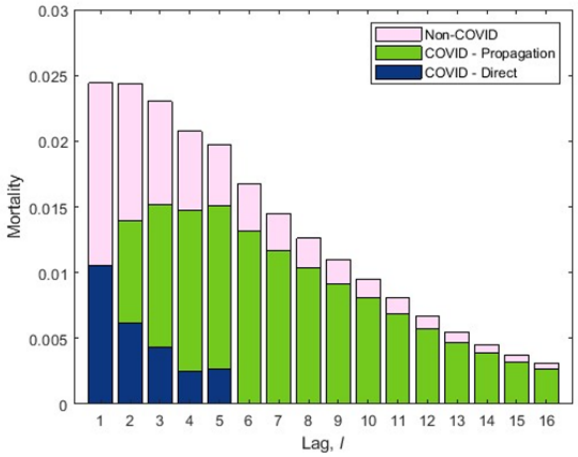

Notes: This figure shows the effect of an additional COVID-19 case in a county in week t on mortality in weeks $t+1$ through $t+L^*$ in that county. The total height of each bar shows the effect on mortality of all causes in the origin county for each lag l relative to week t, $\text{ACMCFR}_{(i,t)\mapsto(i,t+l)}$. We decompose this value into direct COVID-19 deaths of the initially infected person, $\text{MCFR}^{\text{Direct}}_{(i,t)\mapsto(i,t+l)}$ in dark blue bars; COVID-19 deaths from newly propagated cases, $\text{MCFR}^{\text{Prop}}_{(i,t)\mapsto(i,t+l)}$ in green bars; and non-COVID deaths, $\text{OCMCFR}_{(i,t)\mapsto(i,t+l)}$ in light pink bars. For each lag l, we calculate the mean across counties and calendar weeks, for instance $\overline{\text{OCMCFR}}_{(\cdot,\cdot)\to(\cdot,\cdot+l)} \equiv \frac{1}{nT}\sum_{i=1}^{n}\sum_{t=1}^{T}\text{MCFR}^{\text{Direct}}_{(i,t)\mapsto(i,t+l)}$.

is $\overline{\text{OCMCFR}}_{(i,\cdot)\to(i,\Sigma L^*)} \equiv \frac{1}{T}\sum_{t=1}^{T}\text{OCMCFR}_{(i,t)\to(i,t+l)}$. The standard deviation of $\overline{\text{OCMCFR}}_{(i,\cdot)\to(i,\Sigma L^*)}$ is 0.0565, or 56.26% of the standard deviation of $\overline{\text{MCFR}}_{(i,\cdot)\to(i,\Sigma L^*)}$, indicating relatively large heterogenety. We find that $\overline{\text{OCMCFR}}_{(i,\cdot)\to(i,\Sigma L^*)}$ related to the size of the older population, air pollution, and the frequency of premature deaths (see Appendix C.1 for details).

4.4 Mortality by location

Many policy discussions of COVID-19 focused on the autonomy of states, which makes sense if COVID-19 cases and mortality are highly local. Our estimates indicate substantial cross-county transmission of cases (specifically a_2), which in turn implies considerable externalities generated by a case in a focal county on mortality in other counties. In this section, we investigate the $\text{MCFR}_{(i,t)\to(\mathcal{N},\Sigma L^*)}$ and $\text{OCMCFR}_{(i,t)\to(\mathcal{N},\Sigma L^*)}$ at the national level, which we then decompose based on where the mortality occurs, as described in Section 2.2. As before, we calculate the means across counties in which the focal case originates and calendar weeks for each lag l (e.g., $\overline{\text{MCFR}}_{(\cdot,\cdot)\to(\mathcal{S}_{s(\cdot),\cdot+l})} \equiv \frac{1}{nT}\sum_{i=1}^{n}\sum_{t=1}^{T}\text{MCFR}_{(i,t)\to(\mathcal{S}_{s(i)},t+l)}$). The MCFR in this subsection refers to such averages, unless noted otherwise. Panels (a) and (b) of Figure 5 display the results for COVID-19 and non-COVID mortality, respectively.

The dark red bars represent mortality impacts in weeks $t+l$ in the county in which the focal case originated in week t. For each lag l, the dark red bars in Panel (a) are equal to the sum of the dark blue and green bars for COVID-19 in Figure 4, while the dark red bars in Panel (b) are equivalent to the light pink bars for non-COVID mortality. One week after the additional case occurs ($l=1$), all mortality occurs in the county in which the case originates. This is by construction because a case needs at least one week to propagate to other

Figure 5: Marginal case fatality rate from an additional COVID-19 case by location and cause of death

(a) COVID-19 mortality

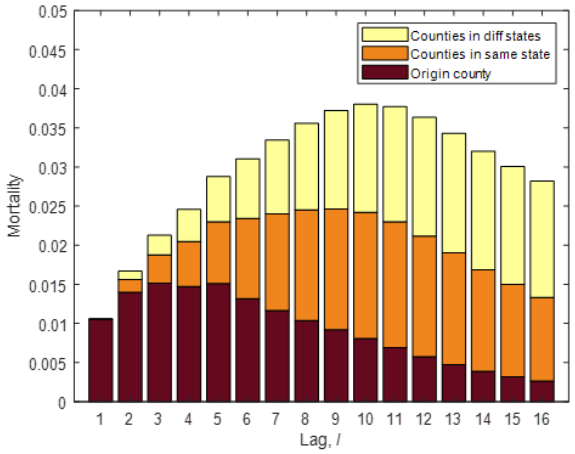

(b) Other cause (i.e., non-COVID) mortality

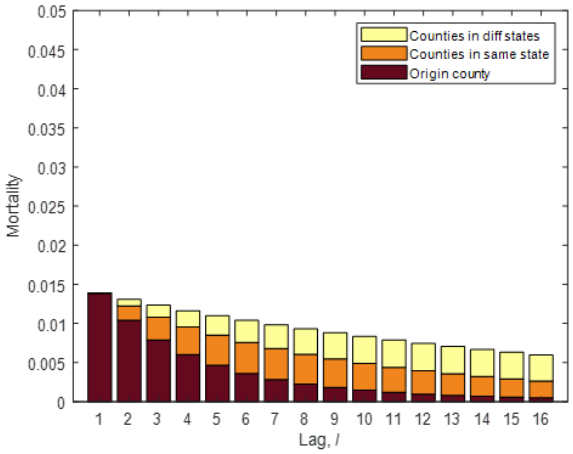

Notes: This figure shows the effect of an additional COVID-19 case in a county in week t on COVID-19 deaths (Panel (a)) and other cause (i.e., non-COVID) deaths (panel (b)) in weeks $t+1$ through $t+L^*$ in different locations. The total height of each bar shows the effect on total deaths at the national level for each lag l relative to week t, i.e., $\text{MCFR}_{(i,t)\mapsto(\mathcal{N},t+l)}$ and $\text{OCMCFR}_{(i,t)\mapsto(\mathcal{N},t+l)}$. We decompose these into deaths in the county in which the focal case originates, $\text{MCFR}_{(i,t)\mapsto(i,t+l)}$ (dark red bars); counties in the same state as the focal county, $\text{MCFR}_{(i,t)\mapsto(\mathcal{S}_{s(i)}\setminus\{i\},t+l)} = \text{MCFR}_{(i,t)\mapsto(\mathcal{S}_{s(i)},t+l)} - \text{MCFR}_{(i,t)\mapsto(i,t+l)}$ (orange bars); and counties in other states, $\text{MCFR}_{(i,t)\mapsto(\mathcal{N}\setminus\mathcal{S}_{s(i)},t+l)} = \text{MCFR}_{(i,t)\mapsto(\mathcal{N},t+l)} - \text{MCFR}_{(i,t)\mapsto(\mathcal{S}_{s(i)},t+l)}$ (bright yellow bars). For each lag l, we calculate the mean across counties and calendar weeks, for instance $\overline{\text{MCFR}}_{(\cdot,\cdot)\to(\mathcal{S}_{s(\cdot)},\cdot+l)} = \frac{1}{nT}\sum_{i=1}^{n}\sum_{t=1}^{T}\text{MCFR}_{(i,t)\mapsto(i,t+l)}$.

counties and another week to cause mortality. On average, one additional case leads to 0.0244 additional deaths from all-causes in the originating county after one week. The $\text{ACMCFR}_{(i,t)\to(i,t+l)}$ then decreases steadily to 0.0031 by week $t+16$.

The orange bars in panel (a) represent COVID-19 mortality in counties in the same state as the focal county less mortality in the focal county, that is $\text{MCFR}_{(i,t)\to(\mathcal{S}_{s(i)}\setminus\{i\},t+l)} = \text{MCFR}_{(i,t)\to(\mathcal{S}_{s(i)},t+l)} - \text{MCFR}_{(i,t)\to(i,t+l)}$. The light yellow bars represent mortality in counties in other states, that is $\text{MCFR}_{(i,t)\to(\mathcal{N}\setminus\mathcal{S}_{s(i)},t+l)} = \text{MCFR}_{(i,t)\to(\mathcal{N},t+l)} - \text{MCFR}_{(i,t)\to(\mathcal{S}_{s(i)},t+l)}$. The MCFR outside the focal county takes longer to peak and dissipates rather slowly, especially for mortality outside the focal state. On average, one additional case in a focal county leads to 0.0016 and 0.0011 additional COVID-19 deaths in week $t+2$ in other counties within the same state, and counties in different states, respectively. As l increases, these numbers steadily increase and then peak at 0.0161 in week $t+10$ for counties within the same state (i.e., it peaks 9 weeks after mortality is first realized) and at 0.0153 in week $t+13$ for counties in different states (i.e., 12 weeks after). (In contrast, $\text{MCFR}_{(i,t)\to(i,t+l)}$ peaks just 5 weeks after.) The corresponding numbers in week $t+16$ are 0.0107 and 0.0149 for counties in the same state and counties in different states, respectively. These patterns can be explained by the large values of a_1 and a_2, which sum to 0.9487, indicating a highly persistent transmission process that leads to mortality long after the focal case occurs but not a unit root (see Appendix D.1). In Section D.3 of the appendix, we include additional results with longer lags, L^* and show more clearly that the MCFR outside of the focal county dissipates over time, although quite slowly.

The $\text{MCFR}_{(i,t)\to(\mathcal{S}_{s(i)}\setminus\{i\},t+l)}$ and $\text{MCFR}_{(i,t)\to(\mathcal{N}\setminus\mathcal{S}_{s(i)},t+l)}$ are inverse U-shaped over time because it

takes time for a case in county i to generate cases in other counties. The lag process in mortality accentuates the inverse U-shape of the $\text{MCFR}_{(i,t)\to(\mathcal{S}_{s(i)}\setminus\{i\},t+l)}$ and $\text{MCFR}_{(i,t)\to(\mathcal{N}\setminus\mathcal{S}_{s(i)},t+l)}$. As the MCFR formula can be considered as a set of geometric series - each new case that propagates across county borders creates its own series which then leads to an initial increase in the $\text{MCFR}_{(i,t)\to(\mathcal{S}_{s(i)}\setminus\{i\},t+l)}$ and $\text{MCFR}_{(i,t)\to(\mathcal{N}\setminus\mathcal{S}_{s(i)},t+l)}$. These values eventually decrease because the spatial-dynamic process in equation (2) is stable, as we note in footnote 33.

The effect of a case on non-COVID mortality exhibits a similar pattern as that of COVID-19, although the magnitude is much smaller. Mortality within the same state (orange bars in panel (b)) increases from 0.0018 in week $t+2$ to 0.0040 in week $t+6$ and then decreases to 0.0022 in week $t+16$. Mortality in other states (light yellow bars) increases from 0.0009 in week $t+2$ to 0.0035 in week $t+11$ and then decreases to 0.0033 in week $t+16$.

Over 16 weeks, one additional case in a county generates 0.6255 additional deaths from all causes nationwide. The increase in all-cause mortality is roughly evenly divided between the originating county (0.2083 additional deaths or 33% of the $\text{ACMCFR}_{(i,t)\to(\mathcal{N},\Sigma L^*)}$), other counties within the same state (0.2154 or 35%), and counties in different states (0.2018 or 32%). These results highlight the importance of incorporating cross-border effects when assessing the marginal mortality from a case and evaluating optimal disease control policy.

4.5 Effects of a lockdown

Just as cases impact mortality beyond the county in which the case originates, disease mitigation policies have effects across places. While many states emphasized autonomy in setting their social distancing policies, our estimates imply that a lockdown imposed by one state affects mortality in other states through geographic transmission of cases. We evaluate the benefit of imposing a one-week full lockdown in state s in week t (increasing $\text{LRO}_{i,t}$ from 0 to 5 for $i \in \mathcal{S}_s$) on mortality in all counties in our sample using the estimated coefficient $\hat{\beta}_4^H$ from equation (2).[39] We express the marginal benefit in dollars per person subjected to the lockdown. For each state s, we evaluate the following:

$$\text{MB}_{s,t} = -\sum_{i\in\mathcal{S}_s}\sum_{j=1}^{n}\sum_{l=1}^{L^*}\frac{d(\text{mortality}_{j,t+2+l} + \text{mortality}^{\text{othercause}}_{j,t+2+l})}{d(\text{LRO}_{i,t})} \times 5 \times \frac{\text{VSL}}{\text{pop}_s}.$$

We convert the estimated change in mortality from a full lockdown, $\sum_{i\in\mathcal{S}_s}\sum_{j=1}^{n}\sum_{l=1}^{L^*}\frac{d(\text{mortality}^{\text{all-cause}}_{j,t+2+l})}{d(\text{LRO}_{i,t})} \times 5$, to dollars using the value of statistical life (VSL). Although estimates vary, a plausible range of VSL estimates for an average American is between \$10 and \$12 million (Sunstein, 2024). For simplicity, we consider VSL=\$10 million.[40] We also normalize the value by population size $\text{pop}_s = \sum_{i\in\mathcal{S}_s}\text{pop}_i$.

The estimated per capita benefits of a one-week full lockdown vary substantially across states. Figure 6

[39] Recall that LRO affects cases with a 2-week lag and cases affect mortality with a 1-week lag, so the mortality impact of a lockdown in week t does not materialize until $t+3$. Consistent with MCFR calculation, we estimate the impact across $L^* = 16$ weeks, that is from week $t+3$ through week $t+19$.

[40] This value is also in line with the VSL used in cost-benefit analyses by the US Environmental Protection Agency, which was \$7.4 million in 2006 dollars, or about \$9.5 million in CPI-adjusted 2020 dollars (Lavetti, 2023).

reports the mean value for each state across calendar weeks, $\overline{\text{MB}}_s = \frac{1}{T}\sum_{t=1}^{T} \text{MB}_{s,t}$. The estimates range from \$219.23 per person in Vermont to \$836.43 per person in the District of Columbia, with a mean value of \$576.02 per person locked down. On average, 82.37% of the marginal benefit (\$474.45) is due to reduced COVID-19 deaths, while 17.63% (\$101.57) comes from reduced non-COVID mortality.

Figure 6: Marginal benefit of a lockdown by state, in dollars *per capita*

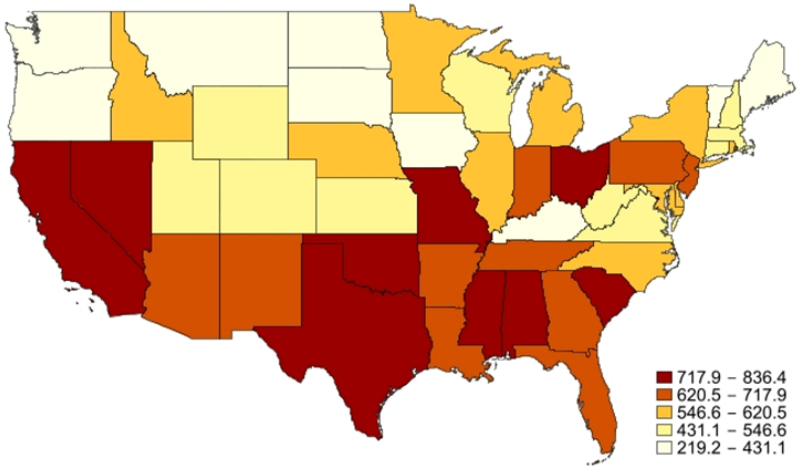

Notes: This map shows the benefits of imposing a state-level, one-week full lockdown for each state s in a week t (increasing $\text{LRO}_{i,t}$ from 0 to 5 for $i \in \mathcal{S}_s$) on mortality in all counties in our sample in weeks $t+3$ through $t+19$. The benefit is expressed in dollars based on the assumed value of statistical life (VSL) of \$10M and normalized to the population size of the state imposing the lockdown. It can be interpreted as the impact per person subjected to the lockdown. For each state, we calculate the average across all calendar weeks t, that is $\overline{\text{MB}}_s = \frac{1}{T}\sum_{t=1}^{T} \text{MB}_{s,t}$.

With the per capita benefits of a state-level lockdown varying across states by a factor of 4, we explore the factors related to that variation. Here we focus on the role of the geospatial connectedness of states, plotting the log of the benefits against the log of the total population flows within and across states, $\vec{w}_s$.[41] Figure 7 shows a strong positive relationship (corr=.72) with a 1% increase in the geospatial connectedness of a state being associated with a 1.32% increase in the benefit of a lockdown. From a policy perspective, some of the states with high values of lockdowns like California did impose strong lockdowns, while others like Florida were less restrictive. This result is consistent with the findings of Balcan et al. (2009), who show that connectivity and population heterogeneity shape the spatial spread in simulations with a generic influenza-like pathogen.

The value of controlling cases also varies across time. Panel (a) in Figure 8 plots the marginal benefit of a lockdown averaged across states (i.e., national level), $\frac{1}{n_s}\sum_{s=1}^{n_s} \text{MB}_{s,t}$, over the year 2020. The values range from \$348.14 per person (second week of July) to \$907.02 per person (first week of November). We next consider how this temporal variation relates to mortality. Figure 8 additionally plots the average LRO policies implemented across states, $\frac{1}{n_s}\sum_{s=1}^{n_s} \text{LRO}_{s,t}$, and the total COVID-19 mortality in all the counties in our sample, $\sum_{i=1}^{n} \text{mortality}_{i,t}$. The benefits of a lockdown tend to precede mortality by a couple of weeks, so that imposing a lockdown before the start of an outbreak (when cases start to increase instead of when mortality is already high)

[41] We calculate $\vec{w}_s = \sum_{i \in \mathcal{S}_s}\sum_{j=1}^{n}(\text{popflow}_{ij} + \text{popflow}_{ji} + \text{popflow}_{ii})/\text{pop}_s$. Note that $\vec{w}_s$ is normalized by the population size of the state and incorporates population flows within counties, popflow_{ii}, in addition to the bilateral flows across counties, $\text{popflow}_{ij} + \text{popflow}_{ji}$.

Figure 7: Correlation between the benefit of a lockdown and geospatial connectedness

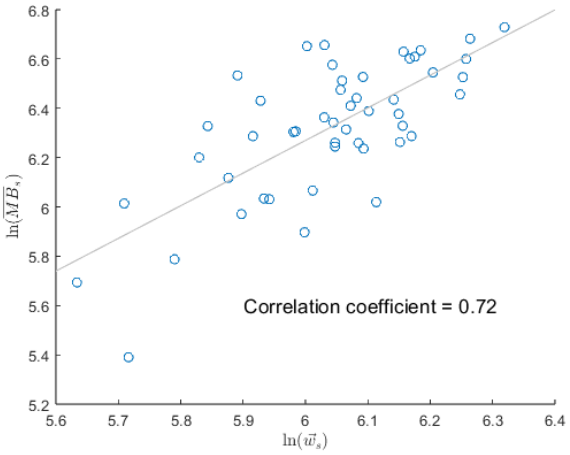

Notes: The vertical axis gives the log of the marginal benefit of imposing a state-level, one-week, full lockdown for state s (increasing $\text{LRO}_{i,t}$ from 0 to 5 for $i \in \mathcal{S}_s$), averaged across calendar weeks, $\overline{\text{MB}}_s = \frac{1}{T}\sum_{t=1}^{T} \text{MB}_{s,t}$. The horizontal axis gives the log of total population flows within and across states, $\vec{w}_s = \sum_{i \in \mathcal{S}_s} \sum_{j=1}^{n} (\text{popflow}_{ij} + \text{popflow}_{ji} + \text{popflow}_{ii})/\text{pop}_s$. Each point in the figure denotes a state. The grey line shows the best linear fit ($\ln(\overline{\text{MB}}_s) = -1.68 + 1.32 \ln(\vec{w}_s)$).

yields the highest marginal benefit.[42] Intuitively, when transmission is high, the compounding effect increases the number of additional cases that each focal case generates, implying a higher benefit of a lockdown. This point highlights a temporal policy misalignment. Rather than taking preemptive action and imposing lockdowns at the start of an outbreak when marginal benefits are the highest, states appear to have (belatedly) reacted to higher COVID-19 mortality. Quantitatively, the correlation between states' LRO policies and COVID-19 mortality is 0.8365. By contrast, the correlation between LRO policies and the marginal benefit is considerably lower at 0.2267.

Panels (e) through (g) in Figure 8 illustrate the marginal benefits of lockdowns and the LRO policies for five representative states plus the District of Columbia, which has the highest marginal benefit. The District of Columbia's approach to its LRO decisions tends to mirror the overall pattern of trailing COVID-19 mortality. California also shows a delayed response to the marginal benefit of lockdowns, reacting primarily to COVID-19 mortality. Conversely, Pennsylvania implemented stricter lockdowns prematurely, generating high economic costs associated with early, stringent lockdown measures. New York's LRO policy appears to align with its marginal benefits. Florida's lockdown stringency actually declines as the marginal benefit increases. Lastly, Texas did not exhibit any response to either COVID-19 mortality or the marginal benefits of lockdowns. Detailed state-level analyses are provided in Appendix C.2. These discrepancies underscore the challenges of timing policy interventions to optimize their effectiveness and minimize adverse impacts, highlighting the value of quantifying the marginal impact of lockdowns through our framework.

[42] Similar patterns are observed when we compare the marginal benefits of lockdowns with cases.

Figure 8: Marginal benefits of a lockdown, COVID-19 mortality and implemented LRO

(a) National level

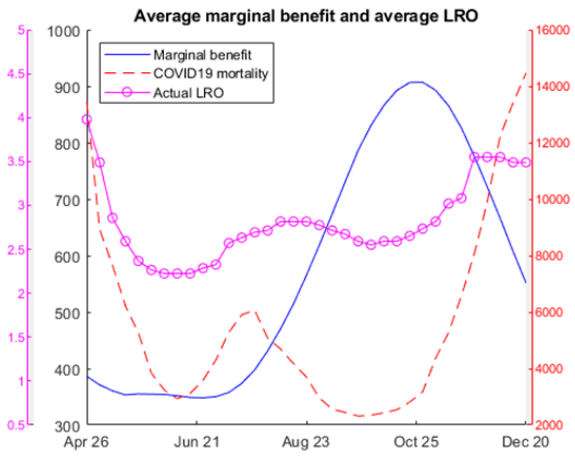

Corr(mortality, LRO) $= 0.8365$, Corr(MB, LRO) $= 0.2267$

(b) California

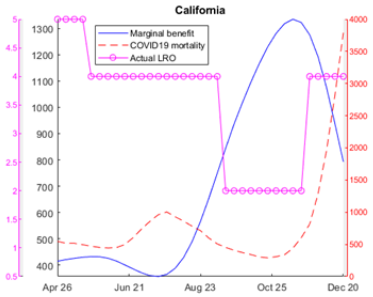

Corr(mortality, LRO) $= 0.2727$
Corr(MB, LRO) $= -0.7447$

(c) Texas

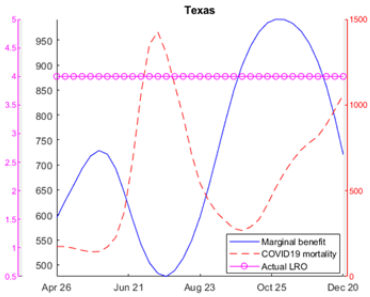

(d) Florida

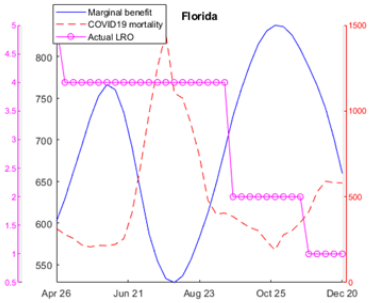

Corr(mortality, LRO) $= 0.2004$
Corr(MB, LRO) $= -0.6220$

(e) New York

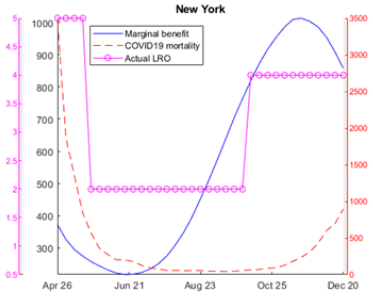

Corr(mortality, LRO) $= 0.5928$
Corr(MB, LRO) $= 0.4987$

(f) Pennsylvania

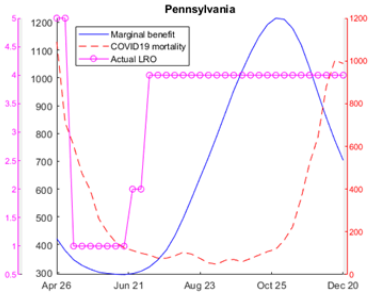

Corr(mortality, LRO) $= 0.1097$
Corr(MB, LRO) $= 0.5652$

(g) District of Columbia

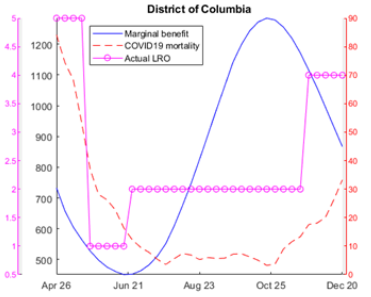

Corr(mortality, LRO) $= 0.6938$
Corr(MB, LRO) $= 0.0761$

Notes: This figure shows the marginal benefits of imposing a state-level full lockdown (blue), actual lockdown and reopening (LRO) policies (pink), and COVID-19 deaths (red). Panel (a) shows the series at the national level where we calculate the means across states of the marginal benefits, $\frac{1}{n_s}\sum_{s=1}^{n_s} \text{MB}_{s,t}$ and the LRO policies, $\frac{1}{n_s}\sum_{s=1}^{n_s} \text{LRO}_{s,t}$, as well as total COVID-19 mortality, $\sum_{i=1}^{n} \text{mortality}_{i,t}$. Panels (b) through (g) show the corresponding series for selected states plus the District of Columbia. We also provide correlations between (i) LRO policies and mortality and (ii) LRO policies and marginal benefits of a lockdown for states with variation in LRO policies (i.e., for Texas, the correlation is undefined because its LRO policy does not change).

4.6 Disparities by subgroups

We apply the MCFR framework to evaluate the mortality impact from an additional case for different demographic and socioeconomic groups. While the literature has documented disparate impacts of the pandemic on vulnerable groups (e.g., Alsan, Chandra and Simon (2021); Finkelstein et al. (2024)), much of this work uses measures that describe the average mortality (e.g., rates) or do not explicitly link the increase in mortality to cases (e.g., excess deaths). We add to this literature by proposing a new framework to measure differences across groups with the advantages of the MCFR.

We focus on all-cause mortality of individual demographic and socioeconomic groups in the origin county, normalized by the respective size of each group, $\text{ACMCFRpop}_{g,(i,t)\to(i,\Sigma L^*)}$. For uniformity, we use a common number of lags, L, for all groups. We set $L = 4$, which is between the numbers of lags used for COVID-19 and non-COVID mortality in previous sections, because θ_4 is small for most subgroups. The coefficient estimates are reported in Appendix C.3.1. Figure 9 reports the mean values across all counties and weeks for each group; that is, for each group g, we calculate $\frac{1}{nT}\sum_{i=1}^{n}\sum_{t=1}^{T}\text{ACMCFR}_{g,(i,t)\to(i,\Sigma L^*)}$. In this subsection, ACMCFRpop refers to this mean value unless noted otherwise. We consider differences by age, race/ethnicity, education, and gender.

Figure 9: Differences in mortality risk by demographic and socioeconomic groups

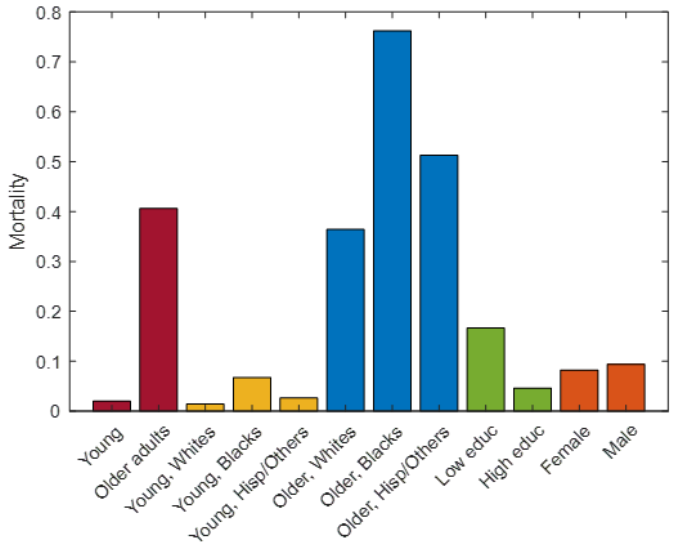

Notes: This figure shows the effect of one additional COVID-19 case in a county in week t on deaths from all causes in the next 16 weeks in the same county for each demographic and socioeconomic group g per 100,000 individuals in each group. For each group, we calculate the mean across counties and calendar weeks, that is $\frac{1}{nT}\sum_{i=1}^{n}\sum_{t=1}^{T}\text{ACMCFRpop}_{g,(i,t)\mapsto(i,\Sigma L^*)}$. Young is defined as under age 65; older is defined as age 65 or older.

There are large differences across age groups. An extra case in a county leads to an increase of 0.4061 deaths from all-causes per 100,000 older adults (i.e., individuals age 65 or older) and only 0.0198 all-cause deaths per 100,000 people under 65. This result corresponds to large differences across age groups measured using the CFR in the Wuhan area (Verity et al., 2020). The pandemic also had widely disparate impacts across

racial and ethnic groups conditional on age.[43] Blacks and Hispanics have considerably higher ACMCFRpop than Whites among both young and older individuals. Specifically, one more case in a county increases mortality by 0.7623 among older Blacks, by 0.5130 among older Hispanics/Others, and 0.3641 among older Whites per 100,000 population in each group.[44] The ranking of mortality risks among the three groups is the same when we consider mortality within the young population, although the estimates are an order of magnitude smaller.

We also find differences in the mortality risk by education level and, to a much smaller extent, by sex. One more case in a county increases all-cause mortality per 100,000 population by 0.1665 for individuals with a high school education or less ("low educ") and by 0.0461 for those with some college or more ("high educ"). The ACMCFRpop of the former is 3.6 times larger than the latter. These differences likely reflect differences in exposure, age distributions, baseline health, and access to healthcare between the two groups. The sex differences are much smaller. One more case in a county increases mortality per 100,000 population by 0.0821 among females and 0.0939 among males.

The relative magnitude of the ACMCFRpop between groups is closer to that of COVID-19 mortality rate than to the all-cause mortality rate (shown in Appendix Figures C.11 and C.12) despite the ACMCFRpop being a measure of all-cause deaths. For instance, the ACMCFRpop of older Blacks is 2.1 times larger than that of older Whites, while the corresponding relative mortality rates between the two groups are 1.5 for COVID-19 deaths and 1.0 for all-cause deaths. This observation implies that the increase in mortality from an additional case comes largely from COVID-19 deaths rather than those from other causes. It also further highlights that the MCFR is a marginal measure rather than a simple frequency which does not describe how a case is related to mortality levels.

Furthermore, the ACMCFRpop incorporates the impact of an additional case on non-COVID deaths which is difficult to evaluate using only mortality rates. The effects of the pandemic on non-COVID mortaility can be assessed by calculating excess mortality, but this also requires additional assumptions and modeling. Figure C.12 in Appendix C.3.3 decomposes the ACMCFRpop into COVID-19 and non-COVID components, and shows that the spillovers vary across groups. For instance, the fraction of non-COVID deaths out of the ACMCFRpop varies from 28% among Older Hispanic/Others group to 47% among Young Blacks. These findings emphasize that compared to existing measures of infectious diseases, the ACMCFRpop is both more comprehensive and interpretable for policymaking as it evaluates the all-cause mortality that can be avoided from an additional case.

4.7 Joint relationship between the MCFR and measures of mortality and transmissibility

So far, we have shown how the MCFR framework can be used to characterize COVID-19 and offer policy-relevant insights that are difficult to derive from traditional epidemiology measures. Two of the primary features

[43] There are large differences in the age distribution across racial and ethnic groups – in our sample counties, the mean ages of Non-Hispanic Whites, Non-Hispanic Blacks, and Hispanics/Others are 42, 32, and 28, respectively. To account for these age differences, we estimate the ACMCFRpop for each race/ethnicity group separately for young (age$\leq$65) and older individuals (age>65).

[44] In calculating the ACMCFRpop for older Blacks, we limit to counties with at least 200 older Blacks. The ACMCFRpop for counties with small older Black populations are unstable and may overestimate the effect of a case on mortality since the death of just one individual has a sizeable impact on the estimates.

examined in the epidemiology literature are the fatality rate and transmissibility, which are often measured using the CFR and $\mathcal{R}_t$. This section explores how our MCFR relates to these conventional measures in two ways. First, we use regressions to further explore the extent to which the MCFR can be reconstructed from the CFR and $\mathcal{R}_t$ versus providing information that is distinct from them. We then conduct comparative statics exercises in which we vary the values of the main parameters representing fatality and transmissibility in our model to demonstrate the general applicability of the MCFR framework to other infectious diseases. Together, these analyses clarify how fatality and disease transmission separately and jointly relate to the MCFR.

4.7.1 The MCFR and the linear combinations of the CFR and $\mathcal{R}_t$

Here we examine how the $\text{MCFR}_{(i,t)\mapsto(i,\Sigma L^*)}$ in an origin county relates to the conventional CFR and $\mathcal{R}_t$ measures using regressions.[45] That is, we seek to understand the extent to which the MCFR can be reasonably reproduced from the CFR and $\mathcal{R}_t$. We use the weekly state-level $\mathcal{R}_t$ from the website *rt.live* (Systrom, Vladek and Krieger, 2020). For comparability, we also calculate the CFR and the means of the $\text{MCFR}_{(i,t)\mapsto(i,\Sigma L^*)}$ at the state level using the counties in our sample.[46] The $\text{MCFR}_{(i,t)\mapsto(i,\Sigma L^*)}$ in this subsection refers to such averages, unless noted otherwise. Because these variables are right-skewed, we use their natural logarithm in the regressions.

Table 5: The relationship between $\text{MCFR}_{(i,t)\mapsto(i,\Sigma L^*)}$ and the CFR and $\mathcal{R}_t$

	(1)	(2)	(3)	(4)
$\ln(\text{CFR})$	0.642	1.124	0.387	0.571
	(0.063)	(0.074)	(0.075)	(0.082)
$\ln(\mathcal{R}_t)$	2.962	2.657	3.337	2.998
	(0.323)	(0.242)	(0.320)	(0.327)
Constant	-0.031	1.724	-0.968	0.505
	(0.225)	(0.263)	(0.262)	(0.242)
State FE	No	Yes	No	Yes
Week FE	No	No	Yes	Yes
Number of observations	1,715	1,715	1,715	1,715
R^2 (total)	0.440	0.683	0.662	0.805
R^2 (conditional on FE)	0.440	0.599	0.406	0.458

Notes: This table reports estimates from regressions of $\ln(\text{MCFR}_{(i,t)\mapsto(i,\Sigma L^*)})$ on $\ln(\text{CFR})$ and $\ln(\mathcal{R}_t)$. The columns differ in the types of fixed effects included. We calculate both the total R^2 and the partial R^2 conditional on the fixed effects to highlight the role of CFR and $\mathcal{R}_t$ separate from the fixed effects. The latter is calculated by first demeaning the variables at the week and/or state level, depending on the fixed effects included, and then regressing the demeaned variables and calculating the resulting R^2. Standard errors are reported in parentheses.

Table 5 shows estimates with different sets of fixed effects. Consistent with intuition, the CFR and $\mathcal{R}_t$

[45] Given that the basic (or effective) reproduction number is derived from a mathematical model, its value differs depending on the selected model and its inherent parameters. Given this model-specificity, the aim of this analysis is to understand the overarching relationships between the cross-sectional and temporal variations of our MCFR and the conventional measures.

[46] Because *rt.live* reports data for entire states while our main analysis focuses on 369 of the largest counties, there is some non-comparability between our data and that from *rt.live*. At the same time, the counties in our sample account for a disproportionate share of the population, reducing the discrepancy somewhat. For instance, we only include 19 out of the 67 counties in Pennsylvania when calculating the state average, but these counties collectively represent 74% of the state population.

are both positively related to the $\text{MCFR}_{(i,t)\mapsto(i,\Sigma L^*)}$ in all specifications. In Column (4), which includes week and state fixed effects, we estimate that a 1% increase in the CFR and $\mathcal{R}_t$ are associated with a 0.6% and a 3.0% higher $\text{MCFR}_{(i,t)\mapsto(i,\Sigma L^*)}$, respectively. The coefficients on both terms are statistically different from zero in all specifications, indicating that the MCFR incorporates information in each measure.

Furthermore, the estimates indicate that the MCFR is convex in $\mathcal{R}_t$ and generally concave in the CFR (except for the specification with only state fixed effects in column (2) of Table 5, the estimated coefficients on the CFR are less than 1). The log-log specification builds some complementarity in the relationship with the MCFR between the CFR and $\mathcal{R}_t$. For instance, the slope of the MCFR with respect to the $\mathcal{R}_t$ becomes more convex at larger values of the CFR. Figure 10 graphically represents this relationship using the estimates in column (4).

Figure 10: Graphical representation of the relationship between the $\text{MCFR}_{(i,t)\mapsto(i,\Sigma L^*)}$ and the CFR and $\mathcal{R}_t$

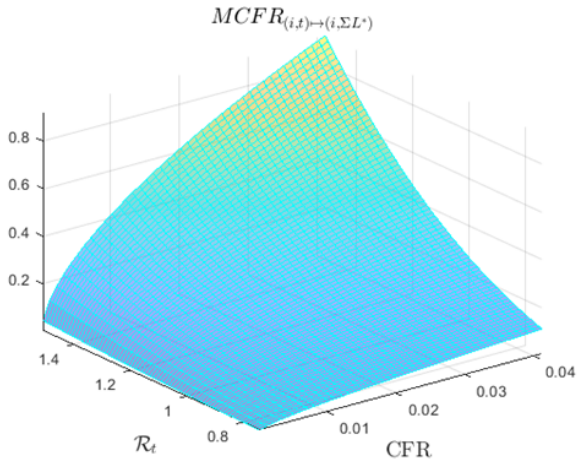

Notes: This figures graphically represents the empirical relationship between the $\text{MCFR}_{(i,t)\mapsto(i,\Sigma L^*)}$ and the CFR and $\mathcal{R}_t$ as described in column (4) of Table 5.

We further explore the robustness to the inclusion of state and week fixed effects and find that including state fixed effects increases the coefficient on the CFR, while the coefficient on $\mathcal{R}_t$ is relatively stable across models. Specifically, while (by construction) both state and time fixed effects improve the overall fit of the model, the coefficient on the CFR and the partial R^2 conditional on the fixed effects are considerably higher in models with state fixed effects and considerably lower in models with week fixed effects. These suggest that the within-state temporal variation in the MCFR is strongly related to the CFR.

Across all specifications, the R^2 values suggest that a substantial share of the variation in the $\text{MCFR}_{(i,t)\mapsto(i,\Sigma L^*)}$ remains unexplained by the CFR and $\mathcal{R}_t$. To investigate further, we extract the state- and week-fixed effects from specification (4) in Table 5 and compare them to key demographic and health characteristics (see Appendix C.5). First, we find that the MCFR includes time components closely tied to current confirmed cases, implying that it captures contemporaneous health shocks that both generate additional infections and lead to future mortality. Second, the region-specific component of the MCFR correlates strongly with higher proportions of older and less-educated populations, greater levels of premature deaths, and higher shares

of uninsured and diabetic residents. These findings suggest that the MCFR incorporates significant local risk factors for COVID-19 that are not captured by the CFR and $\mathcal{R}_t$. This combination of evidence suggests that while the CFR and $\mathcal{R}_t$ separately capture important dimensions of an infectious disease, they cannot be combined easily to assist policymakers in formulating optimal policies that are based on marginal tradeoffs in the costs and benefits of mitigating the spread of diseases.

4.7.2 Comparative statics exercises

The previous analysis shows that our MCFR captures additional factors beyond linear combinations of the CFR and $\mathcal{R}_t$. It is also possible to vary the core parameters in our model to demonstrate scenarios in which the MCFR framework provides substantial value relative to linear combinations of transmission and mortality parameters. In this section, we conduct comparative statics exercises which additionally illustrate the framework's generalizability and applicability to other infectious diseases or COVID-19 as it evolves to have different properties.

We perform three comparative statics exercises. In each one, we vary the values of the parameters governing mortality, $\boldsymbol{\theta}^M = (\theta_1, \cdots, \theta_L)'$, and/ortransmission, $\boldsymbol{\theta}^H = (a_1, a_2)'$, which are analogues in our model of the CFR and $\mathcal{R}_t$ in Section 4.7.1, the two central features of infectious diseases captured in epidemiological frameworks. The first exercise considers diseases with different combinations of transmission and mortality parameters. The second exercise seeks to understand the role of the timing of mortality relative to infection by varying the components of $\boldsymbol{\theta}^M$ while keeping the sum constant. The third exercise approximates various modes of transmission by varying the magnitudes of the components of $\boldsymbol{\theta}^H$ while keeping the sum fixed. We use the superscript " $\widehat{\cdot}$ " to refer to values from our estimation (e.g., $\widehat{\theta}_1 = 0.3552$ from Figure 2) and " $\widetilde{\cdot}$ " to the counterfactual values under a comparative statics exercise. Appendix C.4 details our methods and presents additional results.

Comparative statics exercise 1: Varying the magnitudes of $\boldsymbol{\theta}^M$ and $\boldsymbol{\theta}^H$. Our first comparative statics exercise varies both the mortality and transmissibility parameters, $\boldsymbol{\theta}^M$ and $\boldsymbol{\theta}^H$. For example, measles is highly contagious but has a low fatality rate, while Ebola has the opposite characteristics. We consider the influence of the mortality and transmission channels individually, as well as interactions between them, on mortality. This exercise relates to the analysis in Section 4.7.1 in that both vary measures of mortality and transmissibility. Whereas Section 4.7.1 focused on the empirical relationship between the MCFR and measures of mortality and transmissibility, here we perform comparative statics on those variables using our model.

Specifically, we vary the sum of $\widetilde{\boldsymbol{\theta}}^M$ and $\widetilde{\boldsymbol{\theta}}^H$ while holding the ratio of each of their components the same as those in our baseline estimates. Formally, we define $\widetilde{\theta}_{\text{sum}} = \widetilde{\theta}_1 + \widetilde{\theta}_2 + \widetilde{\theta}_3 + \widetilde{\theta}_4 + \widetilde{\theta}_5$ and $\widetilde{a}_{\text{sum}} = \widetilde{a}_1 + \widetilde{a}_2$, we vary $\widetilde{\theta}_{\text{sum}}$ and $\widetilde{a}_{\text{sum}}$ by scaling $\widehat{\boldsymbol{\theta}}^M$ and $\widehat{\boldsymbol{\theta}}^H$ up or down by constants.[47] For each scenario of counterfactual parameters, we consider a pair $(\widetilde{\theta}_{\text{sum}}, \widetilde{a}_{\text{sum}})$. Figure 11 illustrates the relationship between $(\widetilde{\theta}_{\text{sum}}, \widetilde{a}_{\text{sum}})$ and the counterfactual MCFR averaged across all counties and weeks, for instance, $\widetilde{\text{MCFR}}_{(\cdot,\cdot)\mapsto(\mathcal{N},\Sigma L^*)} =$

[47] Mathematically, we set $\widetilde{\theta}_l = \frac{\widehat{\theta}_l}{\sum_{l'=1}^{L} \widehat{\theta}_{l'}} \cdot \widetilde{\theta}_{\text{sum}}$ for $l = 1, \cdots, L$, and $\widetilde{a}_k = \frac{\widehat{a}_k}{\widehat{a}_1 + \widehat{a}_2} \cdot \widetilde{a}_{\text{sum}}$ for $k = 1, 2$.

$\frac{1}{nT}\sum_{i=1}^{n}\sum_{t=1}^{T}\widetilde{\text{MCFR}}_{(\cdot,\cdot)\mapsto(\mathcal{N},\Sigma L^*)}$ in panel (a). The MCFR in this comparative static exercise refers to such averages, unless noted otherwise. Because the simulated estimates are somewhat irregular, we use polynomial smoothing.

Figure 11: Counterfactual MCFR under various parameter values $(\widetilde{\theta}_{\text{sum}}, \widetilde{\alpha}_{\text{sum}})$

(a) National level MCFR (in blue) and $\text{MCFR}^{\text{Direct}}$ in the focal county

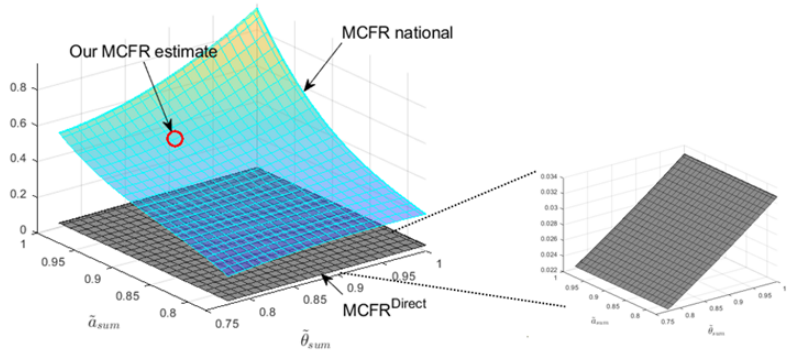

(b) Focal county (c) Counties in the same state (d) Counties in different states

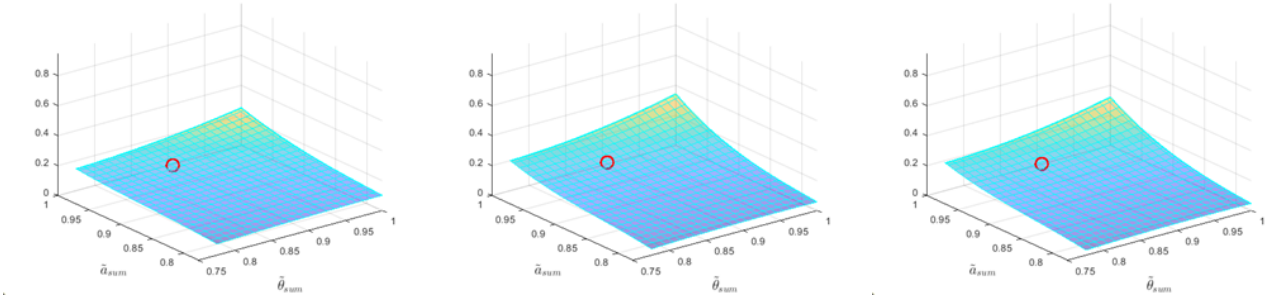

Notes: For all panels, the z-axis gives the counterfactual MCFR from each combination of $(\widetilde{\theta}_{\text{sum}}, \widetilde{\alpha}_{\text{sum}})$. Panel (a) plots the national $\text{MCFR}_{(i,t)\mapsto(\mathcal{N},\Sigma L^*)}$ in blue and the $\text{MCFR}^{\text{Direct}}_{(i,t)\mapsto(i,\Sigma L^*)}$ among the initially infected individuals in the focal county in grey. Panels (b), (c), and (d) plot the MCFR in the origin county ($\text{MCFR}_{(i,t)\mapsto(i,\Sigma L^*)}$), the MCFR in the state in which the focal county is located ($\text{MCFR}_{(i,t)\mapsto(\mathcal{S}_{s(i)}\setminus\{i\},\Sigma L^*)}$), and the MCFR in other states ($\text{MCFR}_{(i,t)\mapsto(\mathcal{N}\setminus\mathcal{S}_{s(i)},\Sigma L^*)}$), respectively. All panels show the MCFR averaged across counties and weeks, for instance, $\widetilde{\overline{\text{MCFR}}}_{(\cdot,\cdot)\mapsto(\mathcal{N},\Sigma L^*)} = \frac{1}{nT}\sum_{i=1}^{n}\sum_{t=1}^{T}\widetilde{\text{MCFR}}_{(\cdot,\cdot)\mapsto(\mathcal{N},\Sigma L^*)}$ in panel (a). The red circle in each plot denotes the MCFR based on our estimated parameters.

The red circles in the figure give the MCFR based on our estimated parameters. A disease with a higher fatality rate but a lower transmissibility (e.g., an "Ebola-type" profile) would have its MCFR in the area to the southeast of the COVID-19 estimate, while a disease with the opposite characteristics (e.g., a "measles-type" with a lower fatality rate and a higher transmissibility) would have its MCFR in the northwest area.

Figure 11 illustrates why the MCFR is indispensable when examining fatality and transmission rates jointly. We find a strong complementarity between $\widetilde{\theta}_{\text{sum}}$ and $\widetilde{\alpha}_{\text{sum}}$ in their relationships to the MCFR. The relationship between one of the parameters and the MCFR becomes more convex as the other parameter increases.[48] Intuitively, when both parameters are large, cases propagate more strongly and each newly transmitted case gen-

[48] Figure C.14 in Appendix C.4 more clearly shows this relationship. For instance, $\text{MCFR}_{(i,t)\to(\mathcal{N},\Sigma L^*)}$ as a function of $\widetilde{\theta}_{\text{sum}}$ is flatter and more linear when $\widetilde{\alpha}_{\text{sum}}$ is small and becomes steeper and more exponential when $\widetilde{\alpha}_{\text{sum}}$ approaches 1.

erate greater mortality, yielding substantial downstream mortality. Moreover, when both $\widetilde{\theta}_{\text{sum}}$ and $\widetilde{a}_{\text{sum}}$ are close to one, the MCFR increases rapidly, indicating "increasing return to scale". Doubling the parameters more than doubles the MCFR.

The MCFR is unsurprisingly more convex in $\widetilde{a}_{\text{sum}}$ than it is in $\widetilde{\theta}_{\text{sum}}$ because the former functions like a multiplier in the transmission process. A larger $\widetilde{a}_{\text{sum}}$ not only increases initial transmission from week t to $t+1$, but also case transmission indefinitely. The relationship between $\text{MCFR}_{(i,t)\to(\mathcal{N},\Sigma L^*)}$ and $\widetilde{a}_{\text{sum}}$ is relatively steep at low values of $\widetilde{\theta}_{\text{sum}}$ and becomes more convex as $\widetilde{\theta}_{\text{sum}}$ increases. In contrast, the relationship between the MCFR and $\widetilde{\theta}_{\text{sum}}$ is less convex as the latter only affects the terminal mortality process. The insights from this exercise, in particular on the interaction between $\widetilde{\theta}_{\text{sum}}$ and $\widetilde{a}_{\text{sum}}$ are difficult to derive separately from the CFR and $\mathcal{R}_t$.

This exercise also highlights the contexts in which the MCFR tends to add the most value relative to traditional epidemiological measures. Panel (a) additionally plots the $\text{MCFR}^{\text{Direct}}_{(i,t)\mapsto(i,\Sigma L^*)}$ among initially infected individuals in the focal county. $\text{MCFR}^{\text{Direct}}_{(i,t)\mapsto(i,\Sigma L^*)}$ increases in $\widetilde{\theta}_{\text{sum}}$ but is flat with respect to the $\widetilde{a}_{\text{sum}}$ because it is not a function of the latter. A side figure reproduces $\text{MCFR}^{\text{Direct}}_{(i,t)\mapsto(i,\Sigma L^*)}$ in a different scale and illustrates this relationship more clearly.

The gap between the $\text{MCFR}_{(i,t)\to(\mathcal{N},\Sigma L^*)}$ at the national level and the $\text{MCFR}^{\text{Direct}}_{(i,t)\mapsto(i,\Sigma L^*)}$, which we take as a proxy for the CFR, widens at larger values of $\widetilde{a}_{\text{sum}}$ and, to a lesser extent, $\widetilde{\theta}_{\text{sum}}$. This divergence stems from increased downstream transmission at larger values of $\widetilde{a}_{\text{sum}}$. These findings indicate that the MCFR framework is likely to be particularly critical in characterizing infectious diseases with high transmissibility like COVID-19. At our parameter estimates, $\text{MCFR}_{(i,t)\to(\mathcal{N},\Sigma L^*)}$ is roughly 20 times the size of the CFR. While a highly infectious disease would also be evaluated using the $\mathcal{R}_t$ in addition to the CFR, it is unclear how to combine the two to quantify increased mortality from downstream cases. This exercise underscores the information the MCFR captures beyond traditional epidemiological measures.

Furthermore, larger values of $\widetilde{a}_{\text{sum}}$ lead to greater externalities in terms of mortality occurring outside the focal county, as shown in the bottom panels of Figure 11. As $\widetilde{a}_{\text{sum}}$ increases, $\text{MCFR}_{(i,t)\to(\mathcal{S}_{s(i)}\setminus\{i\},\Sigma L^*)}$ and $\text{MCFR}_{(i,t)\to(\mathcal{N}\setminus\mathcal{S}_{s(i)},\Sigma L^*)}$ increase at a faster rate than $\text{MCFR}_{(i,t)\mapsto(i,\Sigma L^*)}$. Consequently, the shares of the national MCFR arising in other counties in the original state, $\text{MCFR}_{(i,t)\to(\mathcal{S}_{s(i)}\setminus\{i\},\Sigma L^*)}$, and in other states, $\text{MCFR}_{(i,t)\to(\mathcal{N}\setminus\mathcal{S}_{s(i)},\Sigma L^*)}$ increase, while the share in the origin county, $\text{MCFR}_{(i,t)\mapsto(i,\Sigma L^*)}$, decreases. Intuitively, as transmissibility increases so does geographic spread. In contrast, as $\widetilde{\theta}_{\text{sum}}$ increases, the total MCFR also increases but the geographic shares stay roughly constant. Again, this result arises because $\widetilde{\theta}_{\text{sum}}$ governs the strength of the end-stage mortality process conditional on spread. Figure C.15 in Appendix C.4 decomposes the national MCFR into its geographic components and shows how they vary as a function of $\widetilde{\theta}_{\text{sum}}$ and $\widetilde{a}_{\text{sum}}$.

Comparative statics exercise 2: Varying the components of $\boldsymbol{\theta}^M$. Our second exercise examines the effect of different distributions of the components of $\widetilde{\boldsymbol{\theta}}^M$ on the time path of mortality. This exercise is intended to capture the fact that some conditions lead to death relatively quickly while others operate more slowly. For instance, cholera can lead to severe dehydration and death within hours if untreated (WHO, 2024). By contrast, tuberculosis can have a prolonged course, with symptoms developing slowly and the potential for latent infection

lasting years (CDC, 2025; WHO, 2025). As above, our attempt is less to model specific conditions than to show how our model operates when the underlying parameters are altered in ways that broadly reflect other diseases.

In this exercise, we condition on $\widetilde{\theta}_{\text{sum}} = \widehat{\theta}_{\text{sum}}$ from our estimates. We explore two scenarios:

- Scenario 1 – Rapid mortality: $\widetilde{\theta}_1 = \frac{9}{10}\widehat{\theta}_{\text{sum}}$ and $\widetilde{\theta}_2 = \widetilde{\theta}_3 = \widetilde{\theta}_4 = \widetilde{\theta}_5 = \frac{1}{40}\widehat{\theta}_{\text{sum}}$.
- Scenario 2 – Slow mortality: $\widetilde{\theta}_1 = \widetilde{\theta}_2 = \widetilde{\theta}_3 = \widetilde{\theta}_4 = \frac{1}{40}\widehat{\theta}_{\text{sum}}$ and $\widetilde{\theta}_5 = \frac{9}{10}\widehat{\theta}_{\text{sum}}$.

Figures in Appendix C.4 illustrate these mortality paths.

We calculate the counterfactual aggregate mortality at the national level under each scenario above and compare its dynamics to that of the realized mortality in 2020, as shown in Figure 12. Scenario 1 shows a faster response to increased cases than actual mortality, which is not surprising because placing more weight on θ_1 relative to θ_2 through θ_5 leads to faster mortality than the baseline. On the other hand, Scenario 2 shows a delayed response to increased (and decreased) cases.[49]

Figure 12: Dynamics of mortality across different scenarios

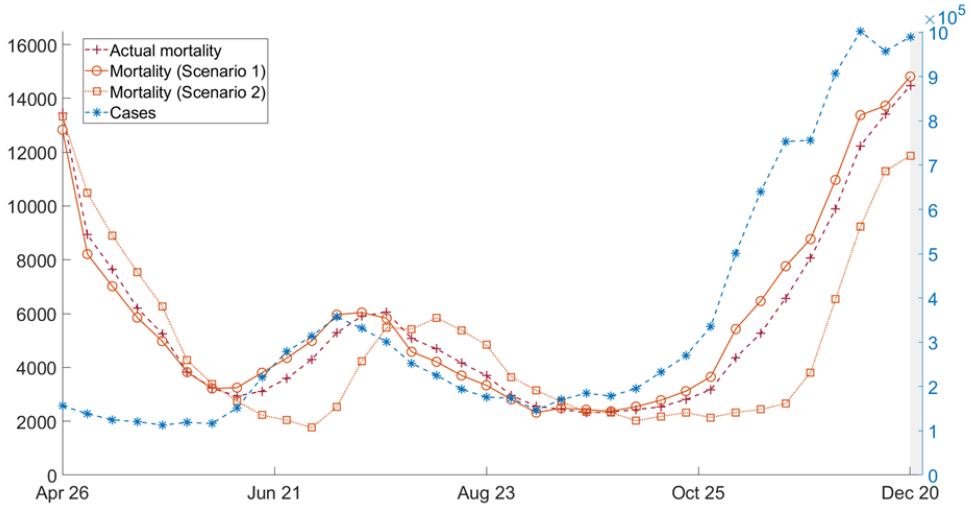

Notes: The three red lines show the dynamics of aggregate mortality at the national level, one gives realized mortality while the other two give mortality under the two counterfactual scenarios. The blue line plots realized cases.

Section 4.5 shows that the lockdown stringency tends to lag cases and seems to track mortality more than the MCFR or anticipated cases. Thus, if policy is assumed to be particularly responsive to mortality, under Scenario 2, in which mortality is realized with a relatively long lag, it seems possible that policy might operate with an even greater lag.

Comparative statics exercise 3: Varying the components of θ^H. Infectious diseases also differ in transmission dynamics. While COVID-19 and many other infectious diseases (e.g., chickenpox and measles) are transmitted largely through respiration, other conditions are transmitted through physical contact with an infected person or object (e.g., Methicillin-resistant Staphylococcus aureus (MRSA)), contact with body fluids

[49] Figure C.17 in Appendix C.4 compares the path of mortality across weeks generated from an additional case in week t (i.e., $\text{MCFR}_{(i,t)\to(i,t+l)}$) based on our estimates and for the two scenarios.

(e.g., Ebola), or intimate contact. Our model does not directly address the biological mechanism through which the disease is spread. Rather, we model disease transmission through our two propagation parameters, which govern local (a_1) and regional (a_2) propagation. Different modes of transmission can be captured (in a reduced form manner) via these parameters. Thus, for a given overall level of transmissibility, a disease that is transmitted through closer contact, such as bodily fluids or intimate contact, likely has a higher a_1 relative to a_2 than a condition that is transmitted through respiration. This is because the level of contact necessary for transmission is more likely to occur among people who have pre-existing relationships and are more likely to be geographically proximate. (We acknowledge that this is a pattern rather than a universal rule as distant contacts may travel to interact with an infected person and bring the infection back to their home.) Our third comparative statics exercise examines the roles of local versus regional propagation for mortality and externalities conditional on the overall level of transmissibility (i.e., the sum of a_1 and a_2).

Figure 13 illustrates the counterfactual MCFR under different values of a_1 and a_2. We take the MCFR averaged across counties and calendar weeks (e.g., $\overline{\widetilde{\text{MCFR}}}_{(\cdot,\cdot)\to(\cdot,\Sigma L^*)} = \frac{1}{nT}\sum_{i=1}^{n}\sum_{t=1}^{T}\widetilde{\text{MCFR}}_{(i,t)\to(i,\Sigma L^*)}$) in the focal county represented by the red area in the figure). As expected, the effects of the marginal case on mortality outside the county in which the focal case originated increase as a_2 grows relative to a_1. A high relative a_1 leads to higher mortality mostly stemming from local propagation, while high mortality can also be generated when a_2 is relatively high (in this case, the main source of mortality is external to the origin county). Total mortality is slightly hump-shaped in the relative values of a_1 and a_2 and it is noteworthy that our estimated value of a_1 relative to a_2 for COVID-19 falls near the global minimum of mortality. Thus, for the same overall level of transmissibility, but with slightly more or less across-region transmission, mortality might well have been slightly higher.

4.8 Empirical relation to epidemiology measures

Our empirical framework is built on the finite distributed-lag and spatial dynamic panel data models that are widely used with well-understood features, which allows us to confidently derive the properties of the MCFR and relate them to well-established epidemiology frameworks. Sections 4.2 - 4.4 show that the MCFR components can be separated into direct-mortality, propagation, and non-COVID-19 elements whereas the previous section examines how the MCFR relates jointly to fatality and disease transmission measures. Here, we relate each MCFR component to conventional measures —CFR and its modification, the SCFR,—as well as $\mathcal{R}_t$ calculated within our own epidemiological framework. This side-by-side comparison demonstrates that the MCFR is empirically consistent with existing measures and that it provides additional insights.

Fatality rates. Figure 14 shows the CFR, SCFR, and $\text{MCFR}^{\text{Direct}}_{(i,t)\mapsto(i,\Sigma L)}$ at the national level. In each calendar week t, we evaluate the average $\text{MCFR}^{\text{Direct}}_{(i,t)\mapsto(i,\Sigma L)}$ across counties (i.e., $\overline{\text{MCFR}}^{\text{Direct}}_{(\cdot,t)\to(\cdot,\Sigma L^*)} = \frac{1}{n}\sum_{i=1}^{n}\text{MCFR}^{\text{Direct}}_{(i,t)\to(i,\Sigma L^*)}$). The MCFR in this subsection refers to national averages, unless noted otherwise. There are a few things to note in this comparison. First, the magnitudes of the three measures are comparable, suggesting that our estimate of the $\text{MCFR}^{\text{Direct}}_{(i,t)\mapsto(i,\Sigma L)}$ is reasonable and captures mortality conditional on be-

Figure 13: Mortality and local versus regional transmission

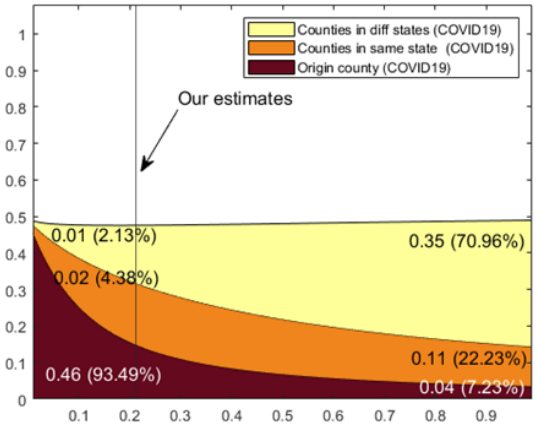

Notes: This figure examines the relative importance of regional relative to local transmission and plots the counterfactual MCFR (y-axis) across different values of $\frac{a_2}{a_1}$ (x-axis). The values of θ_{sum} and $\widetilde{a}_{\text{sum}}$ are set to be the same as the estimated parameters. The national $\text{MCFR}_{(i,t)\mapsto(\mathcal{N}\setminus\mathcal{S}_{s(i)},\Sigma L^*)}$ are decomposed into mortality in the focal county, $\text{MCFR}_{(i,t)\mapsto(i,\Sigma L^*)}$ (in red), mortality in other counties in the same state, $\text{MCFR}_{(i,t)\mapsto(\mathcal{S}_{s(i)}\setminus\{i\},\Sigma L^*)}$ (in orange), and mortality in other states, $\text{MCFR}_{(i,t)\mapsto(\mathcal{N}\setminus\mathcal{S}_{s(i)},\Sigma L^*)}$ (in yellow). For each $\frac{a_1}{a_2}$, we evaluate the average MCFR across counties and calendar weeks (e.g., $\overline{\widetilde{\text{MCFR}}}_{(\cdot,\cdot)\to(\cdot,\Sigma L^*)} = \frac{1}{nT}\sum_{i=1}^{n}\sum_{t=1}^{T}\widetilde{\text{MCFR}}_{(i,t)\to(i,\Sigma L^*)}$). The reported numbers (and the corresponding percentages) show implied mortality in each case when $\frac{a_2}{a_1} = 0.01$ and $\frac{a_2}{a_1} = 0.99$. This figure is generated with $L^* = 16$. Appendix Figure C.18 shows a similar result with $L^* = 51$.

ing infected as intended. Across our study period, the means of SCFR and $\text{MCFR}^{\text{Direct}}_{(i,t)\mapsto(i,\Sigma L)}$ were 0.0179 and 0.0262, respectively, while the CFR at the end of the period was 0.0210.[50]

Figure 14: Comparison of CFR, SCFR, and $\text{MCFR}^{\text{Direct}}_{(i,t)\mapsto(i,\Sigma L^*)}$

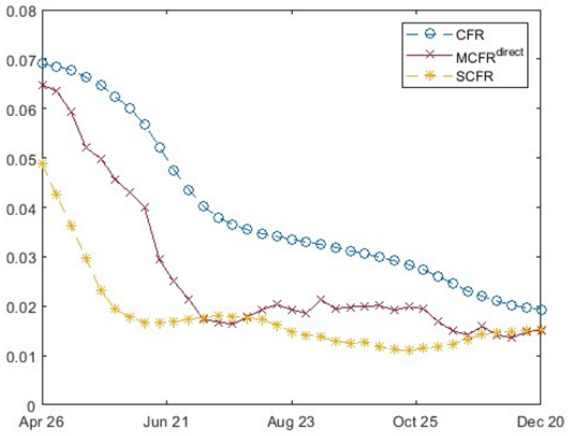

Notes: This figure shows the case fatality rate (CFR), short-run case fatality rate (SCFR), and $\text{MCFR}^{\text{Direct}}_{(i,t)\mapsto(i,\Sigma L^*)}$ at the national level using the counties in our sample. We calculate the mean $\text{MCFR}^{\text{Direct}}_{(i,t)\mapsto(i,\Sigma L^*)}$ in each week t across all counties, that is, $\overline{\text{MCFR}}^{\text{Direct}}_{(\cdot,t)\to(\cdot,\Sigma L)} = \frac{1}{n}\sum_{i=1}^{n}\text{MCFR}^{\text{Direct}}_{(i,t)\mapsto(i,\Sigma L)}$.

[50] See Section 2.3 and footnote 35 on the appropriate statistics when comparing the CFR to the $\text{MCFR}^{\text{Direct}}_{(i,t)\mapsto(i,\Sigma L)}$.

Second, while the CFR, SCFR, and $\text{MCFR}^{\text{Direct}}_{(i,t)\mapsto(i,\Sigma L)}$ all trend downward over time, only the SCFR and $\text{MCFR}^{\text{Direct}}_{(i,t)\mapsto(i,\Sigma L)}$ exhibit substantial short-term fluctuations, so they reflect more information about mortality in specific periods than the smoothly declining CFR. This difference reflects the fact that the $\text{MCFR}^{\text{Direct}}_{(i,t)\mapsto(i,\Sigma L)}$ exhibits substantial short-term fluctuations, so that it reflects more information about mortality in specific periods than the smoothly declining CFR. This difference reflects the fact that the $\text{MCFR}^{\text{Direct}}_{(i,t)\mapsto(i,\Sigma L)}$ and SCFR capture the current mortality rate, while the CFR estimates overall mortality since the origin of the disease. The CFR declines both because a disease outbreak tends to initially claim the lives of vulnerable people (e.g., individuals with chronic conditions) and because treatments are not well established leading to an initial high fatality rate (Verity et al., 2020; Ioannidis, 2021), although viruses may mutate to become more or less deadly. As medical providers developed better strategies to diagnose and treat the disease, the fatality rate decreased. Another statistical artifact contributing to a declining CFR is the shortage of COVID-19 tests at the beginning of the pandemic, which led to an undercount of cases and an overestimate of the case fatality rate. As access to COVID-19 tests increased, the measured case fatality rate decreased. Since the CFR is a ratio of cumulative mortality and cases from the start of the pandemic, these factors suggest that the CFR should steadily decline and possibly converge to a steady state value (in the absence of different disease variants that may have higher mortality rates). In contrast, the SCFR and $\text{MCFR}^{\text{Direct}}_{(i,t)\mapsto(i,\Sigma L)}$ vary more temporally as they capture the relationship between cases and mortality over shorter time horizons (i.e., within L weeks) and are not affected by values of cases and mortality from early periods. We calculate that the standard deviations of SCFR, $\text{MCFR}^{\text{Direct}}_{(i,t)\mapsto(i,\Sigma L)}$ and CFR are 0.0129, 0.0305, and 0.0088, respectively. Thus, both the SCFR and $\text{MCFR}^{\text{Direct}}_{(i,t)\mapsto(i,\Sigma L)}$ exhibit richer temporal and regional variation than the CFR.

Disease transmission. As introduced in Section 2.3, our framework generates a marginal measure of disease transmission, $\frac{\partial \text{case}_{j,t+1}}{\partial \text{case}_{i,t}} = [\mathbf{A}]_{ij} \cdot \frac{\text{case}_{j,t+1}}{\text{case}_{i,t}}$ that is integral to the MCFR, particularly its components that incorporate case propagation, such as the $\text{MCFR}^{\text{Prop}}_{(i,t)\mapsto(i,t+1)}$. We find that an additional case generates, on average, 0.8736 new cases in the same county in the following week (i.e., the average of $\frac{\partial \text{case}_{i,t+1}}{\partial \text{case}_{i,t}}$), and 1.2095 new cases nationwide (i.e., the average of $\sum_{j=1}^{n} \frac{\partial \text{case}_{j,t+1}}{\partial \text{case}_{i,t}}$), implying that 28% of case transmission represents cross-county spillovers. This highlights the importance of regional transmission, ultimately resulting in 0.3268 COVID-19 deaths outside the focal county (Figure 5 (a)).

We compare our measure of marginal disease transmission to $\mathcal{R}_t$. Since $\mathcal{R}_t$ is inherently model-specific, we evaluate our own $\mathcal{R}_t$ in a Susceptible-Infectious-Deceased (SID) model that is close to our empirical setup. Our SID model incorporates two crucial features in our framework: (i) time-varying transmissibility and (ii) externalities from dynamic spatial transmissions. Following Pesaran and Yang (2022), the SID model allows for multiple groups (counties), with regional transmission modeled similarly to our spatial dynamic panel data approach. We then evaluate $\hat{\mathcal{R}}_t$ by plugging in $\hat{a}_1$ and $\hat{a}_2$, as the upper bound on the number of secondary cases generated by an initial infection (see Appendix C.5 for details).[51]

[51] $\hat{\mathcal{R}}_t$ is derived from the epidemiological model's system and reflects the system's potential infections from an extra case in a county at time t (see Heffernan, Smith and Wahl (2005)). The state-level time-varying reproduction number, $\mathcal{R}_{S,t}$ for state S, in Table 5 corresponds to the diagonal element of $\mathbf{G}(t)$ when a geographic unit is a state (instead of a county). Given that our model incorporates time-varying features through our log-log specification, the corresponding next-generation matrix, $\mathbf{G}(t)$, varies over time as well. Con-

Panel (a) of Figure 15 plots the $\text{MCFR}^{\text{Direct}}_{(i,t)\mapsto(i,\Sigma L^*)}$, $\text{MCFR}^{\text{Prop}}_{(i,t)\mapsto(i,\Sigma L^*)}$, $\text{ACMCFR}_{(i,t)\mapsto(\mathcal{N},\Sigma L^*)}$, and $\hat{\mathcal{R}}_t$ at the national level. We take the means across counties in which the focal case originates (e.g., $\overline{\text{ACMCFR}}_{(\cdot,t)\mapsto(\mathcal{N},\Sigma L^*)} = \frac{1}{n}\sum_{i=1}^{n}\text{ACMCFR}_{(i,t)\mapsto(\mathcal{N},\Sigma L^*)}$). Our estimate for $\hat{\mathcal{R}}_t$ (mean=1.7564) aligns with reproduction numbers from the literature, which range between 1 and 5 (Al-Raeei, 2021; Chinazzi et al., 2020; Li et al., 2020; Liu et al., 2020; Park et al., 2020; Salje et al., 2020; Fernández-Villaverde and Jones, 2022).

Figure 15: Comparison of the MCFR, transmission rate, and counts of cases and deaths

(a) The MCFR and the transmission rate

(b) Counts of cases and mortality

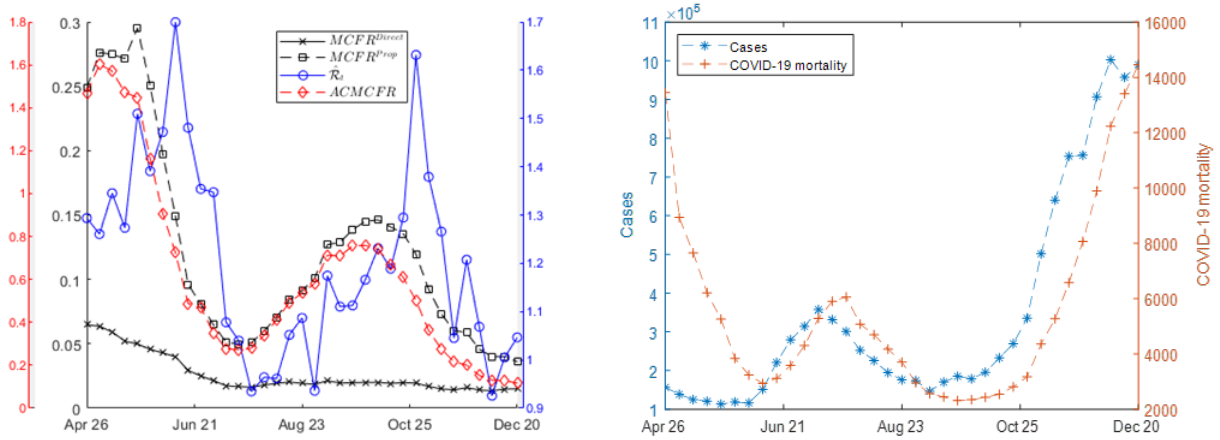

Notes: Panel (a) plots four series at the national level: the number of secondary cases generated by an initial infection in each week (denoted by $\hat{\mathcal{R}}_t$) estimated from our own Susceptible-Infectious-Deceased (SID) model, the $\text{MCFR}^{\text{Direct}}_{(i,t)\mapsto(i,\Sigma L^*)}$, the $\text{MCFR}^{\text{Prop}}_{(i,t)\mapsto(i,\Sigma L^*)}$, and the $\text{ACMCFR}_{(i,t)\mapsto(\mathcal{N},\Sigma L^*)}$. The MCFRs refer to average across all counties in our sample (e.g., $\overline{\text{MCFR}}^{\text{Direct}}_{(\cdot,t)\mapsto(\cdot,\Sigma L^*)} = \frac{1}{n}\sum_{i=1}^{n}\text{MCFR}^{\text{Direct}}_{(i,t)\mapsto(i,\Sigma L^*)}$). Panel (b) plots the total counts of cases and COVID-19 deaths across all counties in our sample (i.e., $\sum_{i=1}^{n}\text{case}_{i,t}$ and $\sum_{i=1}^{n}\text{mortality}_{i,t}$).

There are a couple of reasons why our $\hat{\mathcal{R}}_t$ is at the lower end of the range in the literature, a finding that we believe is sensible. First, our $\hat{\mathcal{R}}_t$ covers the period between April and December 2020, while the larger estimates of $\mathcal{R}_t$ tend to come from the earlier period of the pandemic when transmission may have been substantially higher. While such high estimates may hold early in the pandemic, they are not credible long-term. Thus, even with a moderate $\mathcal{R}_t$ of 2 throughout 2020, exponential growth would predict that $\sum_{t=1}^{49} 2^{t-1} \simeq 5.63 \times 10^{14}$ individuals would be infected by the end of our study period. Moreover, a consistently large $\mathcal{R}_t$ is also implausible because there are extended periods when the number of cases declines, which implies that $\mathcal{R}_t$ must be below 1, at least in those periods. A reasonable model requires time-varying transmissibility that is not consistently 'explosive'. In a compartmental model, $\mathcal{R}_t$ must also eventually decrease because of the shrinking susceptible population. At the same time, our $\hat{\mathcal{R}}_t$ does a reasonable job of matching existing estimates of the time path of $\mathcal{R}_t$. For instance, Fernández-Villaverde and Jones (2022) find that R_t increases in May and that our estimates of $\hat{\mathcal{R}}_t$ approach 2 around early May 2020, significantly higher than the average for our entire period.[52]

sequently, $\hat{\mathcal{R}}_t$ is dynamic, offering insights into the temporal implications of the MCFR. In Appendix C.5, we also discuss other statistics from $\mathbf{G}(t)$ such as diagonal elements of $\mathbf{G}(t)$.

[52] At the same time, the $\hat{\mathcal{R}}_t$ values around April and May 2020 are at the higher end of existing estimates (Katul et al., 2020; Sanche et al., 2020; Ke et al., 2021; Korolev, 2021; Chudik, Pesaran and Rebucci, 2022; Johnsson, Pesaran and Yang, 2023), as we account

The second reason why our estimate of $\hat{\mathcal{R}}_t$ should be at the low end of estimates is that our $\hat{\mathcal{R}}_t$ is a marginal measure of disease transmission, while the traditional $\mathcal{R}_t$ represents the total or average impact of a case. (Our analysis of the total impact can be found in Appendix C.5.) There are some tradeoffs between our approach and the compartmental model. The standard compartmental model does not include incidental components, which we include to improve our model's ability to fit observed data on disease spread (e.g., by addressing unobservable factors, like behavioral changes across places and times). However, the inclusion of these incidental components means that some portion of disease transmission is explained by them. Therefore, a small number of cases (1.432 cases per county per week or 0.62% of all cases) are explained by these incidental components, resulting in lower $\hat{\mathcal{R}}_t$. Ultimately, the value of $\hat{\mathcal{R}}_t$ is an empirical one. Our approach imposes no constraints on the transmission parameters. Rather, these are estimated from the data based on the model specification, as justified in Appendix A.1.

Panel (a) of Figure 15 also shows that $\hat{\mathcal{R}}_t$ displays dynamic patterns mirroring those of the $\text{MCFR}^{\text{Prop}}$ and ACMCFR, although they slightly precede $\hat{\mathcal{R}}_t$ because they reflect disease transmission over a longer period (i.e., the next 16 weeks) while $\hat{\mathcal{R}}_t$ represents the contemporaneous spread of infections. We next compare these temporal patterns with those of realized cases and mortality in Panel (b) of Figure 15. Measures incorporating case transmission rise and peak before an outbreak. For instance, during the summer 2020 outbreak, cases peaked in the week of July 12, with COVID-19 deaths peaking a couple of weeks later. This outbreak was preceded by a spike in the $\text{MCFR}^{\text{Prop}}_{(i,t)\mapsto(i,\Sigma L^*)}$ in the week of May 24, about seven weeks before the peak in cases. The outbreak in the winter of 2020 displays a similar pattern; the $\text{MCFR}^{\text{Prop}}_{(i,t)\mapsto(i,\Sigma L^*)}$ peaks well before the increase in cases. These patterns are not unreasonable given that the $\text{MCFR}^{\text{Prop}}_{(i,t)\mapsto(i,\Sigma L^*)}$ is forward-looking. The $\text{ACMCFR}_{(i,t)\mapsto(\mathcal{N},\Sigma L^*)}$ and $\hat{\mathcal{R}}_t$ follow the same pattern although compared to the $\text{MCFR}^{\text{Prop}}_{(i,t)\mapsto(i,\Sigma L^*)}$, they peak a bit earlier and later, respectively. These patterns further emphasize that the gains from reducing infections are highest before a rise in cases (or deaths), as seen in Figure 8. In contrast, the $\text{MCFR}^{\text{Direct}}_{(i,t)\mapsto(i,\Sigma L^*)}$ (which excludes disease transmission) remains relatively stable, especially after June 2020, as shown in Panel (a). This measure also does not vary temporally as much as the $\text{MCFR}^{\text{Prop}}_{(i,t)\mapsto(i,\Sigma L^*)}$ or $\text{ACMCFR}_{(i,t)\mapsto(\mathcal{N},\Sigma L^*)}$.

5 Robustness

This section probes the robustness of our results with respect to the total number of lags, L, of cases in the mortality equation (1) and the choice of spatial weights. Appendix D contains additional robustness exercises, including those related to the interpolation of mortality data.

5.1 Number of lags in cases, L

In choosing the number of lags (L) of cases in the mortality equation (1), we consider three criteria. First, we rely on epidemiological evidence regarding the duration of the COVID-19 recovery period as previously discussed. Second, we utilize Hannan and Quinn's (1979) information criterion, calculated based on the

for high potential inter-regional transmission early in the pandemic. This underscores the unique contribution of our MCFR framework beyond traditional epidemiological measures, such as $\mathcal{R}_t$, which often overlook transmission across locales.

log-likelihood and adjusted for the degrees of freedom in each specification. For COVID-19 mortality, we evaluate specifications from $L = 1$ to $L = 12$. The criterion decreases substantially from $L = 1$ (29,112.65) to $L = 5$ (25,956.98), indicating improved model fit with additional lags. However, beyond $L = 5$, the criterion stabilizes and slightly increases: values at $L = 6$, $L = 7$, and $L = 8$ are $25,963.29$, $25,973.29$, and $25,977.23$, respectively. Thus, based on this criterion, $L = 5$ emerges as optimal, balancing explanatory power without excessive complexity. For non-COVID-19 mortality, we consider $L = 1$ through $L = 3$. The optimum is at $L = 1$ ($-24,251.11$), as adding further lags slightly worsens the fit ($-24,249.69$ for $L = 2$ and $-24,234.36$ for $L = 3$). Appendix Figure D.25 illustrates these patterns.

Next, we examine the stability of estimated coefficients with varying lag lengths, confirming our earlier conclusion based on the Hannan-Quinn information criterion. Panels (a) and (b) of Figure 16 show that the estimates of θ_l for COVID-19 mortality generally decline as the lag (l) increases, consistent with a diminishing impact of past cases on current mortality. For instance, the estimate of θ_4 is smaller than θ_3 for our main specification (i.e., $L = 5$). An exception to this pattern is the coefficient on the largest lag in a specification (i.e., θ_L) which is sometimes larger than the coefficient on the second-largest lag (i.e., θ_{L-1}).[53]

Importantly, the estimates of the lagged coefficients are largely stable across different lag specifications, except for the largest lag coefficient in each specification. For example, the estimates of θ_1 through θ_4 in the $L = 5$ specification are statistically indistinguishable from their counterparts in specifications with $L \geq 6$. Similarly, the estimates of θ_1 through θ_3 at $L = 5$ are similar to those obtained when $L = 4$. Furthermore, in specifications with $L \geq 7$, estimated coefficients from θ_6 to θ_{12} are not statistically different from zero. These coefficient patterns corroborate our selection of $L = 5$ for COVID-19 mortality.

For non-COVID-19 mortality, the estimates of θ_1 are not statistically different across specifications with different numbers of lags, as shown in Panel (c). Moreover, estimates of θ_2 and θ_3 are not statistically different from zero. These results support setting $L = 1$ in the main specification for non-COVID mortality.

Overall, these patterns in the estimated coefficients closely align with our findings based on the Hannan–Quinn criterion, reinforcing our lag-length choices for both the COVID-19 and non-COVID mortality equations.

5.2 Spatial weights

The spatial weights in the main specification, w_{ij}, are constructed from estimates of population flows based on mobile phone location data, popflow_{ij}, from Kang et al. (2020). This subsection considers two alternative spatial weights. The first alternative weight is based on the 2011-2015 5-Year commuting flows from the American Community Survey (ACS), which captures movements related to respondents' residences and primary workplace locations. The alternative spatial weight, w_{ij}^C, is constructed the same way as the main specification, including row normalization, but we replace popflow_{ij} with estimates of bilateral commuting flows, comflow_{ij},

[53] For instance, in the specification with $L = 3$, θ_3 is larger than θ_2, indicating that the specification with $L = 3$ suffers from some omitted variable bias. This arises because mortality is positively correlated with lagged cases and the various lags of cases themselves are positively correlated. Intuitively, if there is any omitted variable bias due to excluding longer lags, it tends to be more pronounced for the final lag since there is no subsequent lag that could further influence the estimation.

Figure 16: Estimates of coefficient θ_l from equation (1) with different number of lags, L

(a) COVID-19, $L = 1$ through $L = 6$

(b) COVID-19, $L = 7$ through $L = 12$

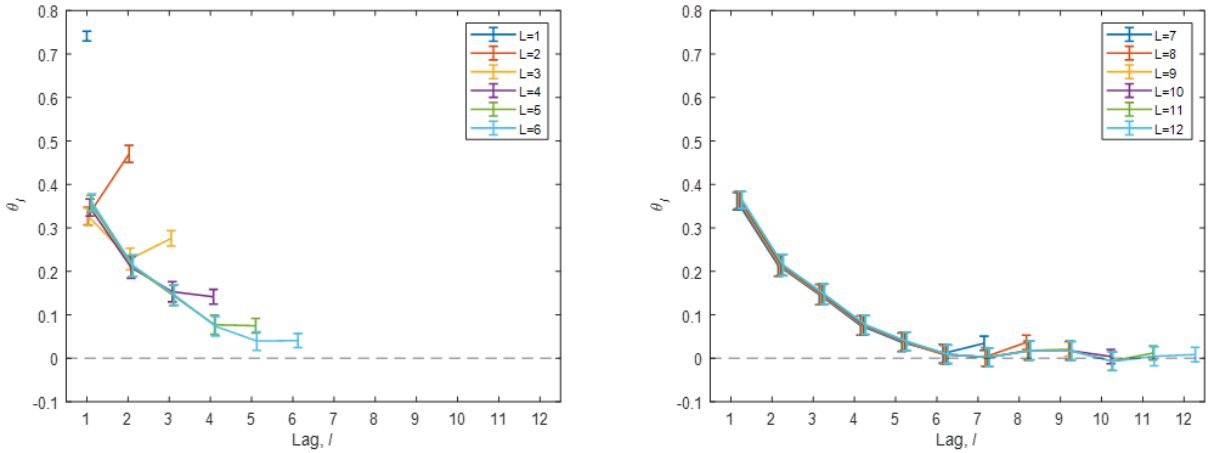

(c) Non-COVID-19, $L = 1$ through $L = 3$

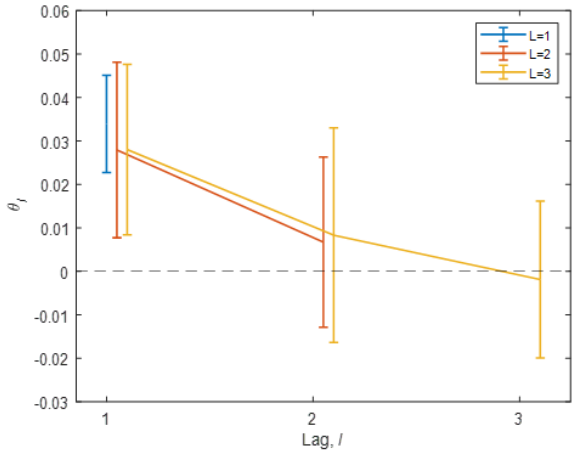

Notes: This figure compares the estimated coefficient θ_l on the lag of log-cases, $h_{i,t-1}$ from various specifications of the mortality equation (1) that differ in the numbers of lags, L. Panel (a) shows the estimates for COVID-19 mortality for specifications with $L = 1$ through $L = 6$, panel (b) for $L = 7$ through $L = 12$, and panel (c) for non-COVID mortality. All specifications have the same covariates as the main specification. The vertical bars denote the 95 percent confidence intervals.

between county j and county i.

The population flows and commuting flows represent different aspects of county networks. Perhaps unsurprisingly, the share of non-zero elements (i.e., network density) when the weighting matrix is defined by population flows is significantly higher (0.9998) than when it is defined using commuting flows (0.2708).[54] Therefore, spatial weights based on the population flows are expected to be a more comprehensive measure of geosocial relations.

The third set of spatial weights is a hybrid of the first and second specifications, where we include two separate spillover effects and estimate separate parameters on each. In this model, we use the commuting flows to generate the weights for county pairs with non-zero commuting flows. For county pairs with zero commuting flows (i.e., $w_{ij}^C = 0$), we use a separate weighting matrix based on the population flows (i.e., a modification of our main specification, w_{ij}). Formally, we define w_{ij}^M as the row-normalized values of bilateral population flows, $\breve{w}_{ij}$ from the first specification among county pairs that have zero commuting flows.[55] In this case, equation (2) is modified as follows:

$$h_{i,t} = a_1 h_{i,t-1} + a_2^C \sum_{w_{ij}^C \neq 0} w_{ij}^C h_{j,t-1} + a_2^M \sum_{w_{ij}^C = 0} w_{ij}^M h_{j,t-1} + \mathbf{x}_{i,t}^H \boldsymbol{\beta}^H + \zeta_i^H + \tau_t^H + e_{i,t}^H.$$

Figure 17 shows estimates of the coefficients on case transmission in a focal county, $\hat{a}_1$, and across counties, $\hat{a}_2$, for different spatial weights. Coefficient $\hat{a}_1$ is similar across the specifications. This is reassuring as the spatial weights govern case transmission across counties, while a_1 governs within-county transmission.

There is greater variation in the coefficients on cross-county transmission, $\hat{a}_2$. The specification based on population flows has a larger estimate (0.2007) than that based on commuting flows (0.1463), and the difference is statistically significant. Moreover, $\hat{a}_2^C$ in specification 3 is similar to $\hat{a}_2$ in specification 2, which is not surprising since they use the same spatial weights. $\hat{a}_2^M$ is smaller than any $\hat{a}_2$, consistent with the former capturing case transmission between counties that are further apart with zero commuting flows. Appendix D.1.2 contains the full estimation results.

Figure 18 the $\text{ACMCFR}_{(i,t)\to(i,\Sigma L^*)}$ in the focal county and the national-level $\text{ACMCFR}_{(i,t)\to(\mathcal{N},\Sigma L^*)}$ in each specification of spatial weights. As before, we calculate the mean across counties and weeks (e.g., $\overline{\text{ACMCFR}}_{(\cdot,\cdot)\to(\cdot,\Sigma L^*)} = \frac{1}{nT}\sum_{i=1}^{n}\sum_{t=1}^{T}\text{ACMCFR}_{(i,t)\to(i,\Sigma L^*)}$). The MCFRs in this subsection refer to such averages, unless noted otherwise. Consistent with the previous figure, specifications using alternative spatial weights differ from the baseline mainly with respect to the components of the ACMCFR that involve case transmission, particularly across counties.

Panel (a) shows the $\text{MCFR}_{(i,t)\mapsto(i,\Sigma L^*)}$ in the origin county for COVID-19 mortality decomposed into the different channels and the $\text{OCMCFR}_{(i,t)\mapsto(i,\Sigma L^*)}$ for other cause (i.e., non-COVID) mortality. The $\text{MCFR}_{(i,t)\mapsto(i,\Sigma L^*)}$ varies across specifications largely following the size of the estimates of a_1.[56] The most

[54] The network density is the number of non-zero relationship between any two units of geography and is defined by $\frac{\#\{w_{ij}>0\}}{n(n-1)}$.

[55] For the hybrid specification, we construct mutually exclusive weights to clearly separate case transmission among counties between which we observe people commute and transmission between counties that are further apart.

[56] The $\text{MCFR}_{(i,t)\mapsto(i,\Sigma L^*)}$ also includes mortality from cases that propagate across county borders before returning to the origin

Figure 17: Coefficient estimates using various specifications of spatial weights

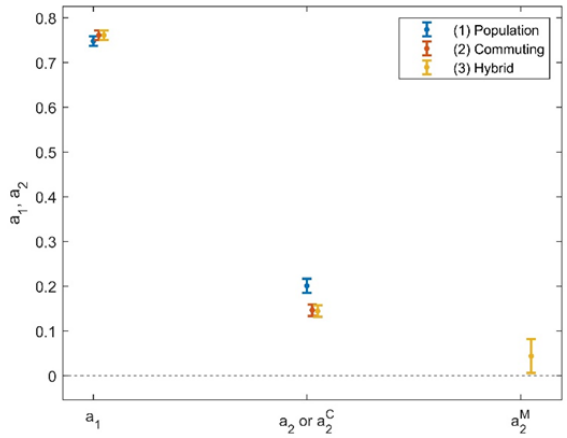

Notes: This figure shows the estimates of the coefficients on the log-cases of the previous week, $h_{j,t-1}$ from equation (2). The different colors refer to specifications using different spatial weights. Specifications 1 and 2 use spatial weights based on the row-normalized values of the bilateral population flows (based on cell phone data) and commuting flows, respectively. Specification 3 is a hybrid of specifications 1 and 2, where we use commuting flows to generate the weights for county pairs with non-zero commuting flows and a separate weighting matrix based on population flows for county pairs with zero commuting flows. The vertical bars indicate the 95 percent confidence intervals. Full estimation results are in Appendix D.1.2.

Figure 18: The ACMCFR under various specifications of spatial weights

(a) Mortality in origin county by causes and channels

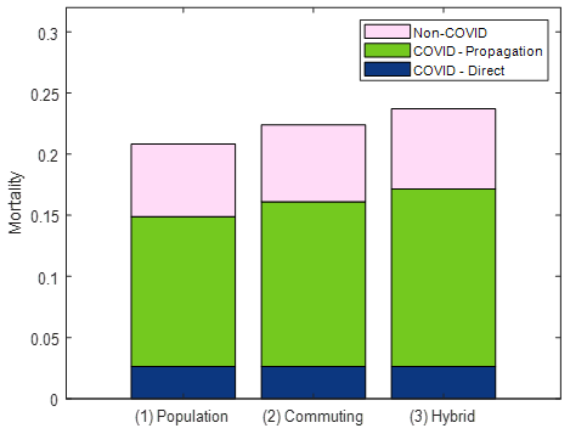

(b) All-cause mortality by location

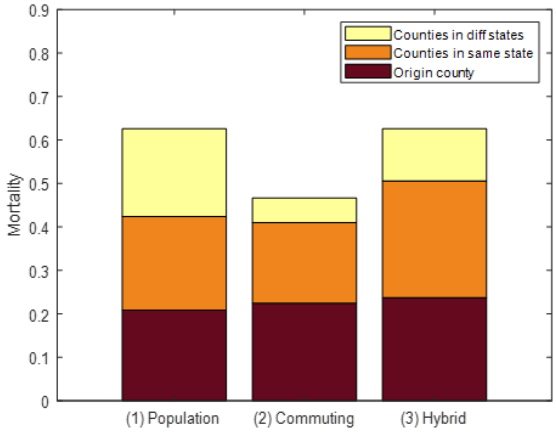

Notes: Panel (a) shows the $\text{ACMCFR}_{(i,t)\mapsto(i,\Sigma L^*)}$ in the origin county, separated into COVID-19 mortality (i.e., $\text{MCFR}_{(i,t)\mapsto(i,\Sigma L^*)}$) further broken down into the direct and propagation channels, and non-COVID mortality (i.e., $\text{OCMCFR}_{(i,t)\mapsto(i,\Sigma L^*)}$). Panel (b) shows the $\text{ACMCFR}_{(i,t)\mapsto(\mathcal{N},\Sigma L^*)}$ at the national level decomposed into different locations. Each vertical bar refers to a specification using different spatial weights. Specifications 1 and 2 use spatial weights based on the row-normalized values of the bilateral population flows (based on cell phone data) and commuting flows, respectively. Specification 3 is a hybrid of specifications 1 and 2, where we use commuting flows to generate the weights for county pairs with non-zero commuting flows and a separate weighting matrix based on population flows for county pairs with zero commuting flows. For each specification, we evaluate the mean across counties and calendar weeks. For instance $\overline{\text{ACMCFR}}_{(\cdot,\cdot)\mapsto(\cdot,\Sigma L^*)} = \frac{1}{nT}\sum_{i=1}^{n}\sum_{t=1}^{T}\text{ACMCFR}_{(i,t)\mapsto(i,\Sigma L^*)}$.

obvious pattern is that the $\text{MCFR}^{\text{Prop}}_{(i,t)\mapsto(i,\Sigma L^*)}$ is larger for the specifications using commuting flows (i.e., specifications 2 and 3). This is mainly because the estimates of a_1 are slightly larger when spillovers are measured using commuting flows instead of population flows (i.e., specification 1). As one would expect, the $\text{OCMCFR}_{(i,t)\mapsto(i,\Sigma L^*)}$ mirrors the propagation channel, with specification 3 having the largest value, followed by specifications 2 and 1. By construction, the $\text{MCFR}^{\text{Direct}}_{(i,t)\mapsto(i,\Sigma L^*)}$ is identical across all specifications because it uses the same estimates $\hat{\theta}_l$ from equation (1). In total, one additional case is estimated to generate between 0.2083 and 0.2371 additional deaths in the origin county within the next 16 weeks.

The differences across specifications are more pronounced in the decomposition of the $\text{ACMCFR}_{(i,t)\to(\mathcal{N},\Sigma L^*)}$ by location, which involves more case transmission than the $\text{MCFR}_{(i,t)\mapsto(i,\Sigma L^*)}$. Given that $\hat{a}_2$ differs more across specifications than $\hat{a}_1$ does, the variation in the $\text{ACMCFR}_{(i,t)\to(\mathcal{N},\Sigma L^*)}$ stems overwhelmingly from mortality outside the focal county, as shown in Panel (b). The magnitude of mortality outside the origin county is positively related to the size of $\hat{a}_2$ and the amount of weight on the off-diagonal terms in the weighting matrix. Marginal mortality outside the focal county in specifications 1 and 3 are similar although their compositions are different. Under specification 1, additional mortality is roughly equal in counties within the same state excluding the focal county (i.e., $\text{MCFR}_{(i,t)\to(\mathcal{S}_{s(i)}\setminus\{i\},t+l)}$) and counties in different states (i.e., $\text{MCFR}_{(i,t)\to(\mathcal{N}\setminus\mathcal{S}_{s(i)},t+l)}$), while specification 3 has a larger share of mortality occurring in the former (43%) than the latter (19%). This pattern can be attributed to specification 3 having a low estimate of a_2^M for counties further away from the focal county. Specification 2 has less mortality occurring outside the focal county, with a larger share in counties in the same state (40%) than in different states (12%). This is consistent with specification 2 having a small estimate of a_2 relative to specification 1 and zero weight on counties outside the commuting area of the focal county, unlike specification 3.

6 Conclusion

Quantifying the impact on aggregate mortality of an additional case of an infectious disease is important for evaluating the costs and benefits of mitigation policies. This paper introduces the marginal case fatality fate (MCFR), a novel measure of the cumulative effect of one additional case on subsequent mortality that incorporates downstream transmission and deaths conditional on infection. This measure innovates over traditional epidemiological metrics such as the case fatality rate (CFR) and the reproduction number, $\mathcal{R}_t$ that separately characterize the fatality rates and transmission of an infectious disease. We operationalize this concept by combining two well-established econometric approaches – finite distributed lag and spatial dynamic panel data models – to model the mortality process and geospatial disease spread. This joint approach captures important features of infectious diseases.

We apply our framework to the early stage of the COVID-19 pandemic and demonstrate how it can characterize aspects of the disease that have so far been unquantified. For instance, we estimate that one additional case generates 0.6255 deaths nationally, 24% of which can be attributed to non-COVID-19 causes, and 70% of which occur outside the county in which the marginal case originates. These results highlight the externalities

county. This subchannel is a function of a_2 but it is quite small.

from an additional infection in terms of spillovers to other causes of deaths and places, which have not been previously studied in a single unified framework. However, despite the large MCFR estimate, we find that the marginal benefits of lockdown policies are modest and vary across states. We also document differences across demographic and socioeconomic groups in the mortality impact of an additional case, which imply that the value of reducing infections might also vary across groups.

Our MCFR framework offers new and deep insights into disease dynamics and can potentially equip policymakers with new tools to guide their decisions. There are numerous epidemiological metrics that characterize the severity of a disease, but many are not directly linked to contemporaneous levels of cases and/or are averages instead of marginals, which cannot directly inform decisions on whether to implement a disease mitigation intervention. For instance, we find that the benefits from reducing infections are the highest in the weeks before an outbreak, when the potential for disease propagation is elevated, while social distancing policies tended to be imposed after cases start increasing. Lastly, our MCFR framework is sufficiently flexible to be applied to other contexts and is particularly valuable for studying diseases with relatively high transmissibility, which increases the scope for geographical spillovers and the mortality impact from downstream cases.

References

Abdulhadi, Adibah, and Bruce Weinberg. 2025. "Imputation Method for Increasing the Temporal Granularity of Data: The Case of Mortality." Working paper.

Almon, S. 1965. "The Distributed Lag between Capital Appropriations and Expenditures." *Econometrica*, 33(1): 178–196.

Al-Raeei, Marwan. 2021. "The basic reproduction number of the new coronavirus pandemic with mortality for India, the Syrian Arab Republic, the United States, Yemen, China, France, Nigeria and Russia with different rate of cases." *Clinical Epidemiology and Global Health*, 9: 147–149.

Alsan, Marcella, Amitabh Chandra, and Kosali Simon. 2021. "The Great Unequalizer: Initial Health Effects of COVID-19 in the United States." *Journal of Economic Perspectives*, 35(3): 25–46.

Atkeson, Andrew G., Karen A. Kopecky, and Tao Zha. 2024. "Four Stylized Facts about COVID-19." *International Economic Review*, 65(1): 3–42.

Auster, R., I. Leveson, and D. Sarachek. 1969. "The Production of Health, An Exploratory Study." *The Journal of Human Resources*, 4(4): 411–436.

Balcan, Duygu, Vittoria Colizza, Bruno Gonçalves, Hao Hu, José J. Ramasco, and Alessandro Vespignani. 2009. "Multiscale mobility networks and the spatial spreading of infectious diseases." *Proceedings of the National Academy of Sciences*, 106(51): 21484–21489.

Barmen, M. P., T. Rahman, K. Bora, and C. Borgohain. 2020. "COVID-19 pandemic and its recovery time of patients in India: A pilot study." *Diabetes & Metabolic Syndrome: Clinical Research & Reviews*, 14(5): 1205–1211.

Beaney, T, JM Clarke, V Jain, et al. 2020. "Excess mortality: the gold standard in measuring the impact of COVID-19 worldwide?" *Journal of the Royal Society of Medicine*, 113(9): 329–334.

Bertozzi, A., E. Franco, G. Mohler, M. B. Short, and D. Sledge. 2020. "The challenges of modeling and forecasting the spread of COVID-19." *Proceedings of the National Academy of Sciences*, 117(29): 16732–16738.

CDC. 2022*a*. "Provisional COVID-19 Death Counts by Week Ending Date and State." US Centers for Disease Control and Prevention. https://data.cdc.gov/NCHS/Provisional-COVID-19-Death-Counts-by-Week-Ending-D/r8kw-7aab. Accessed 2022-10-27.

CDC. 2022*b*. "Provisional Death Counts for Influenza, Pneumonia, and COVID-19." US Centers for Disease Control and Prevention. https://data.cdc.gov/NCHS/Provisional-Death-Counts-for-Influenza-Pneumonia-a/ynw2-4viq. Accessed 2022-10-26.

CDC. 2022*c*. "Weekly Counts of Deaths by Jurisdiction, and Race and Hispanic Origin." US Centers for Disease Control and Prevention. https://data.cdc.gov/NCHS/Weekly-Counts-of-Deaths-by-Jurisdiction-and-Race-a/qfhf-uhaa. Accessed 2022-10-26.

CDC. 2023. "Underlying Medical Conditions Associated with Higher Risk for Severe COVID-19: Information for Healthcare Professionals." US Centers for Disease Control and Prevention. https://www.cdc.gov/coronavirus/2019-ncov/hcp/clinical-care/underlyingconditions.html Accessed: 2023-07-17.

CDC. 2025. "About Inactive Tuberculosis." US Centers for Disease Control and Prevention. https://www.cdc.gov/tb/about/inactive-tuberculosis.html. Accessed: 2025-02-11.

Census Bureau. 2019. "Annual County Resident Population Estimates by Age, Sex, Race, and Hispanic Origin: April 1, 2010 to July 1, 2019." US Census Bureau. https://www.census.gov/newsroom/press-kits/2020/population-estimates-detailed.html. Accessed: 2023-01-17.

Chen, Jiafeng, and Jonathan Roth. 2024. "Logs with Zeros? Some Problems and Solutions." *The Quarterly Journal of Economics*, 139(2): 891–936.

Chetty, Raj, John N Friedman, Michael Stepner, and The Opportunity Insights Team. 2020. "The Economic Impacts of COVID-19: Evidence from a New Public Database Built Using Private Sector Data." National Bureau of Economic Research Working Paper 27431.

Chinazzi, M., J. T. Davis, M. Ajelli, C. Gioannini, M. Litvinova, S. Merler, A. P. Y. Piontti, K. Mu, L. Rossi, K. Sun, C. Viboud, X. Xiong, H. Yu, M. E. Halloran, I. M. Longini Jr., and A. Vespignani. 2020. "The effect of travel restrictions on the spread of the 2019 novel coronavirus (COVID-19) outbreak." *Science*, 368(6489): 395–400.

Chudik, A., M. H. Pesaran, and A. Rebucci. 2022. "Social distancing, vaccination and evolution of COVID-19 transmission rates in Europe." *IMF Economic Review*, 1–35.

Corona, G., A. Pizzocaro, W. Vena, et al. 2021. "Diabetes is most important cause for mortality in COVID-19 hospitalized patients: Systematic review and meta-analysis." *Reviews in Endocrine and Metabolic Disorders*, 22: 275–296.

Coston, Amanda, Neel Guha, Derek Ouyang, Lisa Lu, Alexandra Chouldechova, and Daniel E. Ho. 2021. "Leveraging Administrative Data for Bias Audits: Assessing Disparate Coverage with Mobility Data for COVID-19 Policy." *FAccT '21*, 173–184. New York, NY, USA:Association for Computing Machinery.

Deyle, Ethan, M. Cyrus Maher, Ryan Hernandez, Sanjay Basu, and George Sugihara. 2016. "Global Environmental Drivers of Influenza." *PNAS Biological Sciences*, 113(46): 13081–13086. Accessed July 17, 2023.

Fernández-Villaverde, J., and C. I. Jones. 2022. "Estimating and simulating a SIRD Model of COVID-19 for many countries, states, and cities." *Journal of Economic Dynamics and Control*, 140: 104318.

Finkelstein, Amy, Geoffrey Kocks, Maria Polyakova, and Victoria Udalova. 2024. "Heterogeneity in Damages from a Pandemic." *The Review of Economics and Statistics*.

Griliches, Z. 1967. "Distributed Lags: A Survey." *Econometrica*, 35(1): 16–49.

Hannan, E. J., and B. G. Quinn. 1979. "The Determination of the Order of an Autoregression." *Journal of the Royal Statistical Society: Series B*, 41(2): 190–195.

Han, X., Y. Xu, L. Fan, Y. Huang, M. Xu, and S. Gao. 2021. "Quantifying COVID-19 importance risk in a dynamic network of domestic cities and international counties." *PNAS*, 118(31): 1–8.

Heffernan, J. M., R. J. Smith, and L. M. Wahl. 2005. "Perspectives on the basic reproductive ratio." *Journal of the Royal Society Interface*, 2(4): 281–293.

Heymann, D. L. (Ed.). 2015. *Control of Communicable Diseases Manual.* . 20th ed., American Public Health Association.

HHS. 2023. "COVID-19 Reported Patient Impact and Hospital Capacity by State Timeseries (RAW)." U.S. Department of Health & Human Services. https://healthdata.gov/Hospital/COVID-19-Reported-Patient-Impact-and-Hospital-Capa/g62h-syeh. Accessed 2023-04-14.

Huang, Ian, Michael Anthonius Lim, and Raymond Pranata. 2020. "Diabetes mellitus is associated with increased mortality and severity of disease in COVID-19 pneumonia – A systematic review, meta-analysis, and meta-regression." *Diabetes & Metabolic Syndrome: Clinical Research & Reviews*, 14(4): 395–403.

Ioannidis, J. P. A. 2021. "Infection fatality rate of COVID-19 inferred from seroprevalence data." *Bulletin of the World Health Organization*, 99(1): 19–33F.

Jeong, Hanbat, and L. F. Lee. 2020. "Spatial Dynamic Models with Intertemporal Optimization: Specification and Estimation." *Journal of Econometrics*, 218(1): 82–104.

Jeong, H., Y. Lin, and B. Weinberg. 2023. "Worse than the Problem Itself? The Health and Economic Costs and Benefits of COVID-19 Policy Responses." Working paper.

Johnsson, I., M. H. Pesaran, and C. F. Yang. 2023. "Structural Econometric Estimation of the Basic Reproduction Number for Covid-19 Across U.S. States and Selected Countries." Working paper.

Kang, Yuhao, Song Gao, Yunlei Liang, Mingxiao Li, Jinmeng Rao, and Jake Kruse. 2020. "Multiscale Dynamic Human Mobility Flow Dataset in the U.S. During the COVID-19 Epidemic." *Scientific Data*, 7: 390.

Kastora, S., M. Patel, B. Carter, M. Delibegovic, and P. K. Myint. 2022. "Impact of diabetes on COVID-19 mortality and hospital outcomes from a global perspective: An umbrella systematic review and meta-analysis." *Endocrinology, Diabetes & Metabolism*, 5(3).

Katul, G. G., A. Mrad, S. Bonetti, G. Manoli, and A. J. Parolari. 2020. "Global convergence of COVID-19 basic reproduction number and estimation from early-time SIR dynamics." *PLOS ONE*, 15(9): e0239800.

Ke, R., E. Romero-Severson, S. Sanche, and N. Hengartner. 2021. "Estimating the reproductive number R0 of SARS-CoV-2 in the United States and eight European countries and implications for vaccination." *Journal of Theoretical Biology*, 517: 110621.

KFF. 2022. "State Actions to Mitigate the Spread of COVID-19." (KFF) The Kaiser Family Foundation. https://www.kff.org/state-health-facts/custom/.

Korolev, I. 2021. "Identification and estimation of the SEIRD epidemic model for COVID-19." *Journal of Econometrics*, 220(1): 63–85.

Kudo, Eriko, Eric Song, Laura J. Yockey, Tasfia Rakib, Patrick Wong, Robert Homer, and Akiko Iwasaki. 2019. "Low Ambient Humidity Impairs Barrier Function and Innate Resistance Against Influenza Infection." *PNAS Biological Sciences*, 116(22): 10905–10910. Accessed July 17, 2023.

Kumar, Ashish, Anil Arora, Praveen Sharma, Shrihari Anil Anikhindi, Naresh Bansal, Vikas Singla, Shivam Khare, and Abhishyant Srivastava. 2020. "Is diabetes mellitus associated with mortality and severity of COVID-19? A meta-analysis." *Diabetes & Metabolic Syndrome: Clinical Research & Reviews*, 14(4): 535–545.

Lavetti, Kurt. 2023. "Compensating Wage Differentials in Labor Markets: Empirical Challenges and Applications." *Journal of Economic Perspectives*, 37: 189–212.

Li, Q., et al. 2020. "Early transmission dynamics in Wuhan, China, of novel coronavirus-infected pneumonia." *New England Journal of Medicine*, 1199–1207.

Liu, Y., A. A. Gayle, A. Wilder-Smith, and J. Rocklöv. 2020. "The reproductive number of COVID-19 is higher compared to SARS coronavirus." *Journal of Travel Medicine*, 27(2): taaa021.

Mecenas, P., R. T. d. R. M. Bastos, A. C. R. Vallinoto, and D. Normando. 2020. "Effects of temperature and humidity on the spread of COVID-19: A systematic review." *PLOS ONE*, 15(9): e0238339.

MEDSL. 2017. "U.S. President 1976–2020." MIT Election Data and Science Lab, Harvard Dataverse. https://doi.org/10.7910/DVN/42MVDX. Accessed 2002-11-03.

Morgan, David, Junya Ino, Gabriel Di Paolantonio, and Fabrice Murtin. 2020. "Excess Mortality: Measuring the Direct and Indirect Impact of COVID-19." Organisation for Economic Co-operation and Development OECD Health Working Papers No. 122.

NCEI. 2023. "Climate at a Glance: County Mapping." National Centers for Environmental Information, National Oceanic and Atmospheric Administration. https://www.ncei.noaa.gov/access/monitoring/climate-at-a-glance/county/mapping. Accessed 2023-03-27.

Notari, Alessio. 2021. "Temperature dependence of COVID-19 transmission." *Science of The Total Environment*, 763: 144390.

Park, M., A. R. Cook, J. T. Lim, Y. Sun, and B. L. Dickens. 2020. "A Systematic Review of COVID-19 Epidemiology Based on Current Evidence." *Journal of Clinical Medicine*, 9(4): 967.

Pesaran, M. H., and C. F. Yang. 2022. "Matching theory and evidence on Covid-19 using a stochastic network SIR model." *Journal of Applied Econometrics*, 37: 1204–1229.

Polyakova, Maria, Victoria Udalova, Geoffrey Kocks, Katie Genadek, Keith Finlay, and Amy N. Finkelstein. 2021. "Racial Disparities In Excess All-Cause Mortality During The Early COVID-19 Pandemic Varied Substantially Across States." *Health Affairs*, 40(2): 307–316.

Population Health Institute. 2023. "County Health Rankings and Roadmaps." *http://www.countyhealthrankings.org*, Accessed January 23, 2023.

Qiu, Yun, Xi Chen, and Wei Shi. 2020. "Impacts of Social and Economic Factors on the Transmission of Coronavirus Disease 2019 (COVID-19) in China." *Journal of Population Economics*, 33: 1127–1172.

Ruhm, Christopher. 2015. "Recessions, Healthy No More?" *Journal of Health Economics*, 42(C): 17–28.

Salje, H., C. Tran Kiem, N. Lefrancq, N. Courtejoie, P. Bosetti, J. Paireau, A. Andronico, N. Hozé, J. Richet, C. L. Dubost, Y. Le Strat, J. Lessler, D. Levy-Bruhl, A. Fontanet, L. Opatowski, P. Y. Boelle, and S. Cauchemez. 2020. "Estimating the burden of SARS-CoV-2 in France." *Science*, 369(6500): 208–211. Jul 10.

Sanche, S., Y. T. Lin, C. Xu, E. Romero-Severson, N. Hengartner, and R. Ke. 2020. "High Contagiousness and Rapid Spread of Severe Acute Respiratory Syndrome Coronavirus 2." *Emerging Infectious Diseases*, 26(7): 1470–1477.

Schwandt, Hannes, Janet Currie, Till von Wachter, Jonathan Kowarski, Derek Chapman, and Steven H. Woolf. 2022. "Changes in the Relationship Between Income and Life Expectancy Before and During the COVID-19 Pandemic, California, 2015-2021." *JAMA*, 328(4): 360–366.

SeyedAlinaghi, S., L. Abbasian, M. Solduzian, et al. 2021. "Predictors of the prolonged recovery period in COVID-19 patients: a cross-sectional study." *European Journal of Medical Research*, 26(41): 26–41.

Shaman, Jeffrey, and Melvin Kohn. 2009. "Absolute Humidity Modulates Influenza Survival, Transmission, and Seasonality." *PNAS Biological Sciences*, 106(9): 3243–3248. Accessed July 17, 2023.

Shaman, Jeffrey, Virginia Pitzer, Cécile Viboud, Bryan Grenfell, and Marc Lipsitch. 2010. "Absolute Humidity and the Seasonal Onset of Influenza in the Continental United States." *PLOS Biology*, 8(2): e1000316. Accessed July 17, 2023.

Shi, Peng, Yinqiao Dong, Huanchang Yan, Chenkai Zhao, Xiaoyang Li, Wei Liu, Miao He, Shixing Tang, and Shuhua Xi. 2020. "Impact of temperature on the dynamics of the COVID-19 outbreak in China." *Science of The Total Environment*, 728: 138890.

Shi, W., and L. F. Lee. 2017. "Spatial dynamic panel data models with interactive fixed effects." *Journal of Econometrics*, 197: 323–347.

Stokes, Erin, Laura Zambrano, Kayla Anderson, Ellyn Marder, Kala Raz, Suad El Burai Felix, Yunfeng Tie, and Kathleen Fullerton. 2020. "Coronavirus Disease 2019 Case Surveillance – United States, January 22–May 30, 2020." *Morbidity and Mortality Weekly Report*, 69(24): 759–765.

Sunstein, Cass R. 2024. "The Economic Constitution of the United States." *Journal of Economic Perspectives*, 38(2): 25–42.

Systrom, Kevin, Thomas Vladek, and Mike Krieger. 2020. "Rt.live." *https://web.archive.org/web/20210430035552/https://rt.live/*, Accessed August 26, 2023.

Tamerius, James, Jeffrey Shaman, Wladmir Alonso, Kimberly Bloom-Feshbach, Christopher K. Uejio, Andrew Comrie, and Cécile Viboud. 2013. "Environmental Predictors of Seasonal Influenza Epidemics across Temperate and Tropical Climates." *PLOS Pathogens*, 9(3): e1003194. Accessed July 17, 2023.

Taubenberger, J. K., and D. M. Morens. 2006. "1918 Influenza: the mother of all pandemics." *Emerging Infectious Diseases*, 12(1): 15–22.

The New York Times. 2021. "See Reopening Plans and Mask Mandates for All 50 States." *https://www.nytimes.com/interactive/2020/us/states-reopen-map-coronavirus.html*, Accessed May 16, 2022.

Tsegaye, Serkalem, Firomsa Bekele, Yohanes Lulu, Gebiso Roba Debele, Teshome Bekana, Leta Deressa Tolesa, and Kebebe Bidira. 2022. "Time to recovery and its predictors among COVID-19 positive patients admitted to treatment centers of Southwestern Ethiopian hospitals: A multicenter retrospective cohort study." *Annals of Medicine and Surgery*, 84: 104917.

USAFacts. 2022. "Detailed Methodology and Sources: COVID-19 Data." *https://usafacts.org/articles/detailed-methodology-covid-19-data/*, Accessed July 10, 2023.

Verity, R., L. C. Okell, I. Dorigatti, P. Winskill, C. Whittaker, N. Imai, G. Cuomo-Dannenburg, H. Thompson, P. G. T. Walker, H. Fu, A. Dighe, J. T. Griffin, M. Baguelin, S. Bhatia, A. Boonyasiri, A. Cori, Z. Cucunubá, R. FitzJohn, K. Gaythorpe, and N. M. Ferguson. 2020. "Estimates of the severity of coronavirus disease 2019: A model-based analysis." *The Lancet Infectious Diseases*, 20(6): 669–677.

Weinberger, Daniel M., Jenny Chen, Ted Cohen, Forrest W. Crawford, Farzad Mostashari, et al. 2020. "Estimation of Excess Deaths Associated With the COVID-19 Pandemic in the United States, March to May 2020." *JAMA Internal Medicine*, 180(10): 1336–1344.

WHO. 2024. "Cholera." World Health Organization (WHO). https://www.who.int/news-room/fact-sheets/detail/cholera. Accessed: 2025-09-10.

WHO. 2025. "Tuberculosis." World Health Organization (WHO). https://www.who.int/news-room/fact-sheets/detail/tuberculosis. Accessed: 2025-09-10.

Wu, Yu, Wenzhan Jing, Jue Liu, Qiuyue Ma, Jie Yuan, Yaping Wang, Min Du, and Min Liu. 2020. "Effects of temperature and humidity on the daily new cases and new deaths of COVID-19 in 166 countries." *Science of The Total Environment*, 729: 139051.

Wu, Zunyou, and Jennifer M. McGoogan. 2020. "Characteristics of and Important Lessons From the Coronavirus Disease 2019 (COVID-19) Outbreak in China: Summary of a Report of 72-314 Cases From the Chinese Center for Disease Control and Prevention." *JAMA*, 323(13): 1239–1242.

Yu, J., R. de Jong, and L. F. Lee. 2008. "Quasi-maximum Likelihood Estimators for Spatial Dynamic Panel Data with Fixed Effects when Both n and T are Large." *Journal of Econometrics*, 146: 118–134.

Zhang, Jonathan. 2021. "Hospital Avoidance and Unintended Deaths during the COVID-19 Pandemic." *American Journal of Health Economics*, 7(4): 405–426.

Ziedan, Engy, Kosali I. Simon, and Coady Wing. 2022. "Mortality Effects of Healthcare Supply Shocks: Evidence Using Linked Deaths and Electronic Health Records." National Bureau of Economic Research Working Paper 30553.